CHEMISTRY OF MATERIALS

pubs.acs.org/cm Review

Area-Selective Deposition: Fundamentals, Applications, and Future Outlook

Gregory N. Parsons and Robert D. Clark

Cite This: https://dx.doi.org/10.1021/acs.chemmater.0c00722 Read Online

ACCESS | Metrics & More | Article Recommendations

ABSTRACT: This review provides an overview of area-selective thin film deposition (ASD) with a primary focus on vapor-phase thin film formation via chemical vapor deposition (CVD) and atomic layer deposition (ALD). Area-selective deposition has been successfully implemented in microelectronic processes, but most approaches to date rely on high-temperature reactions to achieve the desired substrate sensitivity. Continued size and performance scaling of microelectronics, as well as new materials, patterning methods, and device fabrication schemes are seeking solutions for new low-temperature (<400 °C) ASD methods for dielectrics, metals, and organic thin films. To provide an overview of the ASD field, this article critically reviews key challenges that must be overcome for ASD to be successful in microelectronics and other fields, including descriptions of current process application needs. We provide an overview of basic mechanisms in film nucleation during CVD and ALD and summarize current known ASD approaches for semiconductors, metals, dielectrics, and organic materials. For a few key materials, selectivity is quantitatively compared for different reaction precursors, giving important insight into needs for favorable reactant and reaction design. We summarize current limitations of ASD and future opportunities that could be achieved using advanced bottom-up atomic scale processes.

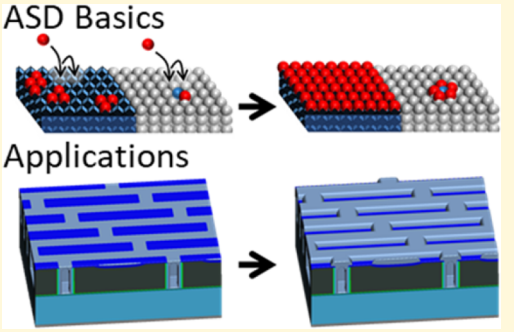

Downloaded via NORTH CAROLINA STATE UNIV on June 22, 2020 at 13:44:41 (UTC).
See https://pubs.acs.org/sharingguidelines for options on how to legitimately share published articles.

I. INTRODUCTION

I.A. Nanoscale Chemical Patterning. Nanoscale materials, thin films, and patterning are important in electronics, energy conversion and storage, catalysis, chemical separations, environmental protection and health, and many other technologies. Scientific and technological advances in these fields require new capabilities to control chemical reactions that determine material composition, dimensions, density, texture, and structural shape with nanoscale or subnanoscale precision. Nanoscale lines, spaces, and other complex features are routinely patterned on surfaces using photolithography, using light to transfer a physical mask pattern to a photoresist. Ultimately, controlling chemical synthesis requires understanding and manipulating reactions at the earliest steps in material formation. Insight is needed in mechanisms during thin film heterogeneous nucleation, driven by the complex chemistry and thermodynamics of molecule/surface and molecule/vapor interactions.

A most basic example of controlling deposition reactions is the ability to achieve "area-selective deposition", ASD, where a process is adjusted to allow a desired film to form in one region of a surface while simultaneously avoiding deposition in an adjacent region. In place of a physical lithographic mask, ASD utilizes chemical information available on a surface and in the deposition source reactants to guide pattern growth on a surface. The term "patterning" is commonly used to indicate control over feature shape, size, and geometry. Indeed, feature patterning often begins using a substrate that is uniform and chemically homogeneous. Area-selective deposition, on the other hand, starts on a prepatterned substrate. On this pattern, ASD can work to selectively adjust surface composition, as well as feature height and/or feature width. Therefore, ASD can be considered as "chemical patterning" in the sense that, after ASD, the surface features become chemically and physically distinct from those present before ASD.

Area-selective deposition refers to any chemical or physical process that controllably forms a desired material layer on a desired "growth" region of an exposed surface without forming a layer on other adjacent "nongrowth" areas of different compositions or surface terminations.[1−11] The growth and nongrowth regions can be differentiated by material composition, surface termination, lattice structure, or physical topography. When the film forms on all exposed surfaces, it is referred to as uniform or "blanket" deposition. "Selectivity loss" refers to a point or range in time when a process transitions from selective to blanket deposition.

Received: February 19, 2020
Revised: May 12, 2020
Published: May 14, 2020

© XXXX American Chemical Society

The purpose of this review is to provide an overview of area-selective deposition, with primary focus on vapor−solid reaction processes. Vapor-based processes for ASD include chemical vapor deposition, CVD, atomic layer deposition, ALD, and molecular layer deposition, MLD, with most recent studies addressing area-selective ALD. Several previous articles have reviewed selective deposition by CVD[3,5−7,9,12,13] and by ALD.[14−19] Also, many excellent articles describe basic ALD reactions and applications,[20−30] as well as how ALD impacts outstanding challenges in semiconductor manufacturing.[31,32] This article expands upon previous reviews to present a cohesive examination of ASD, including discussion of metals, semiconductors, dielectrics, and organic thin films, as well as provide a contrast between ALD, CVD, and related processes for ASD. Interest also includes mechanisms in vapor−solid thin film nucleation, as well as quantification and modeling of ASD. Detailed needs and possible applications for ASD in electronic device manufacturing are also presented. Recent ASD research is also summarized, including ASD of metals, dielectrics, and other materials on a range of desired growth and nongrowth substrates.

The concept of "selective deposition" extends to other processes beyond ASD. For example, "phase-selective deposition" could describe a process to isolate a specific phase of a material or form different phases simultaneously in different regions on a surface.[5,9] The deposition of diamond thin films, for example, is designed to selectively promote sp^3 diamond bonds while minimizing sp^2 graphitic bonding. Facet-selective deposition involves film formation on a preselected exposed crystal face, without reaction on neighboring crystal planes.[33] As another example, "direction-selective deposition" could allow growth to proceed only in one desired direction. Physical deposition via sputtering or evaporation achieves directionality via line-of-sight growth of impinging atoms or clusters. In this sense, direction-selective chemical deposition could be an anisotropic rate process, which is well-known in plasma-based etching. Alternate selective deposition processes are interesting, but area-selective deposition is a current primary concern, particularly in electronics where it is rapidly becoming a required tool to pattern and align nanometer-scale material elements in large-wafer semiconductor manufacturing.

I.B. Top-Down and Bottom-Up Patterning. Significant research in thin film materials has been directed to electronic device systems, leading to rapid advances described by Moore's law.[31,34] Photolithography is the key enabling step in feature scale definition. Photolithography is described as a "top-down" method because it starts with a uniform blanket dielectric and metal films and uses a patterned photoresist to remove material from regions where the blanket film is not wanted. The regions to be removed are defined by a physical mask which allows only part of the resist to be exposed to a lithography UV light source. The pattern formed in the resist is then transferred to the underlying film by chemical etching. Deep UV photolithography using 193 nm light is highly reliable and economically robust, even at sub-10 nm feature nodes. Achieving these feature sizes in manufacturing relies on litho etch litho etch (LELE) multi-patterning, where more than one exposure step is used in a single patterning layer to produce features with size and pitch that are much smaller than those imaged by a single mask.[35,36] In contrast, "bottom-up" or "additive" processes work to deposit or create material only in regions where it is needed, avoiding the need for material removal. Aspects of bottom-up processing are employed in several alternatives to lithography, including nanoimprinting or embossing, scanning probes, direct printing, electrostatic self-assembly, directed self-assembly (DSA) of block copolymers, and chemical assembly of organic electronics.[37−45] "Bottom-up" methods can significantly reduce material waste and energy consumption, so they remain an important direction for research exploration.

As critical device dimensions approach 5 nm or less, new problems are being encountered in photolithography, including the high cost of transitioning from deep UV to extreme EUV 13.5 nm light sources and resists, and by fundamentals of statistical variability. These problems are pushing industry to find new reliable bottom-up methods. Area-selective deposition is a promising approach for bottom-up "chemical patterning". As such, future ASD holds promise to allow molecular-scale chemical sensitivity and reaction design to augment traditional patterning methods.

I.C. Area-Selective Deposition via Vapor−Solid Reactions. Area-selective deposition uses the chemical information available in the reactants and the exposed surface to guide the creation of a desired material design. Figure 1 shows schematic diagrams of an ideal vapor-source area-selective deposition process where deposition occurs only in the desired growth region, and a more realistic ASD process showing unwanted nuclei in the targeted nongrowth region. The growth and nongrowth regions for ASD are usually identified by how the reactants adsorb and react on these regions. Surface preparation, therefore, is a critical part of the overall ASD process. Materials including metal oxides, nitrides, organics, and semiconductors require terminal species, such as hydrogen, hydroxyl, amine, or methyl groups to stabilize and maintain a "clean" surface. Many metal surfaces are also terminated with oxygen or other species, but "clean" metals often only have the metal atoms exposed. Clean surfaces can be used directly for ASD or they can be chemically or physically modified to enhance or inhibit nucleation and deposition.

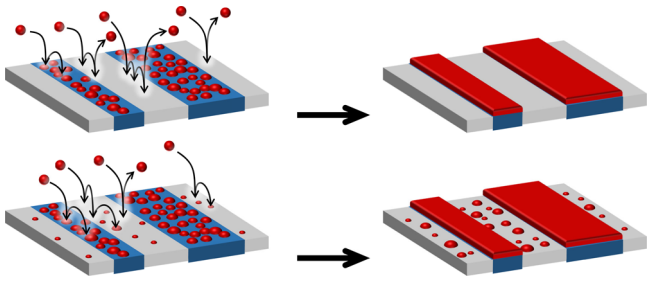

Figure 1. (top) Ideal area-selective deposition producing a thin film only on desired regions of the substrate and (bottom) more realistic ASD producing thin films in desired regions with unwanted nuclei in targeted nongrowth regions.

Deposition can be locally enhanced using patterned surface excitation via electron, ion, or photon beams[5,9,46,47] or locally passivated by adsorbing molecule monolayers or nonreactive polymers.[48,49] Ideally, the process that enhances or inhibits nucleation will be selective, so that it occurs only on regions where it is desired without modifying other regions. As described in detail below, localized enhancement and passivation can substantially improve area-selective deposition, but difficulties can arise in extending the preparation to features with very small size or complex shapes, as well as in scaling the surface preparation to large areas and high throughput.

https://dx.doi.org/10.1021/acs.chemmater.0c00722
Chem. Mater. XXXX, XXX, XXX−XXX

Approaches for ASD of thin film semiconductors, metals, dielectrics, organics, and other complex materials have been of interest for several decades. An early motive for area-selective deposition was to reduce the number of masking steps required in device preparation. Epitaxial silicon and GaAs were observed to grow on silicon at 700 °C without depositing on an adjacent metal oxide.[1,2,4,10,11] Area-selective epitaxy of silicon-based materials by CVD at temperatures in the range of 700−1200 °C is well developed and used in "front-end" processing, to form source/drain contact in Fin-FET transistors, minimizing contact resistance and improving device performance.[50,51] The high deposition temperature controls the local chemical termination of the growing surface, helping to direct ASD. For silicon CVD using SiH_4,[52] desorption of the passivating Si-H species activates the Si surface promoting area-selective silicon deposition. Tungsten has also been used as a transistor contact material and was an early target for ASD.[8,53−57] Tungsten makes a good ohmic contact to silicon, and W and Si have compatible thermal expansion coefficients. Tungsten is also one of the metals that can undergo an area-selective reaction with silicon to form a self-aligned metal silicide, or "salicide".[58,59] In this approach, lithography is used to open via holes in an oxide layer, exposing silicon contact regions in the underlying transistors. A layer of tungsten, or other metals such as Ti, Mo, Ta, or Co, is then deposited on top and then heated to allow metal silicide to form only in the exposed junction regions. The unreacted metal is then removed, leaving the silicide, now covering the previously open silicon vias.

After completing the "front-end" transistor structure, hundreds of "back-end" process steps are needed to form metal and dielectric lines that complete the device. The transistors and interconnects are engineered with complex dopant profiles and ultrathin metal diffusion barriers. Heating above 400 °C can lead to unwanted metal diffusion which degrades the device.[60] Therefore, to extend into back-end manufacturing, ASD processes are needed that work at $T < 400$ °C, where selective thermal activation is not as effective. This low temperature limitation therefore adds significant complexity to the problem of achieving reliable and scalable ASD. Atomic layer deposition can generally proceed at lower temperatures than CVD and the sequential reactant delivery in ALD provides additional flexibility in processing, so recent attention has pushed toward area-selective ALD[24,26,33,61] and related techniques such as molecular layer deposition, vapor infiltration, and atomic layer etching.

I.D. Liquid−Solid Patterned Deposition and Other Nanopatterning Approaches. When considering methods for ASD for microelectronics, it is important to recognize that the combination of small feature size, large-area, and high-throughput manufacturing put extremely stringent demands on ASD processes. Vapor phase reactants are usually preferred over solution-based processes because solutions use a larger amount of material, leading to concerns related to purity. A tactic to overcome this may be to deliver reactants in microdroplets via a microfluidic reaction scheme.[62] Even so, large volume processes can be feasible. A common example of a solution-based manufacturing process is electroless copper plating, which uses a self-catalyzed redox reaction scheme.[63] A copper precursor is reduced by a dissolved reducing agent, such as formaldehyde, which in turn becomes oxidized. To start the process, a catalytic metal seed layer is needed to dehydrogenate the oxidation products, releasing hydrogen and allowing electron transfer through the metal. Using accelerators, it is possible to enable bottom-up filling of interconnect structures with Cu electroplating in order to avoid pinch-off, seams, and voids.[64]

Complementing work in ASD, another important example of solution-based chemically driven patterning that has made impacts in large-scale processing is directed self-assembly of block copolymers.[38,39] Assembling a diblock copolymer, such as polystyrene-*block*-poly(methyl methacrylate) (PS-*b*-PMMA), using predetermined lithographic features can create oriented and registered polymer nanolines and other structures over large wafer-scale areas. The patterns can then be transferred to inorganic layers on the underlying substrate. One pattern transfer method is selective vapor infiltration.[28,65,66] Metal−organic precursors such as trimethyl aluminum will diffuse into the copolymer and preferentially adsorb and react in the PMMA regions.[67] Subsequent reaction with water produces metal oxide layers that precisely duplicate the polymer pattern structure. This method can also be extended to convert arbitrary shaped polymers into patterned metal oxide films.[68]

Research is also ongoing in other solution-based ASD and chemical-patterning processes. One example is spin dewetting for area-selective deposition of polymer films. This method uses a patterned grafted monolayer, such as an alkylsilane, to define local hydrophilic and hydrophobic regions on a substrate surface. A polymer film is then deposited on this surface by spin coating. The localized hydrophobicity combined with the centrifugal forces exerted during the spin coating leads to surface-dependent polymer dewetting and accumulation.[69] The transition from polymer wetting to dewetting depends on details of the materials and spin coating conditions. The resulting polymer thickness and the thickness profile across a feature depend on the feature size and the polymer being deposited and result from complex interactions between the polymer, solvent, and surface termination.[69]

Another means for self-directed pattern formation is vapor−liquid−solid nanowire synthesis.[70] Seed particles selectively collect and direct synthesis of nanoscale crystals, and the tunability of the chemical uptake within the particle allows axial encoding of heterogeneous composition along the length of the growing nanowires. Compositional changes can also be used for selective growth and removal of passivating polymers, creating patterns along the nanowire length.[71] Colloidal assembly,[72,73] DNA scaffolds,[74] and other electrostatic processes also allow patterned surface preparation. Tiles composed of geometrically defined DNA strands can assemble on a surface and guide the subsequent attachment of conductive or other structural elements.[75] Directed folding of designed biomaterials, such as DNA origami, makes use of bottom-up assembly found in nature to create 2D and 3D patterns.[76]

I.E. Review Outline. In the following text, Section II presents background information regarding thin film nucleation from the vapor phase, including discussion of well-known models of nucleation energetics and the insight they provide into current challenges in ASD and quantification of island growth. Before discussing specific ASD processes and mechanisms, Section III brings attention to the importance of considering ASD as a reactive "system", including elementary nucleation reactions as well as effects due to the reaction scheme (i.e., ALD vs CVD) and overall reactor design. Section IV describes applications for ASD, including semiconductor device scaling, catalysis, and other emerging areas. General experimental approaches for ASD are summarized in Section V, and Section VI presents a partial collection of ASD results published to date. Instead of sorting the data based on the experimental approach

https://dx.doi.org/10.1021/acs.chemmater.0c00722
Chem. Mater. XXXX, XXX, XXX−XXX

or material deposited, we chose to sort based on the type of deposited material (i.e., metal or dielectric) and the type of receptive substrate. Because ASD is sensitive to surface reaction, the results in Section VI are further classified by the ligands on the deposition precursors. Section VII then presents a brief summary of outstanding research challenges. The issue of ASD metrology, including comparisons of available procedures to measure and evaluate ASD process, is left for a future review.

II. THIN FILM NUCLEATION DURING VAPOR DEPOSITION: DEFINITION AND MODELING OF SELECTIVITY

II.A. Basics of Nucleation from the Vapor Phase.

Nucleation is any physical or chemical sequence that produces stable nuclei. The rate of heterogeneous nucleation on a substrate surface is determined by the kinetics of the reaction sequence that yields thermodynamically stable nuclei. While thin film nucleation has been extensively studied both theoretically and experimentally, there remain several aspects of nucleation that are not well understood. Most studies of thin film nucleation describe steps that occur when there is a continuous flux of reactants onto a surface, such as during PVD or CVD.[77−79] A benefit of ALD compared to CVD is that the sequential reactant exposure steps can simplify the overall deposition reaction chemistry. However, compared to steady-state CVD, the ALD sequence can add complications to the understanding and modeling of nucleation.[80,81]

When a deposition reactant impinges on a growth surface, it can reflect or become captured into a physisorbed or chemisorbed state through a sequence to minimize its overall Gibbs free energy. Figure 2a shows the basic steps in reactant adsorption and nucleation. Physisorbed molecules are relatively weakly bound, where interactions are driven by dipoles within the molecule or by induced dipoles, i.e., van der Waals or London dispersion forces. Reactants often first become physisorbed and then either desorb or transition into a chemisorbed state. Chemisorbed molecules share electrons with the surface through strong covalent bonds. Surface bonding can also occur via two-electron coordinate or dative bonds formed in Lewis acid/base interactions. These bonds are generally stronger than dipole bonds but weaker than covalent bonds. Many first-principles models show that Lewis acid/base adduct states are important intermediates for covalent bond formation. Therefore, these states can be considered as strongly bound physisorption sites. Adsorbed reactants will diffuse on the surface to find favorable binding sites.[80] Diffusing adsorbates can be energetically repelled or attracted to each other. When multiple reactants are present, nucleus formation will be driven by the adsorption energetics of each reactant on the surface as well as interactive forces between like species and between different species. Multiple substrates, such as during area-selective deposition, will introduce different adsorption energetics for each reactant. Moreover, interactions between species may also be different on each surface. As discussed below, species with different physisorption energies on different surfaces can be used to block adsorption of deposition reactants, thereby helping enable ASD.

Figure 2b shows the expected trend in energy vs nucleus size in classical nucleation theory.[79] When the attractive energy within an adsorbate cluster exceeds the energy cost associated with cluster surface formation, the cluster exceeds its "critical nucleus size" and a stable nucleus is formed. On a stable nucleus, the addition of more adsorbates will reduce the nucleus free

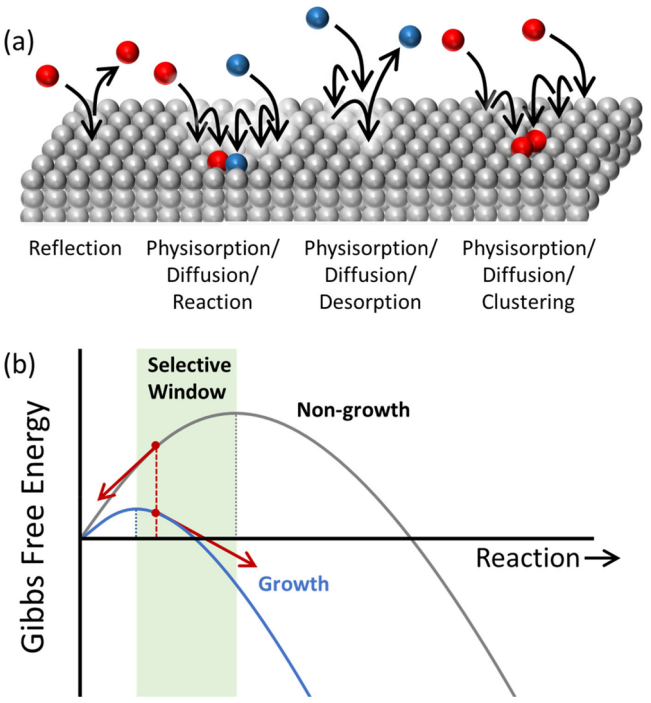

Figure 2. (a) Adsorbate/surface interactions and mechanisms for nuclei formation on a homogeneous surface during CVD using multiple reactants, with a depositing film composition different from that of the substrate. (b) Nucleus free energy vs nucleus radius for nuclei formation on two different surfaces. Selective deposition is achieved when nuclei are stable on the desired growth surface and unstable (i.e., less than the critical nucleus size) on the nongrowth surface.

energy, and growth proceeds. This general description of nucleation applies to many different deposition processes. For example, during sputtering or evaporation, the impinging deposition reactants could be metal atoms or clusters from a single element source. In a CVD process, impinging species may include multiple reactants with different compositions, such as a metal-containing precursor and an oxygen source during metal oxide CVD. Figure 2b also shows that when two different substrates are available for nucleation and deposition, the differences in Gibbs free energy change during nucleation can describe and quantify the expected reaction selectivity. Selectivity is achieved when the reactant chemical potentials and the surface and interfacial free energies enable nuclei with critical size to form rapidly on one surface and not on another.[3,9]

In addition to thermodynamic driving forces, kinetic rate processes also strongly affect nucleation during CVD and ALD. As depicted in Figure 2a, species adsorb, diffuse, and interact to create a stable nucleus. The rate of critical nucleus formation is determined by rates of species impingement and physisorption and the rates of thermally activated diffusion and reaction. A good example where both surface thermodynamics and reaction kinetics are tuned to control film nucleation is high temperature area-selective CVD of silicon using $SiH_4/H_2/HCl$ mixtures, where growth proceeds favorably on crystalline Si and not on SiO_2.[82] In this system, the surface coverage of physisorbed Cl on each surface is determined by the HCl partial pressure and Cl adsorption energy. Selectivity is achieved by controlling the Cl surface coverage which thereby determines the rate of silicon etching by Cl. The bonding between Si atoms in nuclei on SiO_2 tends to be more disordered and therefore etch faster than the Si atoms deposited into the more stable crystal lattice.[82]

https://dx.doi.org/10.1021/acs.chemmater.0c00722
Chem. Mater. XXXX, XXX, XXX−XXX

II.B. Nucleation during Low-Temperature CVD and ALD. Like CVD, ALD uses multiple reactants, but the sequential dose/purge sequence allows the depositing surface to contain only one type of physisorbed reactant at any given time. Therefore, the adsorption/diffusion/reaction pathway shown in Figure 2 for nucleation involving two different physisorbed species that proceeds during CVD will not be present during ALD. This leads to a problem in some ALD processes where desired nucleation can be relatively slow. However, for area-selective ALD, elimination of a nucleation pathway provides an overall benefit compared to CVD. In ALD, chemisorption and reaction saturation occur rapidly on receptive growth regions.

Note that the nucleation mechanisms described above can proceed on a homogeneous defect-free surface. Stable nuclei can form without the need for strong bonding between the adsorbates and the growth substrate. In this case, a "nucleation site" is a random location on the uniform surface where stochastic diffusion and interaction yield an energetically stable cluster. Analysis of nuclei size distribution during ALD of Pt and Ru has indicated that stable clusters are not necessarily bound to the substrate, allowing nuclei to diffuse and agglomerate.[83,84] Other processes, such as Ostwald ripening where atoms transfer from one nucleus to another, can also affect nucleus size and growth rate. When the deposition surface includes sites that react strongly with impinging reactants, the overall process describing nucleation must be adjusted to include additional mechanisms associated with surface/adsorbate reaction energetics and bonding reaction kinetics.

Figure 3 displays some possible mechanisms that may occur during area-selective CVD or ALD to produce nuclei in regions where deposition is not desired. Other mechanisms are also likely. Those depicted are consistent with basic nucleation models[77−79,85] and with example experiments cited in the specific descriptions below. Figure 3a depicts nucleus formation at a defect site (unwanted hydroxyl group, impurity atom, missing ligand, etc.) that exists on the starting surface before deposition. This site could allow reactant chemisorption, or it may promote strong physisorption and subsequent reaction during the coreactant dose.[86−89] An isolated reactant site generally provides few reaction pathways for chemisorption, so multiple cycles may be needed before growth begins. Not all surface defects will act as nucleation sites, and defects that promote nucleation during one ALD or CVD process may not promote nucleation during a different process. It is also important to note that defects may not always be undesired sites for selective deposition. By exploiting defect or impurity sites on a substrate, clusters or possibly single atoms can be synthesized for catalytic or other applications.[25,90] A good example of this is targeted decoration of graphite facet edges using Pt ASD.[91]

Surface impurity "defects" that provide sites for nucleation are often thought to dominate the rate of unwanted nuclei formation during low temperature area-selective ALD or CVD.[49,86,92] Also, in semiconductor manufacturing, unwanted nuclei can degrade device performance, so researchers sometimes refer to the physical unwanted nuclei as "defects", and the term "defectivity" refers to mechanisms that produce unwanted nuclei. Therefore, the definition of "defect" will depend on the context of the discussion. In the analysis of ASD nucleation, it is important to distinguish "defects" that may act as nucleation sites from "defects" which are physical nuclei.

Figure 3b−f shows potential mechanisms for nuclei formation on a clean surface with no impurity atoms initially present. The schemes depict an ALD sequence, but the mechanisms may also pertain to area-selective CVD. As shown in Figure 3b, if physisorbed precursors become stabilized, for example, by clustering, they can remain present after the reactant purge step and be available for chemisorption during the next coreactant dose.[93] Figure 3c shows that, on nonplanar surfaces, feature edges or boundaries between features can be sites for nucleation[94,95] and may also alter the desired growth.[88] These and other "feature" effects are discussed in Section III.A. Further, as shown in Figure 3d, an impinging reactant or reactant byproduct may perturb or otherwise modify a site on the nonreactive surface, leading to favorable chemisorption at the altered location.[49,55,86,96] One example is the removal of surface-

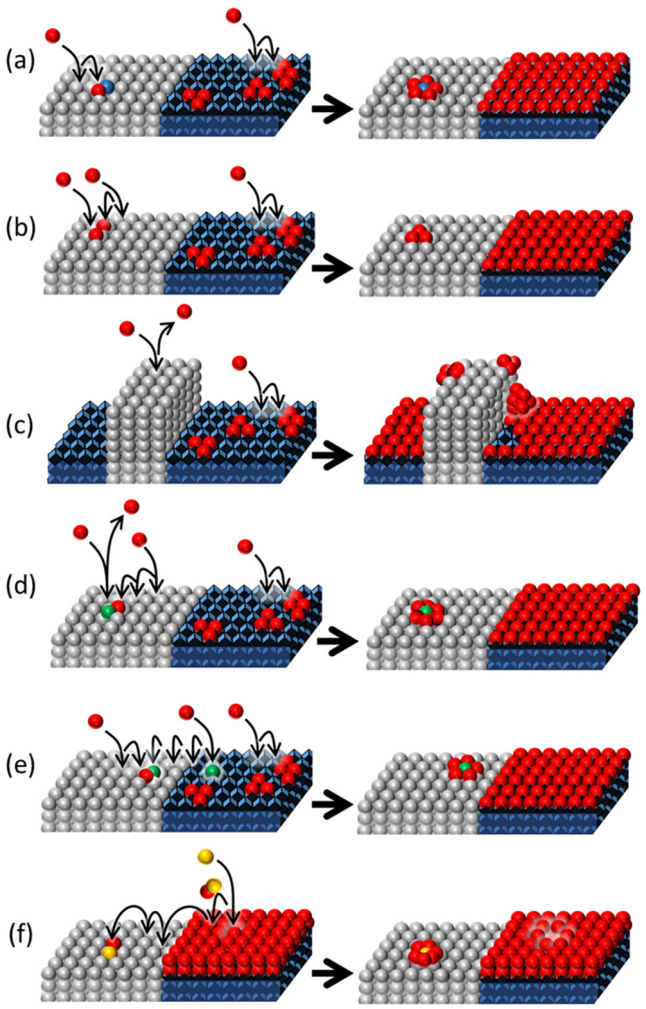

Figure 3. Subset of potential mechanisms leading to unwanted nuclei during area-selective ALD: (a) Chemisorption on a pre-existing surface defect or impurity; (b) nucleus generation by adsorbate stabilization; (c) preferential nucleation or growth inhibition at the feature corner or edge; (d) reactant−surface interaction on the nongrowth surface converting a passive site into a reactive chemisorption site; (e) reactant−surface interaction on the growth surface yielding a reaction byproduct that diffuses and adsorbs, becoming a reactive site in the nongrowth region; and (f) etch product transport and adsorption creating a reactive site. For cases c, e, and f, unwanted nuclei (or inhibition of desired growth) can tend to form near the feature boundaries, so such mechanisms are sometimes referred to as "proximity" or "micro-loading" effects. Note that the mechanisms in panels b−f depict nuclei formation at sites where impurities were not originally present on the starting surface.

https://dx.doi.org/10.1021/acs.chemmater.0c00722
Chem. Mater. XXXX, XXX, XXX−XXX

Table 1. ASD Materials and Example Selectivity

	ASD material	growth/nongrowth surface	substrate preparation	ASD approach	thickness at $S = 0.9$ (nm)	ref
metal on metal	W	Si/SiO_2	inherent	ALD	8	243
	Pt	Pt/SiO_2	ASD-activated	ALD	9	235
metal on dielectric	TiN	Si_3N_4/(a-C+H_2 plasma)	ASD-passivated	ALD	9.5	95
dielectric on metal	Ta_2O_5	TiN/SiO_2	inherent	supercycles: ALD + plasma etch	~7	142
	ZnO	Cu/(Cu+photocross-linked SAM)	ASD-passivated	ALD	>100	140
dielectric on dielectric	Al_2O_3	SiO_2/(Cu+ODPA SAM)	ASD-passivated	ALD	5.5	165
	Al_2O_3	SiO_2/(Cu+ODPA SAM)	ASD-passivated	ALD + postprocessing	>10	165
	Al_2O_3	SiO_2/(W+ODPA SAM)	ASD-passivated	ALD	8	136
	ZnO	SiO_2/(Cu+DDT SAM)	ASD-passivated	supercycles: ALD + regeneration	>100	171
	ZnO	SiO_2/(W+ODPA SAM)	ASD-passivated	ALD	32	136
	TiO_2	SiO_2/Si-H	inherent	supercycles: ALD + ALE	15	96

passivating hydrogen from nonreactive Si-H surfaces creating open sites for reactant chemisorption.[49,86,96] Another mechanism depicted in Figure 3e also involves reactant−surface interactions.[57,97] In this case, an incoming precursor reacts on the growth surface yielding a byproduct that adsorbs on the nongrowth surface, becoming a stable site for subsequent growth. This process is believed to occur, for example, during area-selective CVD and ALD of tungsten metal from WF_6 on silicon vs SiO_2.[57,97] When WF_6 impinges on the growing W surface, it can transfer F to form volatile tungsten subfluorides that then transport and adsorb onto SiO_2, creating sites for continued growth. When the desired deposited surface is involved in creating active nucleating agents, the density of unwanted nuclei will be largest near the growth feature boundary and in regions where growth features are more densely packed. Such mechanisms are sometimes called "edge-" or "proximity effects". "Loading effects" appear when the density of unwanted nuclei depends on the density or ratio of growth vs nongrowth surface presented on the starting substrate. These are discussed in Section III.A. When ASD processes use combined deposition and etching, the etchant species can also create sites for nucleation, even when etching does not occur (Figure 3f). For example, chlorinated reagents will react readily on clean copper to form copper chloride which can be more favorable for growth compared to the starting copper surface.

Desirable ALD reactions are selected to be highly favorable energetically. Therefore, during ALD of a homogeneous material (i.e., without strong effects due to crystal faceting), nuclei or nonplanar surfaces are expected to grow uniformly in all directions, including lateral growth extending over the nongrowth region. As growth proceeds, the resulting shape of the nuclei will be governed by the surface energies of the nucleating substrate and the depositing material, as well as the interfacial energy in the area where the deposited film covers the substrate. A depositing film that does not form strong bonds to the substrate leads to high interfacial free energy, favoring growth of spherical-shaped nuclei. A good example is Pd or Pt ALD on a metal oxide, where spherical metal nuclei can be observed by electron microscopy.[83] Strong interfacial bonding promotes uniform layered growth, as expected during metal oxide ALD on a receptive reactive surface.

II.C. Quantifying Selectivity in Film Deposition. A basic quantified definition of selectivity in thin film deposition, S, can be obtained from surface reaction thermodynamics, where the driving force for any selective deposition is the ratio of the Gibbs free energy change for species reacting on the desired growth surface to that on the nongrowth surface.[3,6,8,9] Unfortunately, the reactions that lead to unwanted nucleation, such as reactant chemisorption on an impurity site, are often not known, making thermodynamic predictions difficult.[7,8] Since more favorable energetics often (but not always) leads to faster reaction kinetics, an alternate definition of selectivity can be made from the relative rate of nucleation on the growth vs nongrowth surface.[6,18] Nucleation rates are difficult to measure directly. Because faster nucleation leads to more rapid surface coverage, a reasonable estimate of the nucleation rate comes from measurements of net surface coverage on the desired growth and nongrowth surfaces, θ_1 and θ_2, respectively, or from the net amount of material deposited, t_1 and t_2. Any selective process seeks to maximize thickness in the desired growth region while minimizing nuclei and film growth in the nongrowth region. The selectivity, S, formally defined by nucleation rate can be estimated as

$$S(n) = \frac{\theta_1 - \theta_2}{\theta_1 + \theta_2} \approx \frac{t_1 - t_2}{t_1 + t_2} \quad (1)$$

The equation indicates that the value of S will depend on n, the number of ALD cycles (or time during a CVD process). Note that the relation between surface coverage and amount of material deposited depends on the nuclei shape and extent of coalescence,[18] which can be modeled under limiting assumptions as discussed below. Surface coverage gives a better estimate of the nucleation rate because different nuclei with the same surface coverages can contain different amounts of material depending on the nuclei shape. It is usually easier to measure film thickness than surface coverage, but as shown below, the value for S determined using t_1 and t_2 will be systematically larger (i.e., better) than the value obtained using θ_1 and θ_2.

In eq 1, the value for S ranges from 1 to 0, where $S = 1$ (i.e., $\theta_1 = 1$ and $\theta_2 = 0$) corresponds to "perfect" selectivity and $S = 0$ indicates full selectivity loss, i.e., $\theta_1 = \theta_2$. For good ASD, the goal is to maintain a large value for S as the film thickness in the desired growth region, t_1, increases. To evaluate the selectivity of any ASD process, the surface coverage or thickness values, θ_1, θ_2, t_1, and t_2, can be measured or inferred by scanning electron microscopy, ellipsometry, surface profilometry, Rutherford backscattering, electron spectroscopy (e.g., Auger spectroscopy or X-ray photoelectron spectroscopy), and other tools. After a long deposition time, we expect $\theta_1 = \theta_2$ (i.e., $S = 0$), but $t_1 > t_2$ (i.e., $S > 0$). The systematic error for S is smallest, however, for small values of θ_2 and t_2, i.e., when S is relatively large.

https://dx.doi.org/10.1021/acs.chemmater.0c00722
Chem. Mater. XXXX, XXX, XXX−XXX

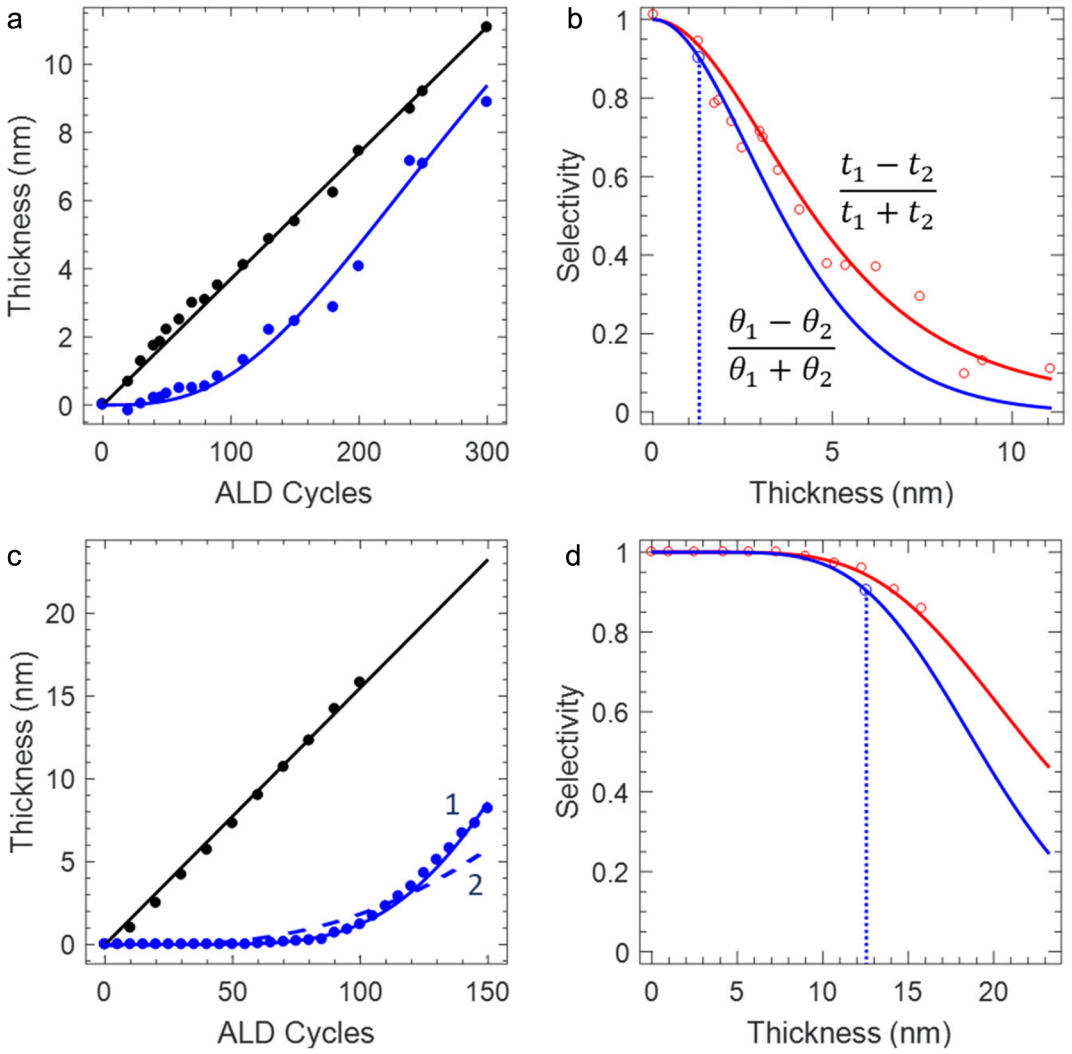

Figure 4. Example experimental thickness vs cycle for two different ASD processes: (a, b) TiO_2 ALD on SiO_2 vs Si-H (data from Song et al., ref 96) and (c, d) electron-activated ZnO ASD on SiO_2 vs a-Si-H (from Mameli et al., ref 101). Panels a and c show data and model fits for thickness versus cycle on the growth and nongrowth surface for each process, and panels b and d show values of S plotted vs thickness on the desired growth surface. The plots of S include data points obtained from the thickness data $[S = (t_1 - t_2)/(t_1 + t_2)]$ and the lines for S calculated from the thickness data fits (solid lines in panels a and c). The model fits to the thickness data also give the expected surface coverage θ_1 and θ_2 vs cycle to determine values for $S = (\theta_1 - \theta_2)/(\theta_1 + \theta_2)$ vs thickness on the growth surface. Highlighted on the plots are the values for $t_{S=0.9}$, i.e., the thickness on the growth surface when $S = 0.9$. Note that the values of S from t_1 and t_2 are systematically larger than those obtained using the surface coverage θ_1 and θ_2. The model parameters associated with the fits, including an alternate fit shown as a dashed line in panel c, are given in the text.

Equation 1 provides a method to estimate S for any ASD process. For data comparison, a useful figure-of-merit is $t_{S=0.9}$, the film thickness in the desired growth region when the selectivity $S = 0.9$. For manufacturing applications, S values exceeding 0.999 may be needed, but $t_{S=0.9}$ is currently a reasonable value for comparison because many published ASD processes show selectivity in this range, as indicated in Table 1. An alternate figure of merit is the selectivity of a process at a target thickness value. If the target thickness is 10 nm, then $S_{t=10nm}$ may be useful to compare different processes.

Comparing different ASD methods requires results that include both process capabilities and overall process limits. To best understand the potential impact and performance of an ASD approach, it is helpful to have data reporting the transition to selectivity loss ($\theta_2 > 0$) as well as the amount of material deposited in the desired growth region when selectivity loss occurs. An example comparison of two different ASD data sets, including selectivity loss and desired growth thickness values, is shown in Figure 4.

II.D. Analytical Model for Nucleation, Growth Evolution, and Selectivity Quantification. Further insight into the mechanisms for selectivity and selectivity loss can come by comparing data for surface coverage, thickness, or number of nuclei vs ALD cycle (or time for a CVD process) to quantitative models for nucleation and film growth. Collecting and analyzing experimental data for ASD is a significant challenge, particularly over large wafer areas.[18,98] During any deposition process (without specific etch steps present) the net surface coverage in the nongrowth region at any time will be determined by (1) the number of nucleation sites initially present on the nongrowth surface; (2) the rate of nucleation site generation during deposition; and (3) the rate of film growth and surface coverage extending from any stable nucleus. A number of empirical models have described trends observed when growth proceeds under limited nucleation conditions.[18,85,99,100] A recent model

https://dx.doi.org/10.1021/acs.chemmater.0c00722
Chem. Mater. XXXX, XXX, XXX−XXX

describes growth initiation during ALD or CVD on non-receptive surfaces, combining a model for uniform ALD or CVD film growth with the Avrami formalism for nuclei expansion and coalescence. The uniform growth model presumes that on any stable isolated nucleation site, growth proceeds uniformly in all directions creating isolated hemispherical nuclei that expand and eventually coalesce. The Avrami equation then correlates the film growth with the extent of nuclei coalescence as a function of n, the number of ALD cycles (or CVD time). Parameters in the model are the number of nucleation sites present on the starting surface, $\hat{N}$ [nm^{-2}], the generation rate of nucleation sites per cycle (or time), $\dot{N}$ [nm^{-2} n^{-1}], and the steady growth rate on the desired surface and on available nuclei, $\dot{G}$ [nm $\cdot n^{-1}$]. Note the distinction between a nucleus and a nucleation site. A nucleation site is identified as a dimensionless point on a surface that enables formation of a physical nucleus. The model also considers that nuclei generation may proceed after some incubation or delay time, ν_d, so that $\dot{N} = \dot{N}(n)$. In the Avrami approach, the parameters are first used to calculate the extended covered surface area on the nongrowth surface, $A_{2,ext}$, which is the area that the nuclei would cover if nuclei did not touch:

$$A_{2,ext}(n) = A_{2,0}\pi\left[(\dot{G}^2 n^2)\cdot\hat{N} + \int_0^n \dot{G}^2(n-\nu)^2\cdot\dot{N}\,\mathrm{d}\nu\right] \tag{2}$$

where $A_{2,0}$ is the area of the starting nongrowth surface. When nucleation sites are generated during the deposition period, n (i.e., $\dot{N} > 0$) the integral gives the surface area covered by nuclei on those generated sites. Integrating eq 2 and putting $A_{2,ext}(n)$ into the Avrami expression then gives the expected coverage fraction on the nongrowth surface as a function of $\dot{G}$, $\hat{N}$, $\dot{N}$, and n:

$$\theta_2(n) = \frac{A_{2,film}(n)}{A_{2,0}} = 1 - \exp\left(-\pi\dot{G}^2 n^2\left(\hat{N} + \frac{n}{3}\dot{N}\right)\right) \tag{3}$$

This eq 3 corresponds to eq 8 in the article describing the model.[18] The surface coverage values can also be used to determine $t_2(n)$, the average film thickness on the nongrowth surface as a function of ALD cycles or time, which is solved as the total deposited film volume per unit substrate area:

$$t_2(n, \dot{G}, \hat{N}, \dot{N}) = \int_0^{\dot{G}n} 1 - \exp(-\theta_{2,ext}(h))\,\mathrm{d}h \tag{4}$$

The integrand in eq 4 uses the Avrami formalism to convert the extended surface coverage fraction $\theta_{2,ext} = A_{2,ext}/A_{2,0}$ determined at each n from eq 2, to the physical fractional surface area $A_2/A_{2,0}$ subtended by a plane at arbitrary height h parallel to the surface passing through the set of deposited nuclei. By integrating the values of $A_2/A_{2,0}$ with unit thickness dh for each value of h between $h = 0$ and the maximum film thickness, $h = \dot{G}\cdot n$, eq 4 gives the total nucleus volume per unit substrate area. This eq 4 is a combination of eqs 12−15 in the model article.[18]

Results using eq 4 to fit published experimental ASD data[96,101] are shown in Figure 4. For TiO_2 ALD on Si-H, the model gives a good fit using $\dot{G}$ = 0.037 nm cycle^{-1}, $\hat{N}$ = 0.01 nm^{-2}, and $\dot{N}$ = 0.0 nm^{-2} cycle^{-1}, so that $t_{S=0.9}$ = 1.2 nm. For low temperature electron activated ZnO deposition, the model fit (line 1 in Figure 4c) corresponds to $\dot{G}$ = 0.155 nm cycle^{-1} with $\hat{N}$ = 0.0 nm^{-2}, $\dot{N}$ = 4.2 × 10^{-4} nm^{-2} cycle^{-1}, and ν_d = 150 cycles. The value $t_{S=0.9}$ = 12.6 nm shows the ZnO process has better selectivity than the TiO_2 ALD. Line 2 in Figure 4c shows an alternate fit with $\dot{G}$ = 0.155 nm cycle^{-1}, $\hat{N}$ = 2.5 × 10^{-4} nm^{-2}, and $\dot{N} = 0$. This fit with $\dot{N} = 0$ is not as good as line 1 obtained with $\dot{N} > 0$. On the other hand, the TiO_2 data shows a good fit with $\dot{N} = 0$. Extracting thickness values from ellipsometry for very thin films can be difficult, so this must be considered when fitting ellipsometry data to the model.[18] Also, the model assumes that isolated nuclei are hemispherical until they agglomerate, so the fits may be affected by differences in nuclei shape. The differences in the fits may also be due to real differences in the processes. A better fit with $\dot{N} > 0$ during beam-enhanced ZnO deposition suggests that nucleation on the nongrowth surface occurs at nucleation sites generated during the process, whereas during TiO_2 ALD, a good fit with $\dot{N} = 0$ points to nuclei that predominantly form at nucleation sites present on the starting growth surface.

Since the fit to the thickness data uses the number of nucleation sites $\dot{N}$ and $\hat{N}$ as an input parameter, the model fit can also give the expected number of nuclei present on the nongrowth surface as a function of cycle or time, n:

$$N_2(n) = \hat{N} + \int_0^n \dot{N}\,\mathrm{d}n \tag{5}$$

The number of nuclei on a surface can be measured independently of thickness. Therefore, two separate data sets for $N_2(n)$ and $t_2(n)$ can be fit with a common set of input parameters to gauge the quality of the fit and the accuracy of the information that the model provides.

Some example fits to literature data, including simultaneous fits to $N_2(n)$ and $t_2(n)$, are shown in ref 18. In addition, example literature data sets were fit to the model and some representative results are given in Table 1. The amounts and types of data were different for each data set, so the quality of the fit was not uniform. The results in Table 1 are presented to demonstrate that the model and selectivity parameter, $S(n)$, can be used to quantitatively compare different ASD processes for different materials from different laboratories, analyzed using different analytical techniques.

III. SYSTEMS-LEVEL ISSUES IN ASD: FEATURE DEPENDENCE, REACTORS, AND ALD VS CVD

Successful ASD chemistry is realized by a well-defined deposition sequence that proceeds readily on one surface and not on another. However, transfer from the lab into manufacturing requires more than successful demonstration of ASD reactions. Manufacturing requires a more systems-level view to understand how the ASD process is affected by the substrate pattern and features being deposited and how the reactor design and reaction mode (i.e., ALD vs CVD) influence the product output.

III.A. Surface Loading and Feature Dependence, Including Shape, Edge, and Proximity Effects in ASD.

During area-selective deposition, the amount and resulting shape of the selectively deposited film can be influenced by the density and size of the features presented on the starting patterned substrate. Near a feature edge, species adsorption and reaction will be influenced by the local abrupt changes in surface energy. Therefore, the lateral profile of a film growing on one surface will be determined by complexities of the interfacial energies in the adjacent surface.

Two primary pattern-dependent mechanisms in ASD are "loading" effects, where the net amount of deposition depends on the relative fraction of growth vs nongrowth surface on the

https://dx.doi.org/10.1021/acs.chemmater.0c00722
Chem. Mater. XXXX, XXX, XXX−XXX

substrate, and "feature" effects, when the extent of selectivity is influenced by the patterned feature shape or size. Loading effects are known and analyzed during plasma etching, where it was noticed that the rate of etching decreased when the etch reactor was loaded with more material to be etched. At low loading, the etch rate is determined by the surface etch reaction rate, whereas at high loading, the etch rate becomes limited by the generation rate of etch reactants.[102] This also leads to "micro-loading" when the amount of material to be etched is not uniform within the reactor or across a wafer surface.[103] Etch experiments also show aspect ratio dependent etching, with small features etching more slowly than larger ones (known as "RIE lag") and etch rate also dependent on the feature profile.[103] Feature-dependent etch rates are ascribed to reactant transport effects producing gas phase concentration gradients, surface charging, and byproduct adsorption that alter the local etch rate.[103]

Surface loading and feature-dependent processes have been observed and analyzed during area-selective tungsten CVD[104] and selective silicon epitaxy.[88,105,106] The chemical genesis of loading and feature-dependence in ASD is analogous to that observed in etching. That is, as the composition of the exposed surface changes (i.e., as the desired growth area becomes covered with the deposited material), reactive species concentrations (and supersaturation ratios) in the gas phase and adsorbed on the surface also change in response. For example, for a case where deposition precursors do not chemisorb on the nongrowth surface, the gas-phase reactant concentration in the volume over the nongrowth region will be larger than over the growth region. Resulting concentration gradients affect the rates of lateral surface and gas-phase species diffusion which will influence the local reactant supersaturation and therefore the observed local deposition rate. These effects can be avoided or minimized by using smaller and more uniform features or working at lower pressures. Moreover, local concentration gradients will be more pronounced in continuous CVD as compared to ALD where reactant delivery is separated in time or space. Steady-state gradients can develop during area-selective CVD, whereas during ALD, feature dependent reactant gradients will be transient. In both CVD- and ALD-based ASD, gradients and related microloading effects can result from spatially dependent consumption of deposition precursors and from localized generation of surface reaction byproducts.

In addition to surface loading, several other related feature dependent processes are known to occur during ASD. Feature-dependent "edge" or "corner" effects can appear when surface passivation is less effective at sharp features and feature transitions. Lateral overgrowth or "mushrooming" appears where selective growth extends over the nongrowth region. "Edge" effects can also include the mechanism that causes increased or decreased selective growth rates at feature boundaries. One example is "faceting" during selective epitaxy,[107] leading to a thinner deposited film at the junction edge. Another important feature-dependence in ASD, sometimes denoted as "proximity effects" or "local selectivity", refers to nonrandom generation of undesired nuclei, which may be analogous to microloading. Proximity effects arise when undesired nuclei appear preferentially in regions close to, or away from, the desired growth region. Results can usually be ascribed to local transport of depositing or surface passivating species to locally enhance or deplete reactant concentrations. If one of the deposited or exposed materials in ASD is catalytically active, it could also lead to excess or diminished growth at the feature edge. The mechanisms leading to ASD pattern dependence will of course depend on the ASD materials and substrates but will also be influenced by the specific reactants and process conditions used in the ASD process. Understanding and controlling loading and feature-dependent phenomena presents a critical challenge for ASD in manufacturing.

III.B. Reaction Mode: Area-Selective Deposition Using ALD vs CVD. ALD offers several known advantages compared to CVD for low temperature thin film deposition, and these advantages can also extend into ASD.[79] Separated reactant delivery and self-limiting surface reactions during ALD enables simpler reactor design and avoids detrimental effects of nonuniform reactant delivery to the depositing surface. Another advantage of ALD is that self-limiting reactions allow large reactant exposures, making ASD attractive for batch processing and for conformal coverage in high aspect ratio nanostructures. Separated reactant dose and purge steps makes ALD overall slower than CVD, but this problem is offset by the improved control and uniformity in ALD. As mentioned above in Section II.B, separating the reactants inherently avoids an important route for unwanted nuclei generation that occurs in CVD. Other advantages may help favor CVD for area-selective deposition. For example, since CVD processes often proceed at higher temperatures, CVD films can have better purity and higher density than those formed by ALD.

Control and uniformity achieved using self-limiting surface reactions makes ALD a critical enabling tool in advanced electronics manufacturing. For optimal ALD, reactants are often selected so that each half reaction has a Gibbs free energy change, $-\Delta G$, that is as negative as possible, to energetically *promote* deposition. However, ASD must *avoid* deposition in the nongrowth surface. Therefore, common ALD processes developed for good blanket deposition will likely not be optimal for ASD. For example, the highly exothermic reaction between trimethylaluminum (TMA) and water makes an excellent ALD process, but ASD of Al_2O_3 using TMA/water is notoriously difficult. Another issue in ALD is that the reactant exposure during each half-cycle is tuned for reaction saturation in the growth region. Simultaneously, the nongrowth region also receives a large reactant exposure, increasing the probability of generating unwanted nuclei. The overall shorter reaction times for CVD may therefore be advantageous for ASD. If the ALD process includes nonideal CVD or other slow- or soft-saturation effects, these effects may lead to unexpected outcomes due to the different surface reaction rates at different locations during ASD.

III.C. Reactor Design. Typical ALD and CVD reactors for "blanket" deposition are carefully designed to optimize favorable deposition reactions. On the other hand, ASD also requires control of desired deposition, but it must concurrently optimize (i.e., limit) reactions that lead to unwanted nucleation. Simultaneous optimization of multiple reactions will naturally add complexity to reactor design and optimization. Indeed, the optimum reactor design will depend on the material being deposited and the specific approach being used for ASD, as well as the scale of the deposited pattern features. Design of any thin film deposition reactor must consider reactant and thermal transport, as well as thermodynamics and chemical rate kinetics in surface reaction and diffusion. For any general ASD process, simple design issues can include choice of reactor volume and substrate heating. For ASD, the reactor thermal configuration, i.e., isothermal (hot wall) or nonisothermal (warm or cold wall), can have significant impact. In this regard, for example, it is important to consider if the reactor wall is designed to promote or inhibit nucleation (i.e., is the reactor wall designed to be a

https://dx.doi.org/10.1021/acs.chemmater.0c00722
Chem. Mater. XXXX, XXX, XXX−XXX

"growth" or "nongrowth" surface?), and how the reactant/wall interactions will influence species composition and flux. Types of commercial ALD reactors include single-wafer, batch, and spatial designs. Batch reactors usually have a large volume to coat many wafers simultaneously. The large reactor volume leads to long gas residence times and extended reactant exposure times, making it difficult to inhibit unwanted nucleation. Reactant partial pressure affects the reactant flux and equilibrium surface concentration, so pressure must be considered in any reactor configuration.

IV. MOTIVATION AND APPLICATIONS FOR AREA-SELECTIVE DEPOSITION

IV.A. Current Uses of ASD in Microelectronics.

IV.A.1. Selective Epitaxial Growth. Selective epitaxial growth (SEG) is perhaps the most widely used and studied example of ASD in industrial semiconductor manufacturing. Si SEG was first introduced in 1962 by Joyce and Baldrey as a high temperature CVD semiconductor on semiconductor growth process employing $SiCl_4$ and H_2 as coreactants and oxide masks as the nongrowth area.[1] This process was extended to lower temperatures by employing silane in place of silicon tetrachloride and to selective epitaxial growth of Ge and GaAs over the next decade.[4,10,11] The growth mechanisms and thermodynamic driving factors associated with SEG have been extensively studied and can provide important object lessons for researchers currently developing new ASD processes.[108,109] For instance, the importance of surface-chemistry-driven reaction mechanisms was recognized early in the development of SEG. In addition, the advantages of incorporating an etching component into the deposition process were also demonstrated in early SEG research.[109] More recently the advantages of cyclical deposition and etch processes for SEG have been demonstrated.[110]

In its current form, SEG is an essential process in the formation of leading-edge metal oxide semiconducting field effect transistors (MOSFETs).[111] SEG is utilized in forming the source and drain of both N-type and P-type MOSFETs within the complementary MOS process flows used for advanced logic devices and SRAM memory. SiC and SiGe provide mobility-enhancing tensile and compressive strain for NMOSFETs and PMOSFETs, respectively, which boosts the drive current of the resulting devices. In addition, N-type and P-type dopants are incorporated in situ during the SEG in order to reach dopant levels that can exceed the solid solubility limit of the respective dopants after postgrowth implants are complete and, thus, drive down the source/drain parasitic resistance after contact formation. Figure 5 shows an example image of SEG of SiGe on a silicon fin.[112] In practice, selective SiC (NMOS) and selective SiGe (PMOS) are deposited on Si in the presence of nongrowth areas comprised of Si oxide and nitride, thereby representing an example of semiconductor on semiconductor ASD. Epitaxial and single crystalline SEG structures have preferred growth directions that result in faceted shapes. This gives rise to the diamond-shaped SiGe growth shown in Figure 5.

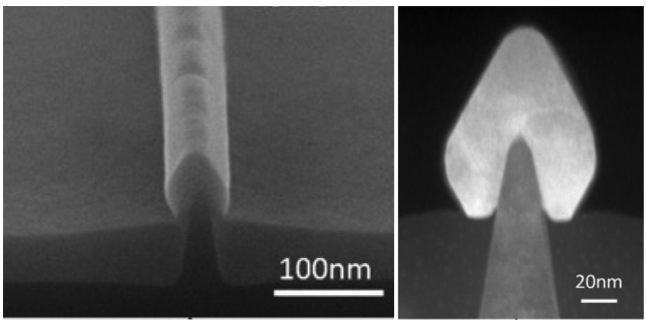

Figure 5. Selective epitaxy of SiGe on a silicon fin. Adapted with permission from G. Wang et al., ref 112. Copyright 2016 Elsevier.

IV.A.2. Selective Co Capping of Copper. Selective cobalt growth via CVD for Cu capping applications is a recent addition to the semiconductor process toolbox.[113,114] As line widths continue to shrink, densities within the narrow vias contacting the bottom-most interconnect levels have reached the point that they provide enough resistive heat and electromotive force to create significant migration of Cu atoms. This eventually results in voiding within the via and ultimately failure of the circuit due to loss of electrical connectivity. To combat this phenomenon, device makers have begun cladding the exterior of the Cu lines with metals that are less prone to electromigration in order to meet the reliability needs for recent devices. State of the art devices currently in manufacturing employ Co for this purpose. Depositing a thin Co layer on top of the Cu metal lines, which is the narrowest point of connection for the vias running between metal layers, provides a significant reliability enhancement. To accomplish this task, devices makers employ a selective CVD Co taking advantage of the inherent selectivity that many metal on metal deposition processes exhibit, as well as the hydrophobic nature of the low k dielectrics surrounding the Cu metal lines.

Semiconductor manufacturing technology tends to advance in evolutionary steps, and the use of selective Co caps represents just such a step for the industry. As line widths continue to narrow, Co capping is likely to reach a reliability limit, and could be replaced by capping with another metal such as Ru that has even higher electromigration resistance. Metal on metal selective CVD and ALD Ru processes are well-known and have been demonstrated for this purpose.[115] In fact, at a certain point it becomes beneficial to replace the Cu lines entirely with less diffusive metals to reduce the relative thickness of the liner seed as well as the resistance due to surface and grain boundary scattering. Co and Ru are leading candidates for this migration. Intel has recently begun to employ Co lines for the tightest pitch interconnect layers in their latest processor generation.[116] Another potential path that future devices might employ is to replace the TaN diffusion barriers currently used for Cu with another, thinner material, that reduces the relative volume of the barrier within the lines while still providing enough resistance to Cu diffusion to maintain reliability of the circuits. Graphene has recently been proposed for this purpose,[34] and since selective graphene deposition can be accomplished via Cu-catalyzed CVD,[261] ASD of graphene is the leading process candidate for realizing this type of structure.

IV.B. Application Needs for ASD in Microelectronics.

SEG and Co capping layers represent prime examples of functional films deposited using ASD in semiconductor manufacturing. As the name implies, functional films serve a purpose related to the operation, function, or structure of the device. Functional materials are also called "leave-behind" films to distinguish them from "sacrificial" films which are formed to serve a temporary purpose during processing. An example "sacrificial" film is a selective hard etch mask, which is formed to transfer a pattern and then removed before the device is completed. For microelectromechanical systems (MEMS), functional films can frequently have a primarily physical

https://dx.doi.org/10.1021/acs.chemmater.0c00722
Chem. Mater. XXXX, XXX, XXX−XXX

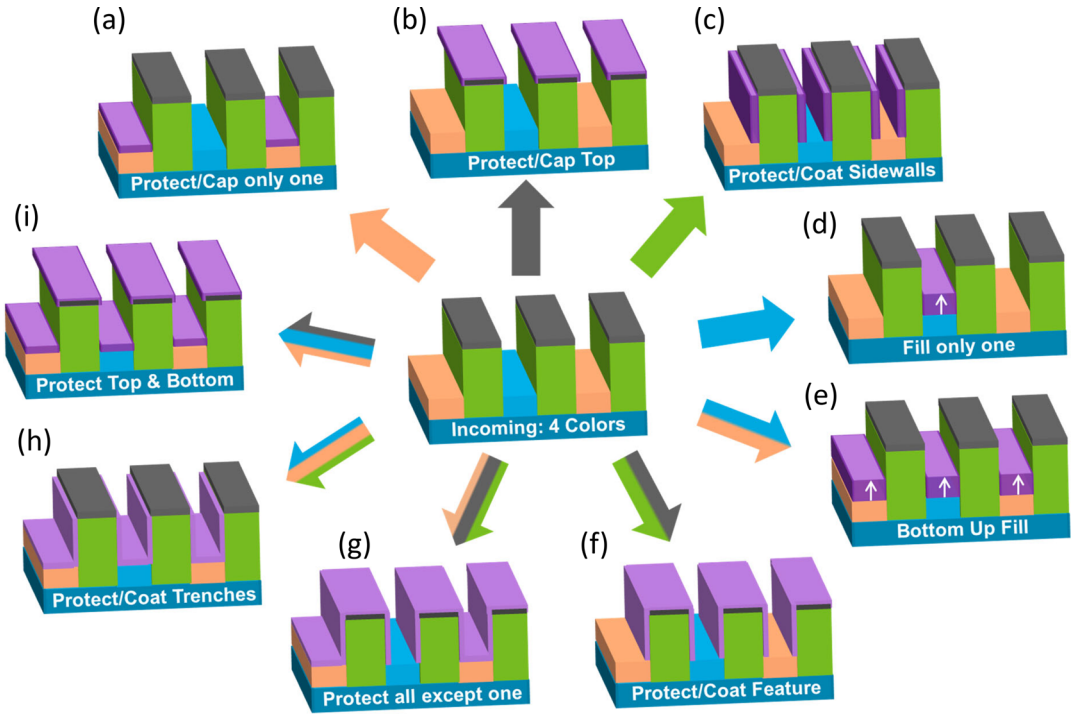

Figure 6. Schematic representation of the "selective deposition toolbox" illustrating the types of structures that ASD could provide given a generic incoming structure with four unspecified materials exposed. By selectively depositing on one or more materials (colors) a variety of structures can be realized. For example, images a–d show ASD on only one color, and images e and f show ASD on two out of four colors. Likewise, images g–i show ASD on three colors. Other color combinations can also be imagined.

purpose. For example, self-assembled monolayers (SAMs) can be employed as functional films in MEMS devices in order to reduce friction or stiction of a moving part.[117,118] In addition, the electrical circuits of a semiconductor device require a certain amount of physical support in order to survive the stresses inherent in the manufacturing and packaging processes. Hardness is a key concern for materials such as interlayer dielectrics, but generally the physical function of the films is a secondary attribute for electronic devices.

A variety of sacrificial films are used during nanomanufacturing processes, primarily for the purpose of patterning or forming the device structures. The distinction between functional and sacrificial films is important because sacrificial films, despite their growing and ubiquitous usage, are rarely maintained in the final product and, thus, can be essentially invisible in product teardowns. Of course the exact identity, nature, and use of sacrificial films employed by a particular device maker in manufacturing are closely guarded secrets. In the case of functional films there may be cases where a selective and a nonselective process results in an indistinguishable structure. Thus, we cannot necessarily say exactly if, when, or how many selective processes might be currently employed by a given manufacturer, even though some use of ASD can be confirmed or at least inferred by device teardowns.

In this section we seek to provide examples of ASD processes that are either currently needed or desired for device manufacturing now or in the near future. These are illustrative examples of known processes and process flows that may be useful for nanomanufacturing of semiconductor devices primarily, and while we are attempting to cover the full scope of potential ASD uses, developing a comprehensive list is impractical and potentially impossible.

IV.B.1. "Selective Deposition Toolbox". Figure 6 is a schematic representation of what we will refer to as the "selective deposition toolbox", designed to illustrate the types of structures that ASD could provide given a generic incoming structure with unspecified materials.[119] Of course for real processes the incoming material set should be known, and the incoming structure is unlikely to match the generic example we are using. But this toolbox should still be useful, along with a fundamental understanding of the nanomanufacturing process flow, for researchers seeking to understand the types of ASD processes that could be useful if they can be developed. Wherever possible we will seek to refer back to this toolbox in the examples below in order to provide clarity as to how these ASD processes might be employed for manufacturing.

For the discussion of ASD materials, it is useful to divide the processes according to the material types being employed. The material set used for semiconductor nanomanufacturing consists of three classes of materials: metals (i.e., conductors), insulators (including dielectrics and organics), and semiconductors. Since most selective deposition processes are selective for a class of materials it becomes useful to group ASD processes according to the class of material being deposited as well as the class of target growth surface material. To illustrate this point, Co capping of Cu metal lines is an example of metal on metal (MoM) ASD in that Co, a metal/conductor, is depositing on Cu, another metal/conductor. The Co is also depositing on Co as the film is formed as well as the conducting liner/seed layers exposed at the edges of the Cu lines. Using this nomenclature we can therefore group ASD processes according to the possible combinations of material classes: dielectric on dielectric (DoD), metal on metal (MoM), dielectric on metal (DoM), metal on dielectric (MoD), semiconductor on semiconductor (SoS), metal on semiconductor (MoS), dielectric on semiconductor (DoS), etc.

https://dx.doi.org/10.1021/acs.chemmater.0c00722
Chem. Mater. XXXX, XXX, XXX−XXX

The nongrowth surfaces are essentially everything else that is exposed during the growth processes. Of course this kind of generalization breaks down in certain circumstances, but given the current status of ASD it is quite useful for the purpose of this discussion and we expect it will remain useful in the future.

Referring to Figure 6, one could envision that if the orange lines represent copper filled interconnect lines, selectively capping those lines with another metal, as in Figure 6a, could provide electrical benefits or impart etch or corrosion resistance. Likewise, if orange and blue lines represent N and P type metal gates, and the other colors are dielectrics that can be selectively blocked, then one might envision a bottom-up filling, as in Figure 6e, of dielectric caps on recessed metal gate features using a DoM ASD process enabled by a selective SAM blocking layer. It should be apparent from Figure 6 that combinations of Figure 6a–d could be used to accomplish any of the other structures pictured in Figure 6e–i, but it is useful to illustrate how targeting different materials might create structures useful for 3D integration. In addition, the use of ASD to realize bottom-up gap filling, as illustrated in Figure 6d,e, provides potential manufacturability benefits as well. By filling structures in this way it is possible to avoid the formation of seams or voids which can trap foreign material and result in etch rate variations.

IV.B.2. Contact over Gate Structure. The use of selective deposition to cap recessed metal gates, mentioned above in reference to Figure 6 and shown directly in Figure 7, allows contact to be made to the gate metals within the active device structure. Making contact on top of the transistor, instead of at an adjacent pad, reduces the transistor footprint on the wafer, thereby providing a critical process margin in the integration of standard logic and SRAM cells. Traditionally, gate metal lines are extended outside of the active device area in order to ensure they can be contacted without shorting to the source or drain contact. By employing a self-aligned gate contact scheme,[120] it becomes possible to safely contact the gates and sources and drains of the transistors within the active area of the logic cell, which results in additional area scaling in terms of cell/transistor areal density. This type of scheme can be realized without the use of selective deposition; however, the use of selective gate and diffusion caps can provide a significant manufacturability advantage.[32] A selective process flow results in reduced CMP overburden, creating a smaller starting stack height and the lack of a seam or void from selective bottom-up processing can result in reduced defectivity as well, increasing the overall process margin and yield.

IV.B.3. Bottom-Up Filling. Eliminating seams and voids in semiconductor processing is becoming more critical as scaling continues. With the migration to three-dimensional device structures and architectures the aspect ratios of features inside semiconductor devices have begun to increase significantly. In addition the actual widths of the structures themselves continue to decrease and can be measured on atomic scales. Seams and voids present multiple problems. For dielectric capping layers a seam can result in a higher etch rate or chemical mechanical planarization (CMP) rate at the center of the feature. In addition seams and voids can trap foreign material during processing which gets released in later steps and forms particles, which impacts the yield of the finished devices. Selective DoM capping layers have previously been proposed to provide relief from the overburdens required for chemical mechanical planarization during CMOS replacement gate integration.[121] In this case DoM capping on recessed contact and gate metal layers is proposed to enable self-aligned gate contact integration with

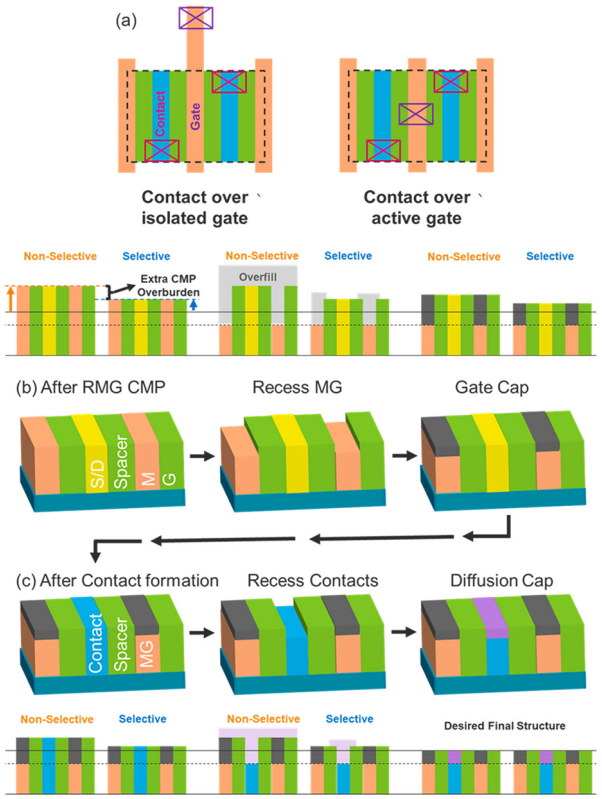

Figure 7. (a) Schematic representation comparing contact over active gate (COAG) versus contacting an isolated gate. The tighter spacing of the gate and diffusion contacts requires the use of (b) gate caps for self-aligned contacts and (c) diffusion caps during for self-aligned gate contacts during transistor fabrication. Cross sections illustrate how selective and nonselective process flows can be used for both structures; however, the selective process flow results in greatly reduced CMP overburden due to reduced overfilling. Adapted with permission from Clark et al., ref 32. Copyright 2018 AIP Publishing.

minimal CMP. A key advantage of this style of process is that when ASD is utilized the growth becomes bottom-up and the resulting structure is therefore free of seams and voids.

For metals, especially in vias, the production of voids and seams are important problems because they increase the resistance of the metal feature, which also increases electromigration, thus causing a reliability issue. For example, buried power rails and supervias, Figure 8, are proposed as scaling boosters for use in future nodes. Buried power rails allow designers to gain area by moving some of the metal lines that normally travel just above the transistors to regions beneath the transistors. In this way the power lines for the sources and drains, which are typically wider than the signal lines, can be routed below the devices providing relief from wire crowding at the densest metal layers. Supervias would span two metal layers, instead of the usual one metal layer, also in order to relieve wire crowding in advanced nodes. Both of these structures require high aspect ratio metal filling without seams or voids to be used in manufacturing. Thus, bottom-up metal filling by MoM ASD of appropriate materials becomes an enabling technology to realize these structures.

IV.B.4. Selective Hard Mask and Etch Stop Depositions. Current nanomanufacturing processes make extensive use of selective etching processes; however, the etching processes employed are rarely perfectly selective or completely damage free with respect to the other materials exposed on the substrate.

https://dx.doi.org/10.1021/acs.chemmater.0c00722
Chem. Mater. XXXX, XXX, XXX−XXX

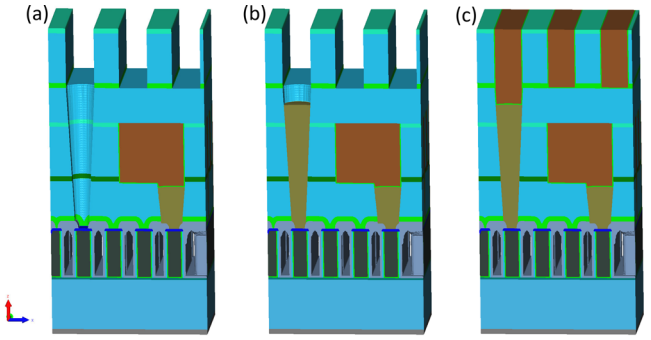

Figure 8. Supervia formation by bottom-up MoM ASD. (a) After forming trenches for the top metal layer, a supervia hole is etched to span down to a metal line two levels below. (b) MoM ASD is used for bottom-up filling of the supervia to avoid seams or voids. (c) After metallization.

In the case of anisotropic etching, a hard mask is frequently employed in order to define features in a single material or in order to protect a functional material from damage during the etching process. As feature sizes have scaled significantly below the resolution limits of state of the art lithography processes, it has become increasingly difficult to form and align hard masks that are robust enough to survive the etching processes to which they are exposed. Figure 9, which depicts a hypothetical selective process flow for forming air gap structures in Cu interconnect structures, can serve as an illustrative example for this discussion.

In this process flow MoM ASD is utilized to form a metal capping layer over pre-existing metal lines. The selective metal serves as a hard mask, and the well-known mushrooming effect

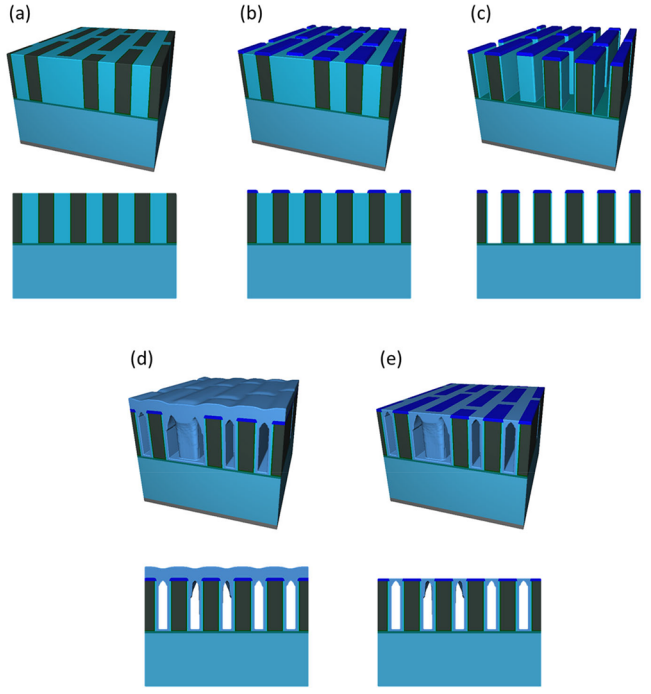

Figure 9. Illustration of the interconnect air gap process utilizing selective metal capping as a hard mask for etching. (a) Incoming metal line and space structure within an interlayer dielectric (ILD) and separated from the previous ILD layer by an SiN etch stop layer (ESL). (b) Selective MoM deposition to form a selective hard mask. (c) Straight ILD etching, stopping on the ESL. (d) Pinch-off PECVD oxide deposition. (e) Final structure after chemical mechanical planarization.

of selective deposition is used to overgrow the edges of the metal lines in order to leave behind a thin layer of interlayer dielectric (ILD) and protect any liner or barrier layers encapsulating the metal lines. After etching, the air gap structure is formed by a topographically selective PECVD process which is tuned to pinch off the gaps between the metal lines. In this case the advantage of the selective process is that a self-aligned hard mask can be deposited with a defined overgrowth in order to protect the sides of the metal lines from plasma and etching damage.

Another example of selective hard mask formation is the ASD-enhanced self-aligned block (SAB) process for metal line and space patterning, Figure 10, recently proposed by IMEC.[115] Traditional SAB relies on recessing a nonselective blocking layer during the first block formation (Figure 10c,d) to below the level of the sidewall spacers, but because of nonuniformity across the wafer, it is extremely difficult to realize this process in practice. If the blocking layer is overetched, then the block is lost, and in the case of under-etching, the block will interfere with the second block patterning. Instead, the ASD-enhanced SAB process flow uses a MoM ASD to form the first blocking layer by selective growing Ru on top of the TiN hard mask used for pattern transfer. Using this process flow it is not necessary to uniformly recess a blocking layer to a controlled height. After forming the second block and transferring the pattern into the TiN hard mask, the Ru first block is removed along with the other patterning layers, and the resulting line and space pattern can be transferred into the underlying ILD.

IV.B.5. Fully Self-Aligned Vias. The fully self-aligned via (FSAV) process flow has recently been proposed in order to provide an additional edge placement error (EPE) margin for via alignment from one level to another during interconnect formation.[122] The ASD enhanced FSAV process flow, Figure 11, provides significant advantages over the originally proposed process flow by avoiding the need for a difficult metal recess etch to form the topography needed for self-alignment at the bottom of the via.[115] In this process flow a selective DoD process is used to create a dielectric scaffold that prevents the vias from coming too close to the neighboring metal features, resulting in a greater process margin for EPE during via formation. A conformal etch stop layer is then deposited over the topography created by the DoD layer (Figure 11c). After ILD and metal trench formation, a traditional self-aligned via approach is used (Figure 11e–g) where via holes are patterned over top of the trench hard mask so that the vias are self-aligned to the trench sidewalls. The via etch process then lands on the conformal ESL below, and after ESL opening the via can be formed with self-alignment to the underlying metal layers. The via is now "fully self-aligned" because it is aligned both to the trenches above and to the metal lines below. In this case, Figure 11 shows via filling by a MoM ASD process. The MoM ASD realizes bottom-up filling and increases the contact area through any subsequent diffusion barrier or liner needed for trench metallization, just as with the supervia described above (Figure 8). It is also worth noting that the supervia integration described previously also benefits from the FSAV bottom topography. Self-aligned hard masks and process flows like the ones discussed above are expected to become more ubiquitous in future manufacturing processes due to the need for an additional EPE margin as well as reduced variability as devices reach atomic scale dimensions.

IV.C. ASD for Catalysis, Nanostructures, and Large-Area Devices. While most ASD research addressed problems in patterning and size scaling in silicon-based logic and memory manufacturing, exploration of ASD in other fields also shows

https://dx.doi.org/10.1021/acs.chemmater.0c00722
Chem. Mater. XXXX, XXX, XXX−XXX

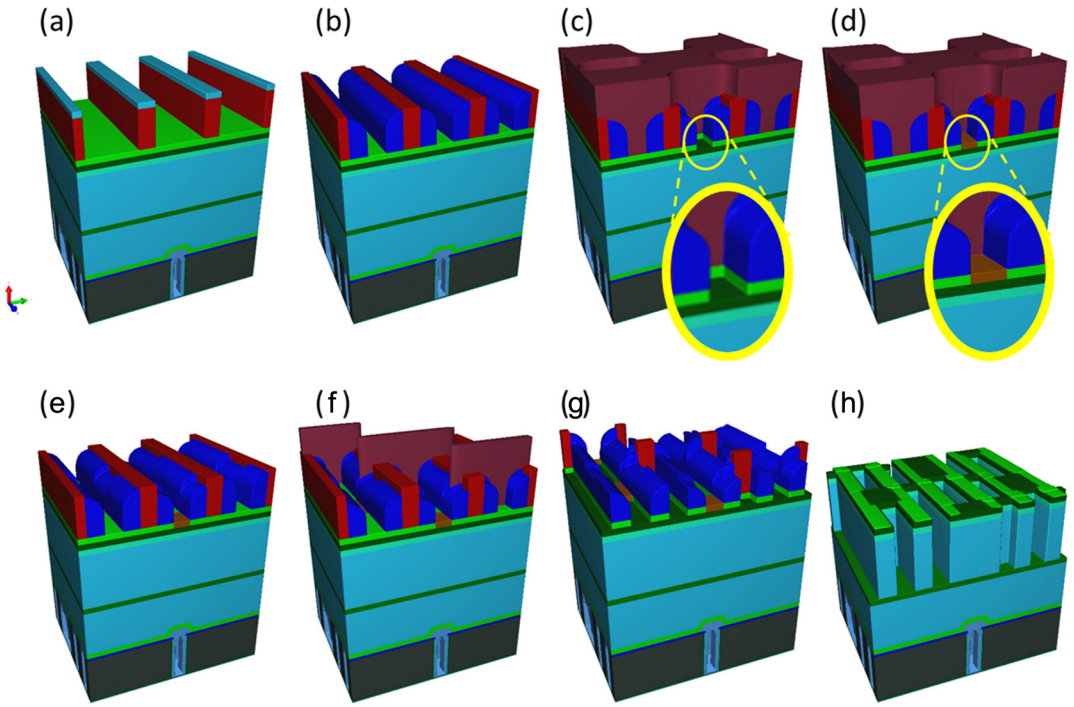

Figure 10. ASD enhanced self-aligned block for metal line space patterning. (a) Si mandrel formation over SiN and TiN hard masks. (b) Conformal oxide spacer and etch. (c) Spin on carbon (SOC) deposition, CMP, and first block patterning followed by SiN hard mask opening. (d) ASD MoM deposition on TiN. (e) SOC removal. (f) SOC deposition, CMP, and second block patterning. (g) Mandrel etch followed by SOC removal and SiN hard mask opening. (h) Transfer into TiN, removal of selective metal, and etch trenches with using the TiN hard mask.

promise for important advances. Moreover, in fields outside of nanoelectronics, the specifications and extent of selectivity may be less demanding to achieve a significant advantage. In catalysis, for example, ASD of very thin Al_2O_3 has been used where the oxide forms on exposed regions of Pd nanoparticles but not on regions where the particles are covered by remnant organic ligands. The ASD Al_2O_3 film then contains nanoscale pores that enable desired reactants to reach the active Pd catalyst sites while blocking reactants that lead to undesired coke formation.[25,123,124] Other uses for ASD in catalysis have also been explored[25,125,126] including formation of tailored core−shell catalysts[125] and stabilization of desired catalytic function by facet-selective coating of nanocatalyst particles.[126] Area-selective epitaxy of nanowires and related structures can be useful for optical, thermal, sensing, and solid state lighting.[70,127,128]

Large area active matrix displays and solar cells[129] can also take advantage of ASD, for example, to reduce process steps and improve the quality of electronic contacts and junctions. Low temperature area-selective plasma enhanced CVD of silicon has been demonstrated in thin film transistors to achieve advanced device designs and reduce mask count.[130,131] Advances in spatial atomic layer deposition[21,132,133] also hold promise for extension of ASD processes to low-cost large-area device manufacturing.

V. EXPERIMENTAL APPROACHES TO ASD

This section describes current experimental approaches and reaction schemes being explored for ASD. The two key steps in ASD are the preparation of a starting patterned substrate surface and exposure to deposition reactants.[5−7,9,16] The surface preparation and deposition reactions must complement each other, and identifying surface preparation steps that favorably pair with deposition is often the key challenge in ASD.

V.A. Inherent, Activation, and Passivation. Approaches to ASD are usually classified by the method of surface preparation, including inherent, activated and passivated. These are shown schematically in Figure 12, and examples are described in Section VI.

"Inherent" ASD describes a process where nucleation occurs at different rates on growth and nongrowth surfaces in their native clean state. The native clean state could include uniform hydrogen, hydroxyl, or other native terminal groups on covalent materials. Clean surfaces often result from previous steps used to create the substrate pattern.

ASD by "surface passivation" uses additional reagents that modify the clean surface and preferentially adsorb only onto part of the starting patterned surface. Passivating species change the exposed surface structure to aviod chemisorption and impede physisorption of depositing species. Passivation can be done using polymer films,[134,135] covalently bound self-assembled monolayers,[40,93,136] or small molecules that preferentially adsorb on one surface versus another.[13,92,137,138] Passivating layers can be patterned by selective adsorption and reaction from the liquid or vapor phase or by photoactive patterning.[139]

A common challenge with passivation layers is inhibiting the diffusion of deposition reactants into or beneath the passivating layer. Cross-linking within a patterned polymer can help solve this problem and substantially enhance inhibition.[140,141] Molecular inhibitors in particular have drawn attention as a means to promote film deposition uniformity[142] and allow bottom-up film growth[143] during CVD.[13] The extent of passivation depends on how well the molecule covers and stays bound to the surface during the process, which will depend on the molecular surface binding energy, vapor pressure, delivery dose, substrate temperature, deposition reactant interactions, and other factors. Generally, lower substrate

https://dx.doi.org/10.1021/acs.chemmater.0c00722
Chem. Mater. XXXX, XXX, XXX−XXX

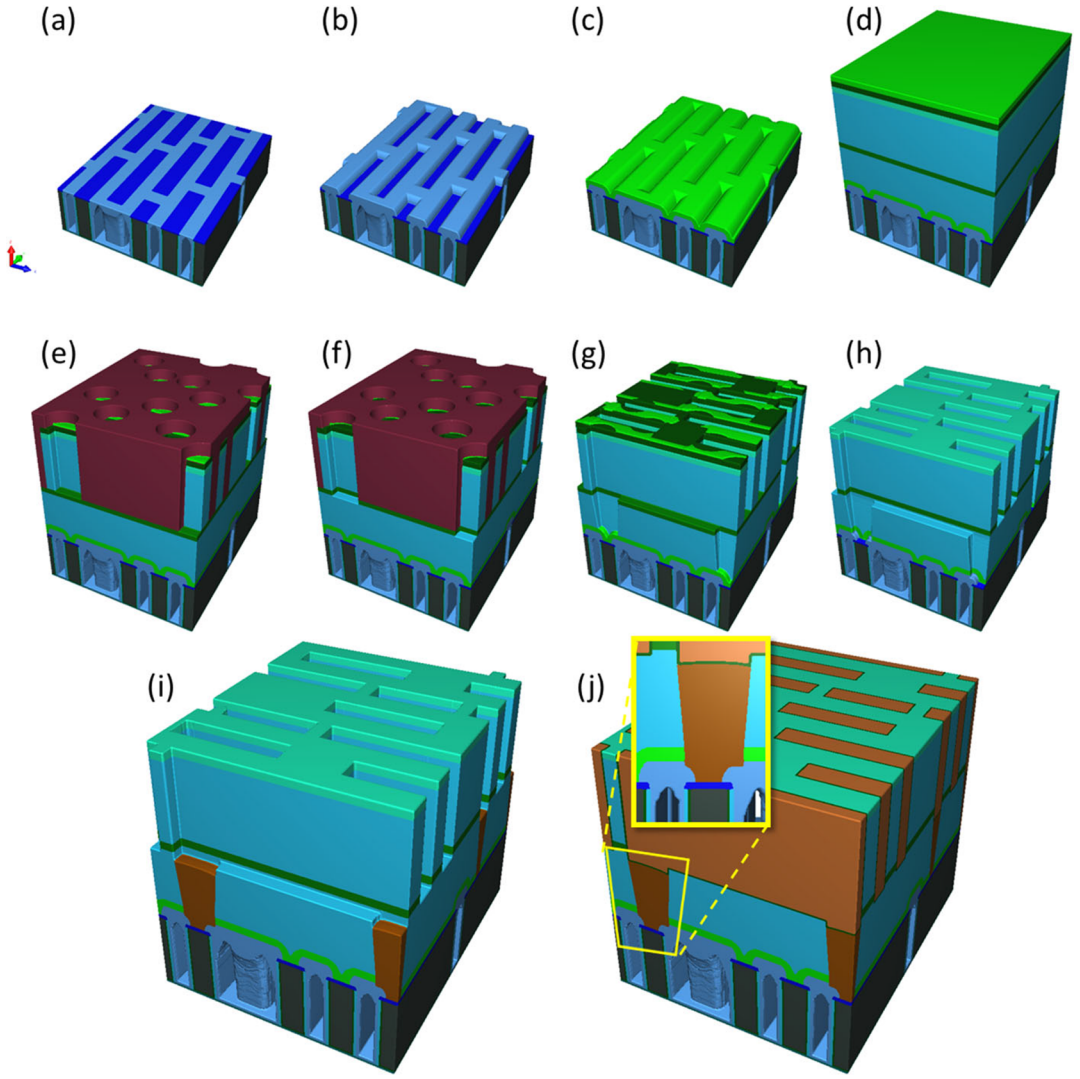

Figure 11. ASD enhanced fully self-aligned via (FSAV) formation. (a) Incoming metal line and space pattern. (b) DoD ASD to create FSAV bottom topography. (c) Conformal etch stop layer (ESL) formation. (d) ILD for via layer, followed by ESL for metal trenches, followed by ILD, capping, and hard mask layers for metal lines. Metal lines and spaces are then patterned e.g. by using an SAB patterning flow (Figure 10). (e) Via holes are patterned over the top of the line space hard mask and down to the metal trench ESL. (f) Open ESL for vias. (g) Removal of the patterning layer and etch via. (h) Open conformal ESL. (i) MoM ASD for via fill. (j) After metallization with the inset showing the detail of the FSAV landing on the metal line below.

temperatures can favor inhibitor binding, so lower temperature ALD may have advantages over higher temperature CVD. On the other hand, because ALD is relatively slow, making it more sensitive to inhibitor loss, molecular inhibitors may ultimately work better with faster CVD than with ALD.

"Surface-activation" can proceed by local energy delivery or using patterned catalytically active surfaces to locally promote growth.[101,144−147] When surface features partially shadow or block incoming irradiation, the deposition can produce "topographic selectivity" where growth regions are determined by surface geometric structure.[148,149] The distinctions within this terminology are not always clear. For example, for ASD of ruthenium on a patterned Ru/SiO_2 surface, the process may be considered "intrinsic" because it uses the original starting surface and requires no passivation steps, but it is also "activated" since the Ru substrate (and the desired film) are catalytically active for dissociation of the O_2 reactant.

V.B. Multistep and Supercycle Methods. Significant improvements on common ASD methods can also be achieved by integrating other processes within ALD or CVD, usually by periodically stopping the deposition. "Supercycle" or "multistep" methods refer to ALD processes with periodic passivation or etch steps coupled to the reactant exposure sequence. Supercycles can be used to regenerate or repair passivation layers,[150] readsorb passivating molecules,[92] or chemically etch unwanted nuclei that form on nongrowth surfaces.[96,151−153] Schemes for supercycle or multistep sequences used for ASD are shown in Figure 13. For the case of small molecule inhibitors, repeated delivery within each ALD cycle can more effectively retain the passivation effect as the process proceeds. Intermittent process modifications during CVD, such as periodic etching,[154,155] have also shown good results. These have been referred to as "alternating", "cyclic", or "pulsed" CVD.[154,155] Because the growth reactions are not self-limiting, these processes are distinct from ALD.

VI. ASD MATERIALS AND PROCESSES

Many materials and surface preparation methods have been explored for ASD. Tables 2−5 provides a partial summary of reports of substrate-dependent film nucleation and area-

https://dx.doi.org/10.1021/acs.chemmater.0c00722
Chem. Mater. XXXX, XXX, XXX−XXX

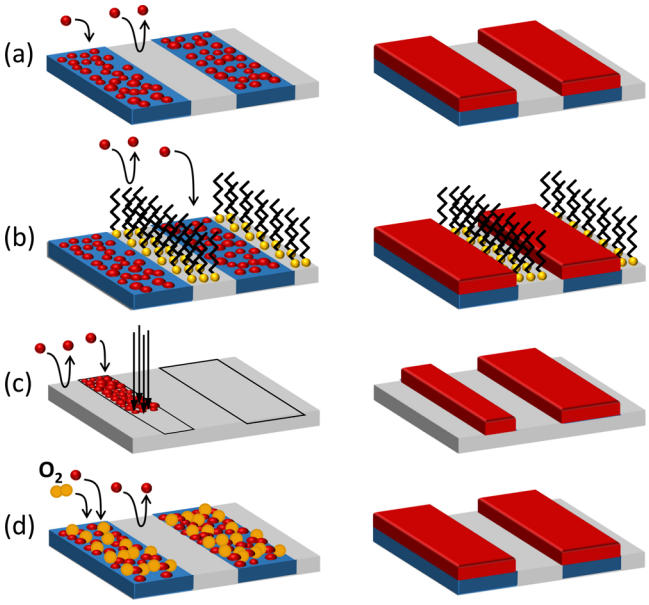

Figure 12. Common approaches for ASD during ALD and CVD: (a) intrinsic ASD; (b) ASD by surface passivation (using, for example, a patterned self-assembled monolayer, SAM); (c and d) surface activation by local energy delivery (panel c) or by local catalytic activation of a reactant (panel d).

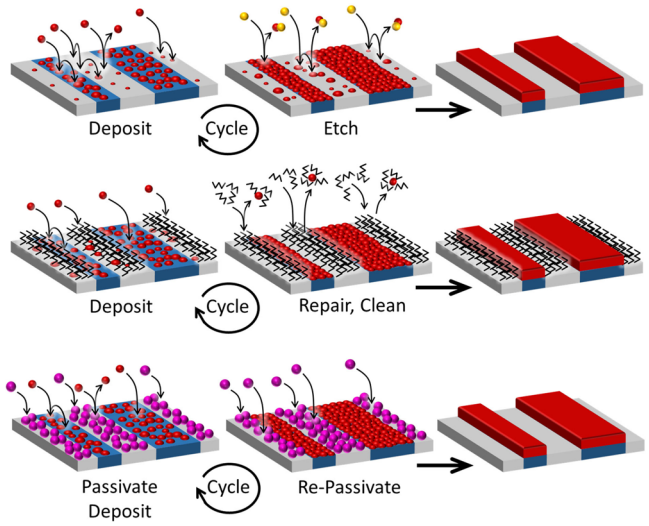

Figure 13. Examples of multistep or supercycle methods for ASD: (a) sequential deposition/etching; (b) surface passivation cleaning and repair; and (c) molecular inhibitor readsorption.

selective deposition. Entries include results from area-selective atomic layer deposition, as well as a few representative examples from selective CVD and epitaxial selective deposition literature. Most recent attention in area-selective ALD has focused on metals for electronics (Cu, Co, Ru, W, etc.) and for catalysis (Pt, Pd, Ir, etc.). Work on metal oxides has mostly focused on high-dielectric-constant materials (TiO_2, HfO_2, ZrO_2, Al_2O_3, etc.), suitable for electronic applications and hard-mask materials. Work has also explored lower-*k* materials and compounds.

Because ASD depends strongly on the precursor used for deposition, the sections below are organized by material deposited as well as precursor type. The types of precursors studied for ASD are broadly distributed, including halides, alkyls, amidinates, cyclopentadienyls, β-diketonates, propoxides, and several heteroleptic precursor systems. The inhibition approach to achieve area-selective ALD is probably the most widely studied, followed by inherent selectivity. The sections below first describe results for dielectric ASD, including dielectric on dielectric (DoD) and dielectric on metal (DoM), followed by metal ASD, including metal on metal (MoM) and metal on dielectric (MoD). Figure 14 shows some images of ASD adapted from the literature for DoD and DoM, and examples of MoM and MoD are in Figure 15. We then describe results of ASD of other materials, including semiconductors, organic and biological materials, and metal−organic frameworks.

VI.A. ASD of Dielectrics. For ASD of dielectrics, the receptive growth surface is usually another dielectric material (i.e., DoD) and the nongrowth surface is a nonoxidized metal, a semiconductor such as hydrogen-terminated silicon, Si-H, or a surface-passivating SAM, polymer, or molecule. The deposition and passivation reactions often depend strongly on the metal precursor ligand. Results to date for ASD of dielectrics on metal (DoM) mostly use patterned passivating layers, where growth occurs on exposed metal. Some examples of DoM ASD without organic passivation layers are also reported and are discussed below.

VI.A.1. DoD Using Alkyl Precursors: Al_2O_3 and ZnO. The metal alkyls trimethyl aluminum (TMA) and dielthyl zinc (DEZ) are widely used for ALD because they are easily delivered to ALD reactors and their reaction with water provides a strong thermodynamic driving force for oxide film formation. Their metal centers are not fully screened by the ligands, making them electrophilic Lewis acids (especially TMA) so they readily form adducts with nucleophilic, i.e., oxy or oxo, or other polar surface groups, leading to nucleophilic displacement, i.e., ligand exchange reaction at the growth surface. Because TMA adsorbs readily on many surfaces, area-selective ALD of Al_2O_3 from TMA and water is challenging. Studies of TMA adsorption and reaction on Si-H vs SiO_2 show only a small tendency for inhibition on Si-H.[86] TMA can react on Si-H to form passivating $Si-CH_3$ groups, but extended exposure overcomes this passivation allowing growth without significant nucleation delay.[156] Approaches for inherent selective patterning of Al_2O_3 or ZnO from alkyls are not common.[157] Using local photoactivation, patterned Al_2O_3 can be deposited using TMA/O_2.[146] ASD using TMA and water can be locally activated by selectively adsorbing reactive molecules, such as perylene-tetracarboxylic dianhydride (PTCDA) onto otherwise nonreactive graphene,[158] and this approach can also extend to other metal precursors.

Most of the work on area-selective ALD of Al_2O_3[129,136,159−165] and ZnO[93,133,136,140,150,159,160,166−172] from alkyl precursors uses inhibition layers. A common issue using TMA with SAMs is that TMA can adsorb within the SAM leading to selectivity loss. The extent of adsorption can be controlled to some extent, for example, by controlling the dose pressure.[162] For growth inhibition, DEZ is better than TMA because it is a weaker Lewis acid, and therefore it physisorbs less strongly. Moreover, the ethyl ligand on DEZ is bulkier than the small methyl-ligand on TMA, decreasing reactant diffusion. In one example showing the influence of precursor ligands on adsorption, ZnO was selectively deposited inside a metal−organic framework due to DEZ preferentially stabilizing within smaller pores, ascribed to more favorable dispersion force interactions.[173]

https://dx.doi.org/10.1021/acs.chemmater.0c00722
Chem. Mater. XXXX, XXX, XXX−XXX

Table 2. ASD Dielectric on Dielectric

material deposited	reactants		growth surface	nongrowth Surface	temperature (°C)	ref
Al_2O_3	TMA	H_2O	PTCDA SAM	graphene	100	158
	TMA	H_2O	PMMA-block	PS-block	85	65
	TMA	H_2O	SiO_2	Si-H	150	86
	TMA	H_2O	Au, SiO_2	Photoresist, PMMA	100−150	163
	TMA	H_2O	SiO_2	PMMA, PVP and C_4F_8 polymers	200	159
	TMA	H_2O	SiO_2	CF_x	200	160
	TMA	H_2O	SiO_2	PVP		161
	TMA	H_2O	SiO_2	polystyrene	150	303
	TMA	H_2O	SiO_2	ODTS, ODPA, DDPA, Si-H	150	162
	DMAI		SiO_2	PVP	100−300	168
	DMAI		SiO_2, ZnO, ZnO:Al	PVP	200	133
	$AlCl_3$	H_2O	SiO_2	PVP	250	161
	TMA	O_2	SiO_2 (light)	SiO_2 (dark)	60	146
ZnO	DEZ	H_2O	small MOF pore	larger MOF pore	125	173
	DEZ	H_2O	SiO_2	DTS	125	93
	DEZ	H_2O	SiO_2	CF_x	200	160
	DEZ	H_2O	SiO_2, ZnO, ZnO:Al	PVP	200	133
	DEZ	H_2O	SiO_2	PMMA, PVP, and C_4F_8 polymers	200	159
	DEZ	H_2O	SiO_2	ODT or DDT	120	171
	DEZ	H_2O	cicada wings		–	172
	DEZ	H_2O	SiO_2	DDT	90	166
	DEZ	H_2O	SiO_2	PFOS	120	167
	DEZ	H_2O	SiO_2	PVP	100−300	168
	DEZ	H_2O	SiO_2	ODPA	150	169
TiO_2	$(EtCp)Ti(NMe_2)_3$	H_2O or O_3	SiO_2	SiO_2	150−300	212
	$Ti(OCH_3)_4$	H_2O	Si_3N_4	a-C	250	95
	TDEAT	H_2O	SiO_2	copper	175	205
	TDMAT	H_2O	SiO_2	Cu_2O	200	206
	TDMAT	H_2O	SiO_2	PMMA, PVP, and C_4F_8 polymers	150	159, 208
	$TiCl_4$	H_2O	SiO_2	Si, Si-H		49
	$TiCl_4$	H_2O	SiO_2	Si-H	100−150	49
	$TiCl_4$	H_2O	SiO_2	Si-H	300	179
	$TiCl_4$	H_2O	SiO_2	Si-H	100	174
	$TiCl_4$	H_2O	SiO_2	Si-H	150	86
	$TiCl_4$	H_2O	SiO_2	PMMA	160	135, 176, 177
	$TiCl_4$	H_2O	PMMA-block	polystyrene-block	85−135	65
	$TiCl_4$	H_2O	SiO_2	trimethylsilane/SiO_2	100	178
	$Ti^i(PrO)_4$	H_2O	photoexposed PtBMA	PtBMA	140	190
	$Ti^i(PrO)_4$	H_2O	SiO_2	ODTS	150	197
	$Ti^i(PrO)_4$	H_2O	MOU SAM	ODT SAM	100	198
	$Ti^i(PrO)_4$	H_2O	SiO_2	ODT or DDT	120	171
	$Ti^i(PrO)_4$	H_2O	SiO_2	PMMA	140	199
	$Ti^i(PrO)_4$	H_2O	SiO_2	PMMA	160	176,177
	$Ti^i(PrO)_4$	H_2O	SiO_2	PFTS SAM	225	200
HfO_2	TDEAHf	H_2O	PTCDA	graphene	100	158
	TDEAHf	H_2O	SiO_2	copper	200	207
	TDEAHf	H_2O	SiO_2	Si-H	150	86
	TEMAHf	H_2O	SiO_2	Si-H	250	304
	$HfCl_4$	H_2O	SiO_2	Si-H	300	85, 181
	$Hf^t(BuO)_4$	H_2O	SiO_2	ODTS on S-layer protein	200	195
	TDMAHf	H_2O	Au, SiO_2	photoresist, PMMA	100−150	163
	TDMAHf	H_2O	SiO_2	PMMA, PVP, and C_4F_8	200	159
	TDMAHf	H_2O	SiO_2	CF_x	200	160
	TDMAHf	H_2O	SiO_2	Si-H	200−325	305
	$HfCl_4$	H_2O	SiO_2	ODTS SAM	300	182
	$HfCl_4$	H_2O	SiO_2	ODTS and other SAMs	300	183
ZrO_2	$ZrCp(DMA)_3$	ethanol	SiO_2	copper	200	211

https://dx.doi.org/10.1021/acs.chemmater.0c00722
Chem. Mater. XXXX, XXX, XXX−XXX

Table 2. continued

material deposited	reactants		growth surface	nongrowth Surface	temperature (°C)	ref
	$Zr\ ^{t}(Bu)_4$	H_2O	SiO_2	ODTS SAM	–	201
	TDMA-Zr	H_2O	nitrogen-doped CNT	oleylamine	250	209
	$ZrCl_4$	H_2O	SiO_2	ODTS	300	182
SiO_2	bis(diethylamino)silane	O_2 plasma/H (acac)	GeO_2, SiNx, SiO_2, and WO_3	Al_2O_3, TiO_2, and HfO_2	150	92
	TEOS		TiO_2	PVP	25	306
Co_3O_4	$Co(NO_3)_2$	O_2 calcination	PS-NH_2, P2VP-NH_2, P2VP-SH	SiO_2	350−450	307
	$CoCp_2$	O_3	Al_2O_3	ODT	150	204
In_2O_3	InCp	O_2 + H_2O	SiO_2	Si-H	100	308, 309
MnO	$Mn(CpEt)_2$	H_2O	porphyrin		130	310
MoO_3	$Si(CH_3)_3CpMo(CO)_2(\eta^3$-2-methylallyl)	O_3	MoO_3	SiO_2	250	87

Table 3. ASD Metal on Metal

material deposited	reactants		growth surface	nongrowth surface	temperature	ref
W	WF_6	H atoms	Co, W	SiO_2, Al_2O_3, TiN	275	311
	WF_6	H_2	Si-H	SiO_2	500−900	8
	WF_6	H_2	Si-H	SiO_2	25−400	57
	WF_6	H_2	Si-H	SiO_2	240−380	56
	WF_6	SiH_4	Si-H	SiO_2	220	189, 243
Mo	MoF_6	Si_2H_6	Si-H	SiO_2, SiN_x	120	312
Cu	$Cu(thd)_2$	H_2	Cu	SiO_2	190	218
	$Cu(thd)_2$	H_2	Pt, Cu	SiO_2, TaO_x, TiN, NiO_x, ITO, FeO_x	190−260	217
	(β-diketonate)CuL_n	--	Pt	SiO_2	100−400	216
Co	Co $(AMD)_2$	--	Cu	SiO_2, $SiOC_x$, SAMs	165−265	223
	(undefined)	--	Cu	organo-silicate glass	200	114
	$Co(DAD)_2$	tertbutylamine	Pt, Cu	Ru, SiO_2, Si-H, $SiOC_x$	160−220	248
	$Co(DAD)_2$	diethylamine	Pt, Cu	Ru, SiO_2, Si-H, $SiOC_x$	160−220	248
	$Co(DAD)_2$	formic acid	Pt, Cu	Ru, SiO_2, Si-H, $SiOC_x$	180	246
	(^{t}Bu-allyl)$Co(CO)_3$	dimethylhydrazine	Si-H	SiO_2	140	313
Ru	(ethylCp) (pyrrolyl)Ru(II)	O_2	Pt, RuO_x	SiO_2	250−330	233
	$Ru(EtCp)_2$	O_2 H_2	Pt, Pd	Al_2O_3, TiO_2, ZrO_2	200	219
	RuO_4	H_2	Si-H	SiO_2	125	314
Pt	$MeCpPtMe_3$	O_2	ebeam Pt	Al_2O_3	300	145, 234−236
	$MeCpPtMe_3$	O_2	Pd, Ru	Al_2O_3, TiO_2, ZrO_2	150	219
	$MeCpPtMe_3$	O_2	graphene edges	graphene faces	300	91
	$MeCpPtMe_3$	O_2	C49 TiSi; Si-, *b* plane	C49 TiSi (other planes)	250	315
	$MeCpPtMe_3$	O_2	SiO_2, Pd	ODTS SAM	300	125
Pd	$Pd(hfac)_2$	--	Cu	SiO_2, Si, Al, W, Ni, Co, Ag	200−425	220
	$Pd(hfac)_2$	H_2	Pt, Ru	Al_2O_3, TiO_2, ZrO_2	150	219
	$Pd(hfac)_2$	formalin	SiO_2, Pt	ODTS SAM	200	125
Ir	$Ir(acac)_3$	O_2	Cu, SiO_2	DDT SAM	250	251
Ag	$Ag(hfac)_2$	--	Cu	Si, Al, W, Ni, Co, Ag	200−425	220

Area-selective ALD of ZnO using DEZ and water has led to some of the best-reported selectivity results, as shown in Table 1. Solution-deposited octadecylphosphonic acid (ODPA) SAMs on Cu can block more than 30 nm of ZnO ASD,[169] and vapor-regenerated dodecanethiol SAMs on Cu extended selectivity to >80 nm on SiO_2.[150] The addition of photocrossing groups within the a SAM has also been shown to give high selectivity for ZnO ALD on Cu vs the SAM layer.[140]

VI.A.2. DoD Using Halide Precursors: TiO_2, HfO_2, and ZrO_2. The most common halides studied for ASD are $TiCl_4$ for TiO_2,[49,86,135,174−180] $HfCl_4$ for HfO_2,[85,181−183] and $ZrCl_4$ for ZrO_2.[182] Between ∼100 and 250 °C, $TiCl_4$ and water show inherent selectivity for TiO_2 ALD on SiO_2 with slow nucleation on Si-H, allowing 1−2 nm of selective growth on SiO_2. The slow nucleation on Si-H is attributed to weak physisorption of $TiCl_4$ on Si-H vs SiO_2.[49,184] Growth occurs on Si-H after multiple ALD cycles, likely due to silicon oxidation by water followed by adsorption and reaction with $TiCl_4$. ALD using $HfCl_4/H_2O$ shows similar trends at 300 °C.[85,181] To avoid silicon oxidation, "water-free" ALD processes have been tested using $TiCl_4$ with titanium isopropoxide as the oxygen source,[180,185] leading to some improvement in selectivity. Water-free HfO_2 ASD has also been studied by pulsed CVD using hafnium tetra-*tert*-butoxide as a single precursor source.[186] At low deposition temperature on SiO_2, $TiCl_4$ can react on single Si-OH sites, whereas reaction at multiple neighboring sites is more favorable at higher temperatures.[187,188] Preselecting the type of hydroxyl sites present on a surface may therefore provide the means to

https://dx.doi.org/10.1021/acs.chemmater.0c00722
Chem. Mater. XXXX, XXX, XXX−XXX

Table 4. ASD Dielectric on Metal

material deposited	reactants		growth surface	nongrowth Surface	temperature	ref
Al_2O_3	TMA	H_2O	Au	dodecanethiol SAM	130	164
	TMA	H_2O	Cu	ODPA SAM	150	165
	TMA	H_2O	Au, SiO_2	photoresist, PMMA	100−150	163
	TMA	O_3	Si	screen printed polymer	125	129
ZnO	DEZ	H_2O	Au	1-dodecanethiol SAM on Au	105−200	170
	DEZ	H_2O	Cu	dodecanethiol	120	150
TiO_2	$TiCl_4$	H_2O	Ge-Cl, Ge-Br	1-octadecanethiolate SAM		175
	TDMAT	H_2O	Au	1-dodecanethiol SAM on Au	105−200	170
HfO_2	TDMAHf	H_2O	Si-H	octadecyltrichlorosilane SAM		183
	TDMAHf	H_2O	Au, SiO_2	photoresist, PMMA	100−150	163
ZrO_2	TDMAZr	H_2O	Au, SiO_2	photoresist, PMMA	100−150	163
Ta_2O_5	TBTDET	O_2/NF_3 plasma	TiN	SiO_2, Si-H	325	151
Si_3N_4	SiH_2Cl_2	NH_3	Si-H	Si_3N_4	375	215
Fe_2O_3	$FeCp_2$	O_3	Pt	Al_2O_3	270	213
	^{t}BuFeCp	O_2	Pt	SiO_2	300	144
CeO_2	$Ce(thd)_4$	O_3	Pt(111)	Pt(100)	200	126
SnO_2	TDMASn	H_2O	Au	1-dodecanethiol SAM on Au	105−200	170

Table 5. ASD Metal on Dielectric

material deposited	reactants		growth surface	nongrowth surface	temperature	ref
Al	$Al(^iBu)_3$		Al_2O_3	SiO_2	240−280	46, 47
Co	Co(AMD)		SiO_2	ODTS SAM	340	245
	$Co(^i$Pr-AMD$)_2$	NH_3, H_2	SiO_2	ODTS SAM	350	244
Cu	CuI(hfac)(vtms)	--	Al_2O_3, SiO_2, TiO_2, ITO	alkoxysilane SAMs	150−200	249
	$Cu(dmap)_2$	DEZ	SiO_2	ODTS SAM	100	250
	Cu(hfac)(vtms)	vtms	RuO_x	--	100	316
Ir	$Ir(acac)_3$	O_2	Cu, SiO_2	DDT SAM	250	251
	$Ir(acac)_3$	O_2	SiO_2	ODTS SAM	225	225
	$Ir(acac)_3$	O_2	SiO_2	PVV		161
	$Ir(acac)_3$	O_2	SiO_2	PMMA		193
	$Ir(acac)_3$	O_2	HfO_2	ODTS SAM		224
Ni	$Ni(dmab)_2$	NH_3	SiO_2	ODTS SAM	300	252
Pd	$Pd(hfac)_2$	formalin	SiO_2	ODTS SAM	200	125
	$Pd(hfac)_2$	formalin	TiO_2	Al_2O_3	200	25
Pt	$MeCpPtMe_3$	O_2	anatase TiO_2	amorphous TiO_2	300	317
	$MeCpPtMe_3$	O_2	SiO_2	ODTS/SiO_2	280−300	318
	$MeCpPtMe_3$	O_2	SiO_2, Pd	ODTS SAM	300	125
	$MeCpPtMe_3$	O_2	SiO_2	CFx implated SiO_2	250	148
	$MeCpPtMe_3$	O_2	SiO_2	PAM	280−300	239
	$MeCpPtMe_3$	O_2	SiO_2	1-octadecene/Si	--	192
Ru	(EBECH)Ru	O_2	SiCN, SiO_2	a-C:H	325	240
	(EtCp)(Py)Ru	O_2	Pt, RuO_x	SiO_2	250−330	233
		O_2	ZrO_2	Si-H, SiO_2, TiN	275−325	238
	$Ru(DMPD)_2$	O_2	HfO_2, $HfSiON_x$	SiO_2	210−300	254
	Ru(DMPD)(EtCp)	O_2	HfO_2, $HfSiON_x$	SiO_2	210−300	254
	$Ru(EtCp)_2$	O_2	SiN_x	SiO_2	300	229
		O_2	HfO_2:NH	HfO_2	350	237
	$RuCp_2$	O_2	SiO_2, HfO_2	Si-H (100)	275−325	228
		O_2	SiO_2	PVP	300	161
		O_2	SiO_2	OTS SAM	275	230
TiN	$TiCl_4$	NH_3	Si_3N_4	a-C	300	95
	TDMATi	NH_3	HfO_2	chlorosilane SAMS	250	94

promote or impede reactant adsorption and growth. Halide precursor adsorption on different types of hydroxyl sites was also studied for the case of area-selective ALD of tungsten.[189]

Organic blocking layers are also used with Ti, Hf, and Zr chlorides for ASD, where SiO_2 is typically the favorable growth surface.[15,135,175−177,182,183,190−192] For SAM blocking layers (e.g., octadecyltrichlorosilane on SiO_2), a high packing density of the SAM is critical.[182,183,191] As with TMA, precursor penetration into the blocking layer can be a problem, so selectivity depends on the density of the packing and the structure and physical length of the SAM molecules.[15] Thicker polymer films are also used as blocking layers,[135,161,176,177,193]

https://dx.doi.org/10.1021/acs.chemmater.0c00722
Chem. Mater. XXXX, XXX, XXX−XXX

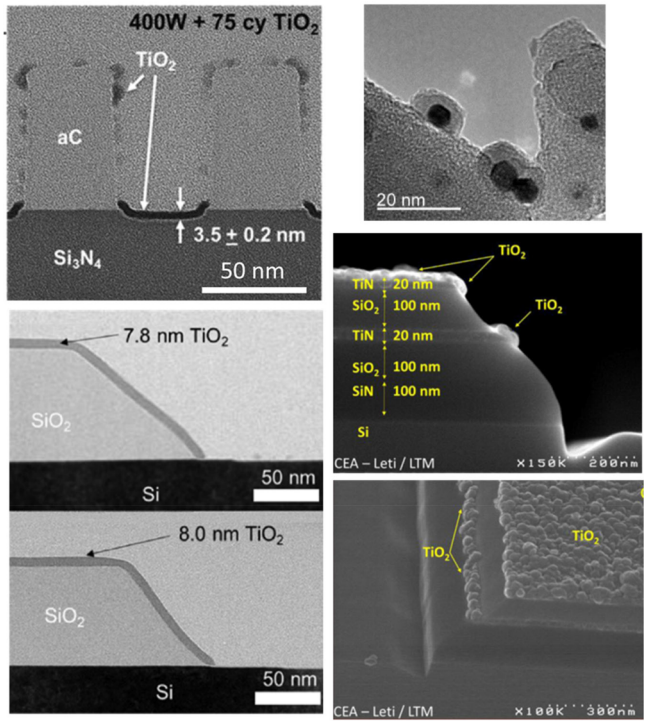

Figure 14. Images of dielectric ASD. (Upper left) TiO_2 on Si_3N_4 vs a-C:H, adapted with permission from Stevens et al., ref 95. Copyright 2018 American Chemical Society. (Upper right) Fe_2O_3 on Pt vs SiO_2, adapted from with permission from Singh et al., ref 144. Copyright 2018 American Chemical Society. (Lower left (two images)) TiO_2 on SiO_2 vs Si-H, adapted with permission from Song et al., ref 96. Copyright 2019 American Chemical Society; (Lower right (two images)) TiO_2 on TiN vs SiO_2, adapted with permission from Vallat et al., ref 151. Copyright 2019 AIP Publishing.

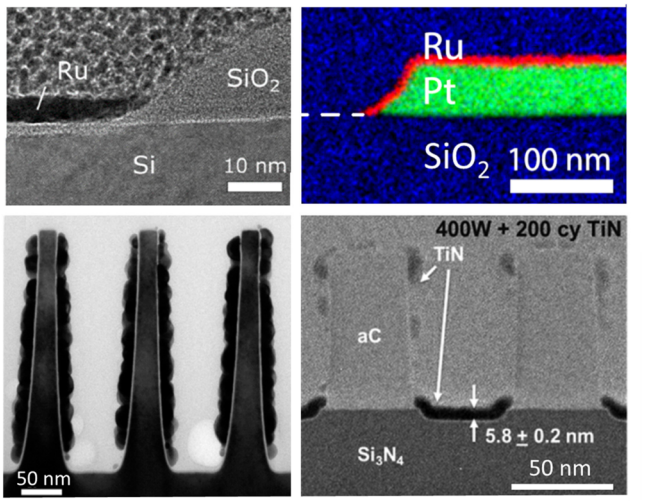

Figure 15. Images of metal ASD. (Upper left) Ru on Si-H vs SiO_2, adapted with permission from Minjauw et al., ref 314. Copyright 2019 American Chemical Society. (Upper right) Ru on Pt vs SiO_2, adapted with permission from Vos et al., ref 153. Copyright 2019 American Chemical Society. (Lower left) Pt on Si vs CF_x, adapted with permission from Kim et al., ref 148. Copyright 2016 American Chemical Society. (Lower right) TiN on Si_3N_4 vs a-C:H, adapted with permission from Stevens et al., ref 95. Copyright 2018 American Chemical Society.

but diffusion can still occur. Diffusion problems can be improved using larger, less-reactive precursors, such as alkoxides, as discussed below.

Instead of reaction blocking, organics can be placed on a surface to specifically promote adsorption of halide precursors. Taking advantage of halide diffusion, $TiCl_4$ can penetrate into a polystyrene-*block*-poly(methyl methacrylate) (PS-*b*-PMMA) copolymer to react selectively in the bulk of the PMMA, while avoiding reaction within the PS regions.[65,66] Infiltrating and reacting TMA in patterned PMMA can also create patterned Al_2O_3 with uniform thickness across large-area wafers.[68] Using patterned SAMs, Zn^{2+} ions dissolved in $ZnCl_2$ solution will react with carboxylic acid-terminated SAMs to form ZnO without reacting on methyl-terminated sites.[194]

VI.A.3. DoD Using Alkoxide and Amino Precursors: Al_2O_3, SiO_2, TiO_2, HfO_2, ZrO_2, CeO_2, and Cobalt Oxides. Alkoxides, including diketonates and other related metal−organic compounds, have been studied for area-selective ALD of Al_2O_3,[133,168] SiO_2,[92,195,196] TiO_2,[95,171,176,177,190,197−200] HfO_2,[195] ZrO_2,[201] CeO_2,[126] and cobalt oxide.[202−204] For ASD using organic blocking layers (e.g., SAM or polymer), the relatively large size of the alkoxides make precursor diffusion less favorable, allowing good results to be obtained for organic inhibition layers formed, for example, by printing,[197] lift-off transfer,[200] or photocatalytic lithography.[201] Polymer films, including PVP and PMMA, can also inhibit nucleation with alkoxide precursors.[133,161,168,176,177,193,199] Reactive SAMs can locally promote growth; TiO_2 ASD using titanium isopropoxide, $Ti(O^iPr)_4$, has been achieved on patterned hydroxyl-terminated SAMs relative to hydrophobic methyl-terminated SAMs.[198]

Amine-based precursors are attractive for ALD because they show good volatility and liquid handling and reasonable stability. For inherent ASD, the oxide-free Si-H surface tends to inhibit precursor adsorption. For TiO_2 ALD using TDEATi or TDMATi at 175−200 °C, the precursors appear to have an inherent preference for adsorption on SiO_2 versus copper or copper oxide surfaces.[205,206] Inhibited growth on copper is also observed for HfO_2 ALD using TDEAHf and water at 200 °C.[207] SAMs and polymer inhibitors have been tested with tetrakis-dimethylamino hafnium (TDMAHf) and analogous TDMATi, TDMAZr, and TDMASn.[94,159,160,163,170,191,208,209] For some polymer blocking layers, undesired growth can also occur on top of the polymer.[163] Octadecyltrichlorosilane (OTS) SAMs on SiO_2 can block TDMAHf adsorption, allowing several nanometers of ASD HfO_2 on Si-H.[191] Similarly, dodecane thoil SAMs on Au[170] can block adsorption of TDMATi and TDMASn. Surface passivation by competitive adsorption of small molecules is an area of growing interest for ASD.[13,138] Acetylacetone vapor, for example, can block adsorption of bis(diethylamino)silane during plasma ALD of SiO_2 by selectively adsorbing onto Al_2O_3 and other materials, while not inhibiting deposition on SiO_2, GeO_2, TiO_2, HfO_2, and others.[92] To maintain good blocking capacity and to counter the effects of plasma exposure during the plasma ALD steps, the ASD process used repeated exposures of the acetylacetone in a multistep "ABC" sequence. The use of molecular inhibitors is a promising area for advancement, but more work is needed to understand the driving forces for selective adsorption and how molecules can be designed to achieve desired selective adsorptive properties.

One limitation of amidinates is that the ligands can undergo β-hydride elimination at low temperatures,[210] and surface-adsorbed dissociation products promote adsorption and unwanted growth. Also, dimers or tetramers in the gas phase

https://dx.doi.org/10.1021/acs.chemmater.0c00722
Chem. Mater. XXXX, XXX, XXX−XXX

can retain their dimerization upon surface adsorption. Dimers can accelerate selectivity loss because they can bind strongly on the nongrowth surface via multiple nitrogen−metal dative bonds.[29] For cerium oxide using $Ce(thd)_4$, growth proceeds via ligand combustion with O_3, where the $Ce(thd)_4$ binds to Pt particles preferentially on the Pt(111) facets, allowing selective growth of CeO_2 before growth occurs over the entire particle.[126]

In another ASD scheme, amino precursors that react on metal oxides can be inhibited using a surface reducing agent. Using ethanol vapor to reduce copper oxide, for example, the adsorption of tris(dimethylamino)cyclopentadienyl zirconium can be impeded on copper while allowing growth on SiO_2.[211]

The effect of precursor structure and ligands on substrate-dependent nucleation reactions is another area that needs more investigation. In situ infrared spectroscopy shows that an amine-based heteroleptic Ti precursor $(EtCp)Ti(NMe_2)_3$ will react at 150 °C with an −OH terminated SiO_2 to form $(O)_3{\equiv}Ti{-}(CpEt)$ surface units, maintaining the intact Cp unit.[212] Reaction with O_3 in an ALD cycle at 250 °C leads to products consistent with combustion of the Cp ligand, and continued ALD shows a few cycles of growth inhibition before reaching the steady-growth regime. However, reaction with D_2O (in place of H_2O) shows no reaction at 250 °C, consistent with the inertness of the Cp ligand system.

VI.A.4. Dielectrics on Metals (DoM). ASD of dielectric on metal versus a dielectric is inherently more challenging than DoD. For DoM, the dielectric precursor must selectively nucleate on the metal, but when the metal becomes covered, the dielectric must selectively deposit on the desired dielectric but not on the undesired dielectric. To avoid this difficulty, schemes for DoM can use nucleation passivation layers adapted from DoM, such as using a SAM pretreatment designed to bind strongly only to exposed metal oxide regions.[129,150,164,165,170,175,183] Catalytic activation is another route to achieve DoM, for example, for ASD of iron or nickel oxide on platinum or iridium.[144,213] Catalytic metal particles on a relatively nonreceptive surface such as Au, SiO_2, or Al_2O_3 readily dissociate oxygen, and oxygen atoms react with ferrocene precursors to form iron oxide predominantly on the catalyst metal. Interestingly, results show that the selective deposition reaction continues to proceed even after the catalytic metal is completely covered by metal oxide. In one example, more than 20 nm of Fe_2O_3 was selectively deposited on Pt.[144] The observed continued growth is ascribed to rapid diffusion of oxygen molecules and atoms in the deposited iron oxide film. $MoSiO_x$ has also been formed selectively on silicon vs SiO_2 using the highly favorable reactivity of MoF_6 with silicon.[214]

Only a few studies show direct preferential growth of a dielectric on noncatalytic conductive or metallic surfaces. For silicon nitride deposition by hot-wire assisted ALD, a few nanometers of silicon nitride will grow on hydrogen-terminated silicon. However, on CVD silicon nitride formed at higher temperatures, growth is impeded due to few available Si-H or N-H reactive sites.[215] Titanium oxide and tantalum oxide have been grown selectively on TiN vs Si/SiO_2 using plasma ALD, with sequential plasma etch steps to remove unwanted oxide nuclei.[151,152] Growth inhibition is ascribed to surface fluorination that occurs during the plasma etch step, and TiO_2 thicknesses of ∼20 nm could be attained. Coupling of deposition and etching offers significant opportunities for ASD, but more work is needed to understand how etching reactions modify the growth and nongrowth surfaces to affect subsequent deposition.[96,151−153]

VI.B. ASD of Metals. Nucleation and area-selective deposition of metals, including W, Cu, Al, and others, have received significant attention, and insights from area-selective CVD continue to help guide the field. Most ASD of metals proceeds on metals (MoM), with dielectrics as the nongrowth surface. Also, unlike many ALD reactions for dielectrics that proceed by acid/base ligand exchange, metal CVD and ALD involve a redox reaction using a reducing agent. Therefore, a substrate that selectively activates a reducing agent (i.e., dissociating H_2 into two H surface atoms) can be a pathway to area-selective deposition.[6]

VI.B.1. MoM Using β-Diketonate, Alkoxide, and Alkyl Precursors: Cu, Al, Pd, Ag, and Ir. Copper is a common interconnect material in microelectronics, and original work in area-selective copper CVD was motivated by the need to create Cu patterns while avoiding difficult copper etch steps. Copper is also currently selectively deposited by electrochemical solution processing. For Cu CVD from copper(II)-hexafluoroacetylacetonate, $Cu(hfac)_2$, kinetic studies indicate growth proceeds through Cu species adsorbed on the clean metal and reaction with surface H atoms from dissociated H_2 at ∼350 °C. Alternate Cu(I) precursors use hfac in combination with a two-electron donating ligand, allowing CVD at lower temperature, and can also help enhance selective nucleation.[216] These precursors are known to disproportionate to the $Cu(II)(hfac)_2$, which may promote selectivity loss. Area-selective Cu ALD can proceed on Pd or Pt using another β-diketonate precursor, bis(2,2,6,6-tetramethyl-3,5-heptadionato)copper(II), $Cu(thd)_2$.[217,218] Selectivity is achieved due to spatially localized activation of the H_2 reductant on catalytic growth substrates, such as Pt and Cu, with no growth on noncatalytic oxides or nitride surfaces. This mechanism also works with $Pd(hfac)_2$ in ALD at 150 °C, yielding Pd growth on Pt or Ru but not on Al_2O_3, TiO_2, or ZrO_2.[219] In the absence of H_2, $Pd(hfac)_2$ deposits on copper via a surface-selective redox transmetalation reaction at 200−425 °C, leaving no deposit on SiO_2 and several other metal surfaces.[220,221] The same trend is reported for deposition of silver from $Ag(hfac)_2$.[220]

Aluminum CVD using Al alkyl precursors is also known to proceed selectively on metals vs oxides.[6,7,46,222] Surface precursor decomposition is expected to proceed via β-hydride elimination from the alkyl ligand through a four-center sp^3-like transition state. Ab initio modeling provides insight into the mechanisms that drive preferential reaction on metal vs oxide.[222] When the precursor metal interacts with a metal surface, the unoccupied out-of-plane p-states in Al remain relatively accessible, allowing a relatively small reaction barrier through the transition state. However, when the reactant adsorbs on an oxide, the more electronegative surface withdraws charge, making the p-state less energetically accessible, increasing the transition state energy, and therefore substantially decreasing the rate of surface decomposition.

Several metal on metal ASD schemes have used organic blocking layers, including ASD of Co,[223] Pt,[125,161] Pd,[125,219] Ru,[161] and Ir.[161,193,224,225] The Pd and Ir studies used β-diketonate precursors, $Pd(hfac)_2$ and $Ir(acac)_2$, with H_2 or formalin (for Pd) or O_2 (for Ir). Using the $Ir(acac)_2/O_2$ ALD combustion process, metal deposition was inhibited on poly(vinylpyrrolidone) polymer layers for up to 17 nm of Ir growth[161] and inhibited on OTS SAM layers for 23 nm of Ir growth.[224]

VI.B.2. MoM from Cyclopentadienyls: Ru and Pt. Cyclopentadienyl (Cp) precursors are used for metal ALD (often Ru

https://dx.doi.org/10.1021/acs.chemmater.0c00722
Chem. Mater. XXXX, XXX, XXX−XXX

or Pt), using an oxidizing coreactant to achieve ligand combustion.[226] Appendages on the Cp ligands and heteroleptic ligand combinations (e.g., $CH_3CpPt(CH_3)_3$ for Pt ALD[227]) are also used to tune volatility and precursor stability. For Ru ALD from Cp precursors, growth is often inhibited on most surfaces, with nitrided surfaces showing less inhibition and oxide-free surfaces (i.e., hydrogen-terminated silicon, or organic layers) showing more inhibition.[161,192,228−230] Ultrahigh vacuum studies of $RuCp_2$ interactions on oxide surfaces show that $RuCp_2$ forms relatively stable clusters on clean amorphous Al_2O_3, even at temperatures as high as 525 °C.[231] For $RuCp_2$, the presence of oxidized Ru clusters led to ligand combustion and Ru deposition at $T \sim 225$ °C. Other cyclopentadienyls also show strong molecule/surface interactions, for example, $FeCp_2$ adsorption on Ag(100) and Cu(100).[232] The stability of the Cp ligands during ALD nucleation is further reinforced by studies using heteroleptic Cp/alkyl precursors. For Pt ALD using $CH_3CpPt(CH_3)_3$, in situ mass spectroscopy analysis of methane production during precursor dosing indicates that adsorption proceeds via methyl ligand elimination with surface Pt-OH groups, and the Cp remains intact to combust during the subsequent oxygen dose. Similarly, for the heteroleptic (EtCp)-$Ti(NMe_2)_3$, infrared analysis showed surface reaction with the methylamine ligands rather than the Cp group.[212]

Findings suggest that Cp based precursors will nucleate more favorably on partially oxidized metals or metals with weakly bound oxygen, compared to metal oxides with strong metal−oxygen bonds. For example, Cp-based Ru or Pt nucleation tends to be favored on noble metals[145,219,233−236] or nitrided surfaces[229,237] and less favorable on oxide-free Si-H[228,238] or organic surfaces (i.e., SAM or polymer inhibition layers).[125,161,192,197,239,240] Area-selective ALD of Ru was also improved using a three-step $RuCp_2/O_2/H_2$ sequence.[219] For Pt ASD, surface catalytic activation can also be used, for example, where patterned Pt acts to activate O_2 and promote localized combustion of $CH_3CpPt(CH_3)_3$ at 300 °C.[145,234−236]

VI.B.3. MoM from Halides: W. Tungsten metal, generally deposited from volatile WF_6, is one of the most studied materials for area-selective CVD.[6−8,53−57,241] Because of the relative strength of Si−F vs W−F bonds, the reaction between WF_6 and silicon to form metallic W and volatile SiF_4 is strongly exothermic. Early studies found that, on patterned Si/SiO_2 surfaces, WF_6 reacts minimally with SiO_2 but readily consumes exposed silicon to locally deposit tungsten. The deposition rate slows as the W film thickness increases, leading to an effective self-limiting ASD process. Further deposition proceeds using a reducing agent, such as H_2 or SiH_4 in a CVD or ALD reaction scheme. As deposition proceeds, W eventually nucleates on SiO_2 and selectivity is lost. The mechanisms for unwanted nucleation are fairly well understood. A common conclusion is that WF_6 impinging on the W surface undergoes ligand transfer, creating reactive volatile tungsten subfluorides (e.g., WF_4) that transport from deposited W regions and adsorb and stick on SiO_2, thereby creating a stable nucleus for growth initiation.[8,189,242,243] This process is an important example of a "proximity effect", discussed above. Because the subfluoride is formed by WF_6 impinging on the growth surface, the rate of nucleation of unwanted W will not be random across the surface. Instead, it will depend on the net surface area and local proximity of the W that is deposited in the desired growth region. The trend to produce unwanted nuclei close to deposited W was also noted during area-selective W ALD studies. Under viscous flow conditions, passing reactants over a stripe of deposited metal led to unwanted nuclei being preferentially formed downstream from the desired W film.[243] Recently, ASD of tungsten on cobalt has been studied as a route for self-aligned gate contact for sub-7 nm transistors.[241]

VI.B.4. MoM Cobalt Using Amino and Carbonyl Precursors. Metal on metal ASD using amine-based precursors has mostly focused on Cu and Co amidinates. Using cobalt amidinate, $Co(AMD)_2$, the amidinate ligand is found to interact favorably with copper allowing deposition at 200 °C with less growth on SiO_2.[223] In contrast, a related amidinate precursor, bis(*N*,*N*)-diisopropyl acetamidinato cobalt, $Co(^iPr\text{-}AMD)_2$, was found to grow readily on SiO_2 at 340−350 °C but be blocked by an OTS SAM,[244,245] suggesting temperature-dependent metal surface association. Cobalt ALD using Co(dialkyl-diazabutadiene) has been studied using formic acid,[246,247] *tert*-butylamine,[247,248] and diethylamine[248] reducing agents, showing preferential Co growth on Pt and Cu versus Ru, SiO_2, Si-H, and $SiOC_x$. While the reaction mechanisms are not very clear, a reason for the observed selectivity was hypothesized to involve Co−Pt and Co−Cu alloy or interfacial layer formation driving selective growth.

Area-selective CVD of cobalt on copper is of particular interest for improved adhesion and electromigration performance of copper interconnects,[113,114] and ∼10 nm of ASD Co has been shown on Cu vs SiO_2.[114] Reports provide few details regarding the precursors and reaction conditions required.

VI.B.5. ASD Metals on Dielectrics. Like the case of DoM, ASD of metal on dielectric, without deposition on metal or another dielectric, presents significant challenges compared to DoD. Like DoM, approaches using SAM or polymer blocking layers can extend to MoD, including ASD of Co,[244,245] Cu,[249,250] Ir,[161,193,224,225,251] Ni,[252] Ru,[161,230] Rh,[253] and TiN.[94]

Of the metals studied, ruthenium ASD, usually using a Cp-based precursor at $T \gtrsim 250$ °C, has shown some propensity to nucleate preferentially on a dielectric vs metal or another dielectric.[84,228,229,233,237,238,240,254] Because the Ru-Cp precursors dissociate via combustion with oxygen, surfaces that more readily provide oxygen are more likely to promote adsorption and nucleation. Once the Ru nuclei reach a sufficient size, they act to catalyze O_2 decomposition and self-promote Ru deposition.[84] The concept of tuning availability of oxygen on a starting surface to impede metal nucleation has also been used for ASD of ALD TiN, where deposition occurred preferentially on Si_3N_4, with the nongrowth surface being H_2-plasma treated hydrogenated amorphous carbon.[95] The hydrogen plasma acted to reduce the carbon by removing surface oxygen impurities, thereby slowing the rate of TDMA-Ti adsorption and reaction. On nanoscale carbon features, unwanted nuclei tended to appear first on feature edges and corners, which was ascribed to more difficult removal of defects that promote nucleation. This is one example that highlights the important challenge of feature size and shape dependence in controlling nucleation during ASD, such as shown schematically in Figure 3c.

VI.C. ASD of Semiconductors. Selective area epitaxy of Si, SiGe, GaAs, GaN, and other compounds typically proceeds at relatively high temperatures (≥700 °C) using halides and hydrides, including SiH_4, $SiCl_4$, SiH_2Cl_2, GeH_4, AsH_3, $AsCl_3$, and HCl.[1,2,4,6,7,10,11,33,50,255−258] The receptive growth surface is usually a semiconductor or metal, with a dielectric as the nongrowth surface. Selective CVD of semiconducting nanowires is also often performed using vapor−liquid−solid growth, where growth occurs only at locations where a catalyst metal particle, such as Au, Ni, or Fe, is available.[259,260] Area-selective epitaxy of

https://dx.doi.org/10.1021/acs.chemmater.0c00722
Chem. Mater. XXXX, XXX, XXX−XXX

SiGe was reported near 500 °C using a mixture of Si_2H_6, GeH_4, and B_2H_6.[257] At high temperature, nucleation thermodynamics promotes rapid formation of stable nuclei on more reactive semiconductor surfaces, and the halogen species helps volatilization of less stable adsorbates on dielectrics. Also at high temperature, silicon deposited on SiO_2 can react favorably to form volatile silicon monoxide: $Si + SiO_2 \rightarrow 2\ SiO(g)$. However, extensive SiO_2 loss is not commonly observed, consistent with nucleation on Si being faster than etching on SiO_2.

Several lower temperature processes (<400 °C) for ASD of semiconductors have also been reported, including silicon,[89,155,262] and ZnS.[194] At $T \leq 250$ °C, microcrystalline silicon films were selectively deposited by plasma-enhanced CVD using intermittent sequential doses of SiH_4 into a continuous H_2 plasma. By varying the duration of the SiH_4 and H_2 plasma exposure times, silicon nuclei were found to grow selectively on silicon and other receptive substrates without deposition on silicon oxide, producing many nanometers of selectively deposited silicon.[89,155,262] This process also shows feature-related phenomena in that nuclei tend to appear in the nongrowth region preferentially at the edge of the desired deposition region.

Two-dimensional semiconductors are an important research area, and there are several reports of ASD of these materials including tungsten disulfide[263] and analogous molybdenum disulfide,[264−268] as well as metallic niobium disulfide[269] and several antimony chalcogenides.[270,271] Surface ribbons of WS_2 were created by reacting lithographically patterned silicon lines with WF_6, forming W, followed by sulfidation under H_2S gas yielding randomly oriented crystals at 450 °C. Basal plane alignment occurred upon annealing at 900 °C under inert gas.[263] Selective CVD of MoS_2 can proceed on patterned seeds or other templates at temperatures above 650 °C.[264−266,268] In the case of antimony compounds, selective deposition at $T = 200$ °C was believed to result from selective passivation of the nongrowth surface by adsorption of Sb.[270]

VI.D. ASD of Organic, Biological, and Metal−Organic Framework Materials. Patterned synthesis of organic materials and organic/inorganic compounds by vapor or solution-based deposition is an important area for continued research. Beyond formation of nucleation inhibitors and resists for selective deposition or etching, other uses for area-selective deposited organics include patterned biofunctional surfaces for medical diagnostics and separations,[272,273] direct patterning of organic light emitting diodes or other organic electronic systems,[274−276] and bottom-up synthesis of de novo heterogeneous catalysts.[277−280] These applications drive the need for improved fundamental understanding of how organic species adsorb, transport, interact, and grow on surfaces. New insight will help understand how surface composition and structure can be tailored to promote desired outcomes and overcome unknown problems of translating organic materials from the lab into large-scale nanomanufacturing.

VI.D.1. Vapor-Delivered ASD of SAMs and Polymers. For SAM-based inhibition layers, preparing a well-defined patterned SAM is a critical step in ASD. SAM patterning can proceed by lift-off or by selective adsorption/reaction from either solution or vapor phases. While some processes require solution-based SAMs to achieve good selective inhibition, SAM vapor delivery is advantageous for simplified processing. Several monolayer materials show the capacity for ASD when delivered in the gas phase, including alkanethiols on metals,[150,164,170,171,251] organosilanes on metal oxide,[167,225] and conjugated carbons on silicon.[48] Careful surface preparation before SAM vapor delivery is important to achieve good coverage and inhibition.[164] Some vapor-delivered monolayers show more favorable inhibition than those formed from solution and allow sequential regeneration of the resist layer.[150] The improved performance for SAMs formed from the vapor phase relative to solution deposition is ascribed to improved surface assembly kinetics for the solvent-free vapor process.

Approaches to remove the SAM or polymer inhibition layers are also important, and solution-based electrochemical reduction[281] and weak acid treatment[165,282] have been used in conjunction with AS-ALD or AS-MLD. In these cases, the SAM removal step functions as a "lift-off" to remove unwanted nuclei or film from the inhibited region. Ideally, vapor-based SAM removal and vapor-surface cleaning processes need to be identified that integrate well with selective deposition.

Area-selective deposition of polymer films is another active research area. Dodecanethiol SAMs that are useful for blocking ALD of iridium can also function to block MLD of polyimide thin films.[251] Interestingly, results showed that good selectivity for the MLD process requires better SAM quality than for the selective inorganic film. Several variations of area-selective MLD of polyurea thin films has also been explored using SAMs as growth inhibition layers,[281−284] resulting in >6 nm of area-selective polymer deposition. SAM removal by weak acid etching could improve the MLD selectivity by eliminating the polymer formed in or on the SAM blocking layer.[282]

Patterned polymer growth has also been studied by surface-initiated polymerization[285,286] and by direct CVD of passivating and chemically active polymers.[12,272−276] During initiated polymerization, metallic surfaces tend to inhibit polymer growth,[274,275] and the mechanism is ascribed to deactivation of the impinging monomer by charge available on the transition metal surface. As with inorganics, patterned monolayers can act to block or selectively promote polymer CVD nucleation and growth.[273,274,276,285] Oxidative- and initiated-CVD[12] are two important processes for polymer film formation, and they allow several approaches for direct patterned deposition. The o-CVD and i-CVD methods use oxidative coreactants and vapor initiators (commonly excited via a hot wire), respectively, to achieve surface polymerization of an impinging vapor monomer. Patterned deposition during o-CVD can be controlled by predepositing, for example, by printing, an amount of the oxidizing metal salt species. The surface polymerization and deposition then proceed only in the regions where the oxidant is present.[287,288] A similar strategy can be used during i-CVD. In this case, a prepatterned transition metal salt, such as $FeCl_3$, acts to locally quench the impinging radicals and thereby inhibit surface polymerization.[289,290] An interesting observation is that in o-CVD the growth occurs only on the metal salt, whereas in i-CVD growth is impeded by the metal salt.

In another approach, patterned polynorbornene thin films have been grown from surface-bound initiators, and the resulting polymers were found to successfully impede nucleation of ZnO and TiO_2 during subsequent ALD.[291] To achieve patterned growth, the initiators were designed to selectively bind onto patterned oxide layers. In contrast to o-CVD, this attachment strategy enables selective deposition of the polymer on the insulator rather than on a metal.

VI.D.2. Biological Materials. Area-selective deposition of biological materials, including viruses,[292] DNA,[293] and dopamine-melanin pigments,[294] is also an interesting area of

https://dx.doi.org/10.1021/acs.chemmater.0c00722
Chem. Mater. XXXX, XXX, XXX−XXX

research. Biomaterial surface patterns can be generated from solution using self-assembled monolayers to promote local adsorption.[294] For example, surface adsorption of dopamine-melanin molecular films occur via dissociation of catechol groups within the molecules, which is inhibited on negatively charged SiO_2 but favored on SAMs with neutral or positively charged terminating groups. In another case, using patterned polymers, genetically engineered M13 viruses were shown to selectively assemble onto polyelectrolyte multilayers, where the polyelectrolyte was first patterned on silica via solvent-assisted capillary molding using a polydimethylsiloxane (PDMS) template.[292] Surface patterns can also be generated using inherent differences in chemical adsorption on different exposed surfaces. An illustration of this is that 2-deoxythymidine-5-monophosphate, a chemical model for DNA, has been shown to preferentially adsorb on Al_2O_3 vs SiO_2.[293] The specific mechanisms that produce the preference for selective adsorption remain unclear.

VI.D.3. Metal−Organic Frameworks. Metal−organic frameworks (MOFs) are porous coordination polymers consisting of a crystalline topological network of well-defined nanoscale inorganic (e.g., metal-oxo/hydroxy) clusters interconnected by organic linker molecules.[295] MOFs have high surface area and large ordered pore volume, and the chemical tunability of the metal nodes and linkers make them interesting for catalysis, gas storage and separation, hazardous gas adsorption, heat transfer agents, and many other uses. MOFs are commonly synthesized in powder form by solution methods, although surface-bound MOF thin films are finding unique uses, including applications in microelectronics,[296] requiring better understanding of MOF heterogeneous nucleation and growth.

For area-selective MOF deposition from solution, surfaces prepared with patterned functional SAMs can promote localized MOF nucleation. For example, a carboxylic-acid terminated SAM will promote solution deposition of MOF-5 (i.e., $Zn_4O(benzodicarboxylate)_3$) through favorable bonding with the linker terminal groups, whereas MOFs avoid growth on SAMs with fluorocarbon termination.[280] For solution-based MOF thin film growth on metal oxides, ALD Al_2O_3 was found to be favorable for MOF growth, whereas SiO_2 was less receptive.[277] This difference was ascribed to the stronger basicity (i.e., larger isoelectric point) of the Al_2O_3, making it more likely to bond to the more acidic end groups of the dicarboxylate linker.[277] In other studies of solution-based MOF nucleation, different metal oxides formed by ALD showed markedly different propensity for growth of copper benzene-tricarboxylate MOF, $Cu_3(BTC)_2$. In this case the MOF was found to preferentially grow on ALD ZnO, with slower nucleation on ALD Al_2O_3 or TiO_2. This trend did not follow differences in the oxide isoelectric point.[297] The rapid nucleation of $Cu_3(BTC)_2$ on ALD ZnO was found to result from the rapid reaction between the ZnO and the copper nitrate reactant, forming a layered hydroxy double-salt compound that allowed rapid linker infusion and conversion to the MOF,[297,298] which in turn promoted further MOF growth. The broad versatility in MOFs, along with new advances in vapor-phase routes for MOF thin film growth,[299−301] makes vapor−surface ASD of MOFs an interesting area for further study.

VII. RESEARCH CHALLENGES AND OUTLOOK

This article has provided an overview of basic surface processes in nucleation and summarized the current understanding and status of substrate-dependent nucleation and area-selective thin film deposition. The primary motive driving research is the emerging need for chemically driven material patterning to supplement current physically based photolithography used for thin film material patterning in high-performance semiconductor devices. Beyond the specific examples described in Section IV above, bottom-up area-selective deposition will accelerate new process design schemes to reduce process complexity, cut material waste, and improve overall energy efficiency in semiconductor manufacturing. As described also above, ASD research is exploring other applications, and it is likely that successful ASD processes will be useful in areas not yet identified. However, to facilitate widespread use, many problems must be overcome and new understanding is needed to enable robust and reliable ASD. For example, following the concepts introduced in Section II, better insight is needed into elementary reaction sequences during low-temperature reactant adsorption and nucleation. As described in Section III, key problems during deposition include feature-dependent phenomena, choice of reaction mode, and detailed reactor design. Process engineering must also consider overall process throughput, material and energy utilization and efficiency, and system reliability.

There are significant opportunities for whole new approaches to ASD, beyond the common CVD, ALD, and etching methods currently studied. Perhaps unwanted nucleation could be avoided, for example, if a reactant acted as a depositing species on one surface but simultaneously operated as an etchant on another. True "bottom-up" processing will also require multiple cooperative ASD processes to work synergistically and sequentially, so that different ASD materials can be stacked on top of each other or side-by-side. Such "dual" or "orthogonal" ASD processes have been described[302] but are not yet demonstrated. It is also expected that advances in modeling, new approaches for in situ analysis and data collection, and innovations in data analysis will be important. Ultimately, more fundamental surface science investigations, likely coupled with targeted precursor design, will be needed to define preferred elementary reaction kinetics to achieve desired material reaction selectivity with true atomic-scale lateral and vertical precision.

A significant challenge not discussed in this article is the problem of ASD metrology. The unwanted nuclei formed during ASD in the desired nongrowth regions can lead to significant loss of semiconductor device yield and performance. This is particularly acute in metal ASD where excess metal leads to electrical shorting. The impact of unwanted nuclei on the device performance will depend on the ASD material and the layout and placement of the ASD step within the device architecture. Understanding this impact requires means to quantify and characterize the surface densities and size distributions of unwanted nuclei. However, at present, experimental tools are not available that can observe and quantify small nuclei defects stochastically dispersed across a large-area, nonuniform patterned surface. Research teams are now diligently working to identify approaches to overcome this obstacle.

AUTHOR INFORMATION

Corresponding Author

Gregory N. Parsons − *North Carolina State University, Raleigh, North Carolina 27695, United States;* orcid.org/0000-0002-0048-5859

Author

Robert D. Clark − *TEL Technology Center, America, LLC, Albany, New York 12203, United States*

https://dx.doi.org/10.1021/acs.chemmater.0c00722
Chem. Mater. XXXX, XXX, XXX−XXX

Complete contact information is available at:
https://pubs.acs.org/10.1021/acs.chemmater.0c00722

Notes

The authors declare no competing financial interest.

■ ACKNOWLEDGMENTS

G.N.P. acknowledges support from the US National Science Foundation Award No. 1704151, EMD Performance Materials, and from the Semiconductor Research Corporation. We also thank Parsons' group members and S. Barry for their help with manuscript review.

■ ABBREVIATION

AMD	amidinato ligand
Cp	cyclopentadienyl ligand
DAD	diazadienyl ligand
DDPA	dodecylphosphonic acid SAM
DDT	dodecanethiol SAM
DMAB	dimethylaminopropoxo
DMAP	dimethylamino-propoxo ligand
DTS	docosyltrichlorosilane SAM
EBECH	ethylbenzyl, ethylcyclohexadienyl ligand system
EtCpPy	ethylcyclopentadienyl, pyrrolyl ligand system
^{i}Bu	isobutyl ligand
$^{i}Pr_2$-Me-AMD	diisopropylacetamidinato ligand
MOU	mercaptoundecanol SAM
ODPA	octadecylphosphonic acid SAM
ODT	octadecanethiol SAM
ODTS	octadecyltrichlorosilane SAM
P2VP	poly-2-vinyl pyridine polymer
PAM	polymethacrylamide polymer
PFOS	perfluorooctylsilane SAM
PFTS	perfluorodecyltrichlorosilane SAM
PMMA	poly(methyl methacralate)
b-PMMA	block-poly(methyl methacralate) polymer
PS	polystyrene polymer
b-PS	block-polystyrene polymer
PtBMA	poly(tertbutyl methacrylate) polymer
PTCDA	perylene-tetracarboxylic dianhydride SAM
PVP	poly(vinyl pyrrolidone) polymer
TDEA	tetrakisdiethylamino ligand system
THD	tetramethyl-heptadionato ligand
VTMS	vinyltrimethylsilane ligand

■ REFERENCES

(1) Joyce, B. D.; Baldrey, J. A. Selective Epitaxial Deposition of Silicon. *Nature* **1962**, *195* (4840), 485−486.
(2) Tausch, F. W.; Lapierre, A. G. A Novel Crystal Growth Phenomenon: Single Crystal GaAs Overgrowth onto Silicon Dioxide. *J. Electrochem. Soc.* **1965**, *112* (7), 706.
(3) Holleman, J. Selective Chemical Vapor Deposition. In *Chemical Physics of Thin Film Deposition Processes for Micro- and Nano-Technologies*; Pauleau, Y., Ed.; Springer: 2002; pp 171−198.
(4) Shaw, D. W. Selective Epitaxial Deposition of Gallium Arsenide in Holes. *J. Electrochem. Soc.* **1966**, *113* (9), 904.
(5) Carlsson, J.-O. Novel and Selective Vapor Deposition Processes. *Vacuum* **1990**, *41*, 1077−1080.
(6) Gladfelter, W. L. Selective Metallization by Chemical Vapor Deposition. *Chem. Mater.* **1993**, *5* (10), 1372−1388.
(7) Hampden-Smith, M. J.; Kodas, T. T. Chemical Vapor Deposition of Metals: Part 2. Overview of Selective CVD of Metals. *Chem. Vap. Deposition* **1995**, *1* (2), 39−48.
(8) Carlsson, J.-O.; Boman, M. Selective Deposition of Tungsten—Prediction of Selectivity. *J. Vac. Sci. Technol., A* **1985**, *3* (6), 2298.
(9) Carlsson, J.-O. Selective Vapor-Phase Deposition on Patterned Substrates. *Crit. Rev. Solid State Mater. Sci.* **1990**, *16* (3), 161−212.
(10) Dumin, D. J. Selective Epitaxy Using Silane and Germane. *J. Cryst. Growth* **1971**, *8* (1), 33−36.
(11) Rai-Choudhury, P.; Schroder, D. K. Selective Growth of Epitaxial Silicon and Gallium Arsenide. *J. Electrochem. Soc.* **1971**, *118*, 107−110.
(12) Wang, M.; Wang, X.; Moni, P.; Liu, A.; Kim, D. H.; Jo, W. J.; Sojoudi, H.; Gleason, K. K. CVD Polymers for Devices and Device Fabrication. *Adv. Mater.* **2017**, *29* (11), 1604606.
(13) Abelson, J. R.; Girolami, G. S. New Strategies for Conformal, Superconformal, and Ultrasmooth Films by Low Temperature Chemical Vapor Deposition. *J. Vac. Sci. Technol., A* **2020**, *38* (3), 030802.
(14) Jiang, X.; Bent, S. F. Area-Selective ALD with Soft Lithographic Methods: Using Self-Assembled Monolayers to Direct Film Deposition. *J. Phys. Chem. C* **2009**, *113* (41), 17613−17625.
(15) Lee, H.-B.-R.; Bent, S. F. Nanopatterning by Area-Selective Atomic Layer Deposition. In *Atomic Layer Deposition of Nanostructured Materials*; Pinna, N., Knez, M., Eds.; Wiley-VCH Verlag GmbH & Co. KGaA: Weinheim, Germany, 2011; pp 193−225.
(16) Mackus, A. J. M.; Bol, A. A.; Kessels, W. M. M. The Use of Atomic Layer Deposition in Advanced Nanopatterning. *Nanoscale* **2014**, *6* (19), 10941−10960.
(17) Mackus, A. J. M. M.; Merkx, M. J. M. M.; Kessels, W. M. M. M. From the Bottom-Up: Toward Area-Selective Atomic Layer Deposition with High Selectivity. *Chem. Mater.* **2019**, *31* (1), 2−12.
(18) Parsons, G. N. Functional Model for Analysis of ALD Nucleation and Quantification of Area-Selective Deposition. *J. Vac. Sci. Technol., A* **2019**, *37* (2), 020911.
(19) Cao, K.; Cai, J.; Chen, R. Inherently Selective Atomic Layer Deposition and Applications. *Chem. Mater.* **2020**, *32* (6), 2195−2207.
(20) *Atomic Layer Deposition of Nanostructured Materials*; Pinna, N., Knez, M., Eds.; Wiley-VCH Verlag GmbH & Co. KGaA: Weinheim, Germany, 2011.
(21) Poodt, P.; Cameron, D. C.; Dickey, E.; George, S. M.; Kuznetsov, V.; Parsons, G. N.; Roozeboom, F.; Sundaram, G.; Vermeer, A. Spatial Atomic Layer Deposition: A Route towards Further Industrialization of Atomic Layer Deposition. *J. Vac. Sci. Technol., A* **2012**, *30* (1), 010802.
(22) Dorsey, K. J.; Pearson, T. G.; Esposito, E.; Russell, S.; Bircan, B.; Han, Y.; Miskin, M. Z.; Muller, D. A.; Cohen, I.; McEuen, P. L. Atomic Layer Deposition for Membranes, Metamaterials, and Mechanisms. *Adv. Mater.* **2019**, *31* (29), 1901944.
(23) Miikkulainen, V.; Leskelä, M.; Ritala, M.; Puurunen, R. L. Crystallinity of Inorganic Films Grown by Atomic Layer Deposition: Overview and General Trends. *J. Appl. Phys.* **2013**, *113* (2), 021301.
(24) Johnson, R. W.; Hultqvist, A.; Bent, S. F. A Brief Review of Atomic Layer Deposition: From Fundamentals to Applications. *Mater. Today* **2014**, *17* (5), 236−246.
(25) Lu, J.; Elam, J. W.; Stair, P. C. Atomic Layer Deposition - Sequential Self-Limiting Surface Reactions for Advanced Catalyst "Bottom-up" Synthesis. *Surf. Sci. Rep.* **2016**, *71* (2), 410−472.
(26) Gregorczyk, K.; Knez, M. Hybrid Nanomaterials through Molecular and Atomic Layer Deposition: Top down, Bottom up, and in-between Approaches to New Materials. *Prog. Mater. Sci.* **2016**, *75*, 1−37.
(27) Brozena, A. H.; Oldham, C. J.; Parsons, G. N. Atomic Layer Deposition on Polymer Fibers and Fabrics for Multifunctional and Electronic Textiles. *J. Vac. Sci. Technol., A* **2016**, *34* (1), 010801.
(28) Leng, C. Z.; Losego, M. D. Vapor Phase Infiltration (VPI) for Transforming Polymers into Organic−Inorganic Hybrid Materials: A Critical Review of Current Progress and Future Challenges. *Mater. Horiz.* **2017**, *4* (5), 747−771.
(29) Barry, S. T.; Teplyakov, V. A.; Zaera, F. The Chemistry of Inorganic Precursors during the Chemical Deposition of Films on Solid Surfaces. *Acc. Chem. Res.* **2018**, *51* (3), 800−809.

(30) Mackus, A. J. M.; Schneider, J. R.; Macisaac, C.; Baker, J. G.; Bent, S. F. Synthesis of Doped, Ternary, and Quaternary Materials by Atomic Layer Deposition: A Review. *Chem. Mater.* **2019**, *31* (4), 1142−1183.
(31) Thompson, S. E.; Chau, R. S.; Ghani, T.; Mistry, K.; Tyagi, S.; Bohr, M. T. In Search of "Forever," Continued Transistor Scaling One New Material at a Time. *IEEE Trans. Semicond. Manuf.* **2005**, *18* (1), 26−35.
(32) Clark, R.; Tapily, K.; Yu, K. H.; Hakamata, T.; Consiglio, S.; O'Meara, D.; Wajda, C.; Smith, J.; Leusink, G. Perspective: New Process Technologies Required for Future Devices and Scaling. *APL Mater.* **2018**, *6* (5), 058203.
(33) Isshiki, H.; Aoyagi, Y.; Sugano, T.; Iwai, S.; Meguro, T. Surface Processes of Selective Growth by Atomic Layer Epitaxy. *Appl. Surf. Sci.* **1994**, *82*−*83* (C), 57−63.
(34) Chau, R. Process and Packaging Innovations for Moore's Law Continuation and Beyond. In *2019 IEEE International Electron Devices Meeting (IEDM)*; IEEE, 2019; pp 1.1.1−1.1.6.
(35) Bencher, C.; Chen, Y.; Dai, H.; Montgomery, W.; Huli, L. 22nm Half-Pitch Patterning by CVD Spacer Self Alignment Double Patterning (SADP). *Proc. SPIE* **2008**, *6924* (May), 69244E.
(36) Raley, A.; Lee, J.; Smith, J. T.; Sun, X.; Farrell, R. A.; Shearer, J.; Xu, Y.; Ko, A.; Metz, A. W.; Biolsi, P.; Devilliers, A.; Arnold, J.; Felix, N. Self-Aligned Blocking Integration Demonstration for Critical Sub-30-nm Pitch Mx Level Patterning with EUV Self-Aligned Double Patterning. *J. Micro/Nanolithogr., MEMS, MOEMS* **2019**, *18* (01), 1.
(37) Stewart, M. E.; Motala, M. J.; Thompson, L. B.; Yao, J.; Nuzzo, R. G. Unconventional Methods for Forming Nanopatterns. *Proc. Inst. Mech. Eng., Part N* **2006**, *220* (3), 81−138.
(38) Ouk Kim, S.; Solak, H. H.; Stoykovich, M. P.; Ferrier, N. J.; de Pablo, J. J.; Nealey, P. F. Epitaxial Self-Assembly of Block Copolymers on Lithographically Defined Nanopatterned Substrates. *Nature* **2003**, *424* (6947), 411−414.
(39) Hu, H.; Gopinadhan, M.; Osuji, C. O. Directed Self-Assembly of Block Copolymers: A Tutorial Review of Strategies for Enabling Nanotechnology with Soft Matter. *Soft Matter* **2014**, *10* (22), 3867.
(40) Crane, E. L.; Girolami, G. S.; Nuzzo, R. G. Additive Fabrication and the Mechanisms of Nucleation and Growth in Chemical Vapor Deposition Processes. *Acc. Chem. Res.* **2000**, *33* (12), 869−877.
(41) Heath, J. R. Wires, Switches, and Wiring. A Route toward a Chemically Assembled Electronic Nanocomputer. *Pure Appl. Chem.* **2000**, *72* (1−2), 11−20.
(42) Theobald, J. A.; Oxtoby, N. S.; Phillips, M. A.; Champness, N. R.; Beton, P. H. Controlling Molecular Deposition and Layer Structure with Supramolecular Surface Assemblies. *Nature* **2003**, *424* (6952), 1029−1031.
(43) Scheibel, T.; Parthasarathy, R.; Sawicki, G.; Lin, X. M.; Jaeger, H.; Lindquist, S. L. Conducting Nanowires Built by Controlled Self-Assembly of Amyloid Fibers and Selective Metal Deposition. *Proc. Natl. Acad. Sci. U. S. A.* **2003**, *100* (8), 4527−4532.
(44) Black, C. T.; Guarini, K. W.; Ruiz, R.; Sikorski, E. M.; Babich, I. V.; Sandstrom, R. L.; Zhang, Y. Polymer Self Assembly in Semiconductor Microelectronics. *Technol. Dig. - Int. Electron Devices Meet. IEDM* **2006**, *51* (5), 605−633.
(45) Jung, W. B.; Jang, S.; Cho, S. Y.; Jeon, H. J.; Jung, H. T. Recent Progress in Simple and Cost-Effective Top-Down Lithography for ≈10 nm Scale Nanopatterns: From Edge Lithography to Secondary Sputtering Lithography. *Adv. Mater.* **2020**, *m*, 1907101.
(46) Fleming, C. G.; Blonder, G. E.; Higashi, G. S. Surface Chemical Modification for Via-Hole Filling Using Tri-Isobutylaluminum Chemical Vapor Deposition. *MRS Proc.* **1987**, *101*, 183.
(47) Higashi, G. S.; Fleming, C. G. Patterned Aluminum Growth via Excimer Laser Activated Metalorganic Chemical Vapor Deposition. *Appl. Phys. Lett.* **1986**, *48* (16), 1051−1053.
(48) Abeln, G. C.; Hersam, M. C.; Thompson, D. S.; Hwang, S.-T.; Choi, H.; Moore, J. S.; Lyding, J. W. Approaches to Nanofabrication on Si(100) Surfaces: Selective Area Chemical Vapor Deposition of Metals and Selective Chemisorption of Organic Molecules. *J. Vac. Sci. Technol., B: Microelectron. Process. Phenom.* **1998**, *16* (6), 3874.
(49) McDonnell, S.; Longo, R. C.; Seitz, O.; Ballard, J. B.; Mordi, G.; Dick, D.; Owen, J. H. G.; Randall, J. N.; Kim, J.; Chabal, Y. J.; Cho, K.; Wallace, R. M. Controlling the Atomic Layer Deposition of Titanium Dioxide on Silicon: Dependence on Surface Termination. *J. Phys. Chem. C* **2013**, *117* (39), 20250−20259.
(50) Radamson, H. H.; Kolahdouz, M. Selective Epitaxy Growth of $Si_{1-x}Ge_x$ Layers for MOSFETs and FinFETs. *J. Mater. Sci.: Mater. Electron.* **2015**, *26* (7), 4584−4603.
(51) Kedzierski, J.; Ieong, M.; Nowak, E.; Kanarsky, T. S.; Zhang, Y.; Roy, R.; Boyd, D.; Fried, D.; Wong, H. S. P. Extension and Source/Drain Design for High-Performance FinFET Devices. *IEEE Trans. Electron Devices* **2003**, *50* (4), 952−958.
(52) Gates, S. M.; Greenlief, C. M.; Kulkarni, S. K.; Sawin, H. H. Surface Reactions in Si Chemical Vapor Deposition from Silane. *J. Vac. Sci. Technol., A* **1990**, *8* (3), 2965−2969.
(53) Broadbent, E. K.; Ramiller, C. L. Selective Low Pressure Chemical Vapor Deposition of Tungsten. *J. Electrochem. Soc.* **1984**, *131* (6), 1427−1433.
(54) Gargini, P. A.; Beinglass, I. WOS: Low Resistance Self-Aligned Source, Drain and Gate Transistors. In *Proceedings of the IEEE IEDM Conference*; IEEE: 1981; pp 54−58.
(55) Creighton, J. R.; Parmeter, J. E. Metal CVD for Microelectronic Applications: An Examination of Surface Chemistry and Kinetics. *Crit. Rev. Solid State Mater. Sci.* **1993**, *18* (2), 175−237.
(56) McConica, C. M.; Cooper, K. Tungsten Nucleation on Thermal Oxide during LPCVD of Tungsten by the Hydrogen Reduction of Tungsten Hexafluoride. *J. Electrochem. Soc.* **1988**, *135* (4), 1003.
(57) Creighton, J. R. A. Mechanism for Selectivity Loss during Tungsten CVD. *J. Electrochem. Soc.* **1989**, *136* (1), 271.
(58) Jung, K. H.; Kwong, D. L.; Swenson, M. S.; Boeck, B. Reliability Comparison of Short-Channel MOSFETs with Cobalt Salicide and Titanium Salicide Structures. *Electron. Lett.* **1989**, *25* (2), 96.
(59) Mann, R. W.; Clevenger, L. A.; Agnello, P. D.; White, F. R. Silicides and Local Interconnections for High-Performance VLSI Applications. *IBM J. Res. Dev.* **1995**, *39* (4), 403−417.
(60) Datta, S.; Dutta, S.; Grisafe, B.; Smith, J.; Srinivasa, S.; Ye, H. Back-End-of-Line Compatible Transistors for Monolithic 3-D Integration. *IEEE Micro* **2019**, *39* (6), 8−15.
(61) Gordon, R. G.; Hausmann, D.; Kim, E.; Shepard, J. A Kinetic Model for Step Coverage by Atomic Layer Deposition in Narrow Holes or Trenches. *Chem. Vap. Deposition* **2003**, *9* (2), 73−78.
(62) Wu, Y.; Döhler, D.; Barr, M.; Oks, E.; Wolf, M.; Santinacci, L.; Bachmann, J. Atomic Layer Deposition from Dissolved Precursors. *Nano Lett.* **2015**, *15* (10), 6379−6385.
(63) Dubin, V. M.; Shacham-Diamand, Y.; Zhao, B.; Vasudev, P. K.; Ting, C. H. Selective and Blanket Electroless Copper Deposition for Ultralarge Scale Integration. *J. Electrochem. Soc.* **1997**, *144* (3), 898.
(64) Kim, H. Atomic Layer Deposition of Metal and Nitride Thin Films: Current Research Efforts and Applications for Semiconductor Device Processing. *J. Vac. Sci. Technol., B: Microelectron. Process. Phenom.* **2003**, *21* (6), 2231.
(65) Peng, Q.; Tseng, Y. C.; Darling, S. B.; Elam, J. W. Nanoscopic Patterned Materials with Tunable Dimensions via Atomic Layer Deposition on Block Copolymers. *Adv. Mater.* **2010**, *22* (45), 5129−5133.
(66) Peng, Q.; Tseng, Y. C.; Darling, S. B.; Elam, J. W. A Route to Nanoscopic Materials via Sequential Infiltration Synthesis on Block Copolymer Templates. *ACS Nano* **2011**, *5* (6), 4600−4606.
(67) Dandley, E. C.; Needham, C. D.; Williams, P. S.; Brozena, A. H.; Oldham, C. J.; Parsons, G. N. Temperature-Dependent Reaction between Trimethylaluminum and Poly(Methyl Methacrylate) during Sequential Vapor Infiltration: Experimental and Ab Initio Analysis. *J. Mater. Chem. C* **2014**, *2* (44), 9416−9424.
(68) Dandley, E. C.; Lemaire, P. C.; Zhu, Z.; Yoon, A.; Sheet, L.; Parsons, G. N. Wafer-Scale Selective-Area Deposition of Nanoscale Metal Oxide Features Using Vapor Saturation into Patterned Poly(Methyl Methacrylate) Templates. *Adv. Mater. Interfaces* **2016**, *3* (2), 1500431.

https://dx.doi.org/10.1021/acs.chemmater.0c00722
Chem. Mater. XXXX, XXX, XXX−XXX

(69) Zhang, Y.; D'Ambra, C. A.; Katsumata, R.; Burns, R. L.; Somervell, M. H.; Segalman, R. A.; Hawker, C. J.; Bates, C. M. Rapid and Selective Deposition of Patterned Thin Films on Heterogeneous Substrates via Spin Coating. *ACS Appl. Mater. Interfaces* **2019**, *11* (23), 21177−21183.
(70) Ek, M.; Filler, M. A. Atomic-Scale Choreography of Vapor−Liquid−Solid Nanowire Growth. *Acc. Chem. Res.* **2018**, *51* (1), 118−126.
(71) Mohabir, A. T.; Tutuncuoglu, G.; Weiss, T.; Vogel, E. M.; Filler, M. A. Bottom-Up Masking of Si/Ge Surfaces and Nanowire Heterostructures via Surface-Initiated Polymerization and Selective Etching. *ACS Nano* **2020**, *14* (1), 282−288.
(72) Jonas, U.; del Campo, A.; Kruger, C.; Glasser, G.; Boos, D. Colloidal Assemblies on Patterned Silane Layers. *Proc. Natl. Acad. Sci. U. S. A.* **2002**, *99* (8), 5034−5039.
(73) Li, J. R.; Lusker, K. L.; Yu, J. J.; Garno, J. C. Engineering the Spatial Selectivity of Surfaces at the Nanoscale Using Particle Lithography Combined with Vapor Deposition of Organosilanes. *ACS Nano* **2009**, *3* (7), 2023−2035.
(74) Seeman, N. C. DNA in a Material World. *Nature* **2003**, *421* (6921), 427−431.
(75) Yan, H.; Park, S. H.; Finkelstein, G.; Reif, J. H.; LaBean, T. H. DNA-Templated Self-Assembly of Protein Arrays and Highly Conductive Nanowires. *Science* **2003**, *301* (5641), 1882−1884.
(76) Rothemund, P. W. K. Folding DNA to Create Nanoscale Shapes and Patterns. *Nature* **2006**, *440* (7082), 297−302.
(77) Venables, J. A. Rate Equation Approaches to Thin Film Nucleation Kinetics. *Philos. Mag.* **1973**, *27*, 697−738.
(78) Venables, J. A.; Spiller, G. D. T.; Hanbucken, M. Nucleation and Growth of Thin Films. *Rep. Prog. Phys.* **1984**, *47* (4), 399−459.
(79) Smith, D. L. *Thin Film Deposition, Principles and Practice*; McGraw-Hill: 1995; pp 119−156.
(80) Freeman, D. L.; Doll, J. D. The Influence of Diffusion on Surface Reaction Kinetics. *J. Chem. Phys.* **1983**, *78* (10), 6002−6009.
(81) Carroll, K. M.; Knoll, A. W.; Wolf, H.; Duerig, U. Explaining the Transition from Diffusion Limited to Reaction Limited Surface Assembly of Molecular Species through Spatial Variations. *Langmuir* **2018**, *34* (1), 73.
(82) Claassen, W. A. P.; Bloem, J. The Nucleation of CVD Silicon on SiO_2 and Si_3N_4 Substrates: I. The SiH_4-HCl-H_2 System at High Temperatures. *J. Electrochem. Soc.* **1980**, *127* (1), 194−202.
(83) Grillo, F.; Van Bui, H.; Moulijn, J. A.; Kreutzer, M. T.; van Ommen, J. R. Understanding and Controlling the Aggregative Growth of Platinum Nanoparticles in Atomic Layer Deposition: An Avenue to Size Selection. *J. Phys. Chem. Lett.* **2017**, *8* (5), 975−983.
(84) Soethoudt, J.; Grillo, F.; Marques, E. A.; van Ommen, J. R.; Tomczak, Y.; Nyns, L.; Van Elshocht, S.; Delabie, A. Diffusion-Mediated Growth and Size-Dependent Nanoparticle Reactivity during Ruthenium Atomic Layer Deposition on Dielectric Substrates. *Adv. Mater. Interfaces* **2018**, *5* (24), 1800870.
(85) Alam, M. A.; Green, M. L. Mathematical Description of Atomic Layer Deposition and Its Application to the Nucleation and Growth of HfO_2 Gate Dielectric Layers. *J. Appl. Phys.* **2003**, *94* (5), 3403−3413.
(86) Longo, R. C.; McDonnell, S.; Dick, D.; Wallace, R. M.; Chabal, Y. J.; Owen, J. H. G.; Ballard, J. B.; Randall, J. N.; Cho, K. Selectivity of Metal Oxide Atomic Layer Deposition on Hydrogen Terminated and Oxidized Si(001)-(2 × 1) Surface. *J. Vac. Sci. Technol., B: Nanotechnol. Microelectron.: Mater., Process., Meas., Phenom.* **2014**, *32* (3), 03D112.
(87) Nanayakkara, C. E.; Vega, A.; Liu, G.; Dezelah, C. L.; Kanjolia, R. K.; Chabal, Y. J. Role of Initial Precursor Chemisorption on Incubation Delay for Molybdenum Oxide Atomic Layer Deposition. *Chem. Mater.* **2016**, *28* (23), 8591−8597.
(88) Fitch, J. T.; Denning, D. J.; Beard, D. The Pattern Dependence of Selectivity in Low Pressure Selective Epitaxial Silicon Growth. *J. Electron. Mater.* **1992**, *21* (4), 455−462.
(89) Boland, J. J.; Parsons, G. N. Bond Selectivity in Silicon Film Growth. *Science* **1992**, *256* (5061), 1304−1306.
(90) Patwardhan, S.; Cao, D. H.; Schatz, G. C.; Martinson, A. B. F. Atomic Layer Deposition Nucleation on Isolated Self-Assembled Monolayer Functional Groups: A Combined DFT and Experimental Study. *ACS Appl. Energy Mater.* **2019**, *2* (7), 4618−4628.
(91) Kim, K.; Lee, H. B. R.; Johnson, R. W.; Tanskanen, J. T.; Liu, N.; Kim, M. G.; Pang, C.; Ahn, C.; Bent, S. F.; Bao, Z. Selective Metal Deposition at Graphene Line Defects by Atomic Layer Deposition. *Nat. Commun.* **2014**, *5*, 4781.
(92) Mameli, A.; Merkx, M. J. M.; Karasulu, B.; Roozeboom, F.; Kessels, W. E. M. M.; Mackus, A. J. M. Area-Selective Atomic Layer Deposition of SiO_2 Using Acetylacetone as a Chemoselective Inhibitor in an ABC-Type Cycle. *ACS Nano* **2017**, *11* (9), 9303−9311.
(93) Yan, M.; Koide, Y.; Babcock, J. R.; Markworth, P. R.; Belot, J. A.; Marks, T. J.; Chang, R. P. H. Selective-Area Atomic Layer Epitaxy Growth of ZnO Features on Soft Lithography-Patterned Substrates. *Appl. Phys. Lett.* **2001**, *79* (11), 1709−1711.
(94) Chopra, S. N.; Zhang, Z.; Kaihlanen, C.; Ekerdt, J. G. Selective Growth of Titanium Nitride on HfO_2 across Nanolines and Nanopillars. *Chem. Mater.* **2016**, *28* (14), 4928−4934.
(95) Stevens, E.; Tomczak, Y.; Chan, B. T.; Altamirano Sanchez, E.; Parsons, G. N.; Delabie, A. Area-Selective Atomic Layer Deposition of TiN, TiO_2, and HfO_2 on Silicon Nitride with Inhibition on Amorphous Carbon. *Chem. Mater.* **2018**, *30* (10), 3223−3232.
(96) Song, S. K.; Saare, H.; Parsons, G. N. Integrated Isothermal Atomic Layer Deposition/Atomic Layer Etching Supercycles for Area-Selective Deposition of TiO_2. *Chem. Mater.* **2019**, *31* (13), 4793−4804.
(97) Creighton, J. R. The Surface Chemistry and Kinetics of Tungsten Chemical Vapor Deposition and Selectivity Loss. *Thin Solid Films* **1994**, *241* (1−2), 310−317.
(98) Saib, M.; Moussa, A.; Charley, A.-L.; Leray, P.; Hung, J.; Koret, R.; Turovets, I.; Ger, A.; Deng, S.; Illiberi, A.; Maes, J. W.; Woodworth, G.; Strauss, M. Scatterometry and AFM Measurement Combination for Area Selective Deposition Process Characterization. In *Metrology, Inspection, and Process Control for Microlithography XXXIII*; Adan, O., Ukraintsev, V. A., Eds.; SPIE: 2019; p 57.
(99) Puurunen, R. L.; Vandervorst, W.; Besling, W. F. A.; Richard, O.; Bender, H.; Conard, T.; Zhao, C.; Delabie, A.; Caymax, M.; De Gendt, S.; Heyns, M.; Viitanen, M. M.; De Ridder, M.; Brongersma, H. H.; Tamminga, Y.; Dao, T.; De Win, T.; Verheijen, M.; Kaiser, M.; Tuominen, M. Island Growth in the Atomic Layer Deposition of Zirconium Oxide and Aluminum Oxide on Hydrogen-Terminated Silicon: Growth Mode Modeling and Transmission Electron Microscopy. *J. Appl. Phys.* **2004**, *96* (9), 4878−4889.
(100) Nilsen, O.; Mohn, C. E.; Kjekshus, A.; Fjellvåg, H. Analytical Model for Island Growth in Atomic Layer Deposition Using Geometrical Principles. *J. Appl. Phys.* **2007**, *102* (2), 024906.
(101) Mameli, A.; Karasulu, B.; Verheijen, M. A.; Barcones, B.; Macco, B.; Mackus, A. J. M.; Kessels, W. M. M. E.; Roozeboom, F. Area-Selective Atomic Layer Deposition of ZnO by Area Activation Using Electron Beam-Induced Deposition. *Chem. Mater.* **2019**, *31* (4), 1250−1257.
(102) Mogab, C. J. The Loading Effect in Plasma Etching. *J. Electrochem. Soc.* **1977**, *124* (8), 1262−1268.
(103) Gottscho, R. A. Microscopic Uniformity in Plasma Etching. *J. Vac. Sci. Technol., B: Microelectron. Process. Phenom.* **1992**, *10* (5), 2133.
(104) Holleman, J.; Hasper, A.; Kleijn, C. R. Loading Effects on Kinetical and Electrical Aspects of Silane-Reduced Low-Pressure Chemical Vapor Deposited Selective Tungsten. *J. Electrochem. Soc.* **1993**, *140* (3), 818.
(105) Qin, C.; Wang, G.; Kolahdouz, M.; Luo, J.; Yin, H.; Yang, P.; Li, J.; Zhu, H.; Chao, Z.; Ye, T.; Radamson, H. H. Impact of Pattern Dependency of SiGe Layers Grown Selectively in Source/Drain on the Performance of 14 nm Node FinFETs. *Solid-State Electron.* **2016**, *124*, 10−15.
(106) Loo, R.; Caymax, M. Avoiding Loading Effects and Facet Growth: Key Parameters for a Successful Implementation of Selective Epitaxial SiGe Deposition for HBT-BiCMOS and High-Mobility Hetero-Channel PMOS Devices. *Appl. Surf. Sci.* **2004**, *224* (1−4), 24−30.
(107) Samavedam, S. B.; Dip, A.; Phillips, A. M.; Tobin, P. J.; Mihopolous, T.; Taylor, W. J.; Adetutu, O. Elevated Source Drain

https://dx.doi.org/10.1021/acs.chemmater.0c00722
Chem. Mater. XXXX, XXX, XXX−XXX

Devices Using Silicon Selective Epitaxial Growth. *J. Vac. Sci. Technol., B: Microelectron. Process. Phenom.* **2000**, *18* (3), 1244−1250.
(108) Loo, R.; Hikavyy, A. Y.; Witters, L.; Schulze, A.; Arimura, H.; Cott, D.; Mitard, J.; Porret, C.; Mertens, H.; Ryan, P.; Wall, J.; Matney, K.; Wormington, M.; Favia, P.; Richard, O.; Bender, H.; Thean, A.; Horiguchi, N.; Mocuta, D.; Collaert, N. Processing Technologies for Advanced Ge Devices. *ECS J. Solid State Sci. Technol.* **2017**, *6* (1), P14−P20.
(109) Tolle, J.; Margetis, J. Selective Epitaxial Growth. Presented at 4th Area Selective Deposition Workshop (ASD2019); Leuven, Belgium, 2019.
(110) Hartmann, J. M.; Benevent, V.; André, A.; Sirisopanaporn, C.; Veillerot, M.; Samson, M. P.; Barraud, S.; Essa, Z.; Sermage, B. Very Low Temperature (Cyclic) Deposition/Etch of in Situ Boron-Doped SiGe Raised Sources and Drains. *ECS J. Solid State Sci. Technol.* **2014**, *3* (11), P382−P390.
(111) Collaert, N.; Rooyackers, R.; Hikavyy, A.; Dixit, A.; Leys, F.; Verheyen, P.; Loo, R.; Jurczak, M.; Biesemans, S. Multi-Gate Devices for the 32 nm Technology Node and beyond: Challenges for Selective Epitaxial Growth. *Thin Solid Films* **2008**, *517* (1), 101−104.
(112) Wang, G.; Qin, C.; Yin, H.; Luo, J.; Duan, N.; Yang, P.; Gao, X.; Yang, T.; Li, J.; Yan, J.; Zhu, H.; Wang, W.; Chen, D.; Ye, T.; Zhao, C.; Radamson, H. H. Study of SiGe Selective Epitaxial Process Integration with High-k and Metal Gate for 16/14 nm Nodes FinFET Technology. *Microelectron. Eng.* **2016**, *163*, 49−54.
(113) Simon, A. H.; Bolom, T.; Niu, C.; Baumann, F. H.; Hu, C.; Parks, C.; Nag, J.; Kim, H.; Lee, J. Y.; Yang, C.; Nguyen, S.; Shobha, H. K.; Nogami, T.; Guggilla, S.; Ren, J.; Sabens, D.; AuBuchon, J. F. Electromigration Comparison of Selective CVD Cobalt Capping with PVD Ta(N) and CVD Cobalt Liners on 22nm-Groundrule Dual-Damascene Cu Interconnects. In *2013 IEEE International Reliability Physics Symposium (IRPS)*; IEEE: 2013; pp 3F.4.1−3F.4.6.
(114) Yang, C. C.; Baumann, F.; Wang, P. C.; Lee, S. Y.; Ma, P.; Aubuchon, J.; Edelstein, D. Dependence of Cu Electromigration Resistance on Selectively Deposited CVD Co Cap Thickness. *Microelectron. Eng.* **2013**, *106*, 214−218.
(115) Altamirano-Sanchez, E.; Chan, B. T.; Delabie, A.; Armini, S.; Scheer, S.; Area Selective Deposition Challenges and Opportunities for Patterning Solution. Preseneted at 4th Area Selective Deposition Workshop (ASD2019); Leuven, Belgium, 2019.
(116) Auth, C.; Aliyarukunju, A.; Asoro, M.; Bergstrom, D.; Bhagwat, V.; Birdsall, J.; Bisnik, N.; Buehler, M.; Chikarmane, V.; Ding, G.; Fu, Q.; Gomez, H.; Han, W.; Hanken, D.; Haran, M.; Hattendorf, M.; Heussner, R.; Hiramatsu, H.; Ho, B.; Jaloviar, S.; Jin, I.; Joshi, S.; Kirby, S.; Kosaraju, S.; Kothari, H.; Leatherman, G.; Lee, K.; Leib, J.; Madhavan, A.; Marla, K.; Meyer, H.; Mule, T.; Parker, C.; Parthasarathy, S.; Pelto, C.; Pipes, L.; Post, I.; Prince, M.; Rahman, A.; Rajamani, S.; Saha, A.; Santos, J. D.; Sharma, M.; Sharma, V.; Shin, J.; Sinha, P.; Smith, P.; Sprinkle, M.; Amour, A. S.; Staus, C.; Suri, R.; Towner, D.; Tripathi, A.; Tura, A.; Ward, C.; Yeoh, A. A 10nm High Performance and Low-Power CMOS Technology Featuring 3rd Generation FinFET Transistors, Self-Aligned Quad Patterning, Contact over Active Gate and Cobalt Local Interconnects. *Technol. Dig. - Int. Electron Devices Meet. IEDM* **2017**, 29.1.1−29.1.4.
(117) Maboudian, R.; Ashurst, W. R.; Carraro, C. Self-Assembled Monolayers as Anti-Stiction Coatings for MEMS: Characteristics and Recent Developments. *Sens. Actuators, A* **2000**, *82* (1), 219−223.
(118) Zhuang, Y. X.; Hansen, O.; Knieling, T.; Wang, C.; Rombach, P.; Lang, W.; Benecke, W.; Kehlenbeck, M.; Koblitz, J. Thermal Stability of Vapor Phase Deposited Self-Assembled Monolayers for MEMS Anti-Stiction. *J. Micromech. Microeng.* **2006**, *16* (11), 2259−2264.
(119) Wallace, C. M. Material Requirements for Self-Aligned Patterning − a Lithographer's Perspective. Presented at AVS 61st International Symposium and Exhibition, 2014.
(120) Mohanty, N.; Smith, J. T.; Huli, L.; Pereira, C.; Raley, A.; Kal, S.; Fonseca, C.; Sun, X.; Burns, R. L.; Farrell, R. A.; Hetzer, D. R.; Metz, A. W.; Ko, A.; Scheer, S. A.; Biolsi, P.; DeVillers, A. EPE Improvement Thru Self-Alignment via Multi-Color Material Integration. *Proc. SPIE* **2017**, *10147*, 1014704.
(121) Clark, R. D. Selective and Self-Limited Thin Film Processes for the Atomic Scale Era. Presented at 2019 Symposium VLSI Technology and Circuits, 2019.
(122) Briggs, B. D.; Peethala, C. B.; Rath, D. L.; Lee, J.; Nguyen, S.; Licausi, N. V.; McLaughlin, P. S.; You, H.; Sil, D.; Lanzillo, N. A.; Huang, H.; Patlolla, R.; Haigh, T.; Xu, Y.; Park, C.; Kerber, P.; Shobha, H. K.; Kim, Y.; Demarest, J.; Li, J.; Lian, G.; Ali, M.; Le, C. T.; Ryan, E. T.; Clevenger, L. A.; Canaperi, D. F.; Standaert, T. E.; Bonilla, G.; Huang, E. Fully Aligned via Integration for Extendibility of Interconnects to beyond the 7 nm Node. *Technol. Dig. - Int. Electron Devices Meet. IEDM* **2017**, 14.2.1−14.2.4.
(123) Lu, J.; Liu, B.; Greeley, J. P.; Feng, Z.; Libera, J. A.; Lei, Y.; Bedzyk, M. J.; Stair, P. C.; Elam, J. W. Porous Alumina Protective Coatings on Palladium Nanoparticles by Self-Poisoned Atomic Layer Deposition. *Chem. Mater.* **2012**, *24* (11), 2047−2055.
(124) Lu, J.; Fu, B.; Kung, M. C.; Xiao, G.; Elam, J. W.; Kung, H. H.; Stair, P. C. Coking- and Sintering-Resistant Palladium Catalysts Achieved Through Atomic Layer Deposition. *Science* **2012**, *335* (6073), 1205−1208.
(125) Cao, K.; Zhu, Q.; Shan, B.; Chen, R. Controlled Synthesis of Pd/Pt Core Shell Nanoparticles Using Area-Selective Atomic Layer Deposition. *Sci. Rep.* **2015**, *5* (1), 8470.
(126) Cao, K.; Shi, L.; Gong, M.; Cai, J.; Liu, X.; Chu, S.; Lang, Y.; Shan, B.; Chen, R. Nanofence Stabilized Platinum Nanoparticles Catalyst via Facet-Selective Atomic Layer Deposition. *Small* **2017**, *13* (32), 1700648.
(127) Li, S.; Waag, A. GaN Based Nanorods for Solid State Lighting. *J. Appl. Phys.* **2012**, *111* (7), 071101.
(128) Madaria, A. R.; Yao, M.; Chi, C.; Huang, N.; Lin, C.; Li, R.; Povinelli, M. L.; Dapkus, P. D.; Zhou, C. Toward Optimized Light Utilization in Nanowire Arrays Using Scalable Nanosphere Lithography and Selected Area Growth. *Nano Lett.* **2012**, *12* (6), 2839−2845.
(129) Cho, Y. J.; Shin, W. C.; Chang, H. S. Selective Deposition Contact Patterning Using Atomic Layer Deposition for the Fabrication of Crystalline Silicon Solar Cells. *Thin Solid Films* **2014**, *568* (1), 1−5.
(130) Parsons, G. N. Enhanced Mobility Top-Gate Amorphous Silicon Thin-Film Transistor with Selectively Deposited Source/Drain Contacts. *IEEE Electron Device Lett.* **1992**, *13* (2), 80.
(131) Yang, C. S.; Read, W. W.; Arthur, C.; Srinivasan, E.; Parsons, G. N. Self-Aligned Gate and Source Drain Contacts in Inverted-Staggered a-Si:H Thin-Film Transistors Fabricated Using Selective Area Silicon PECVD. *IEEE Electron Device Lett.* **1998**, *19* (6), 180−182.
(132) Roozeboom, F.; van den Bruele, F.; Creyghton, Y.; Poodt, P.; Kessels, W. M. M. Cyclic Etch/Passivation-Deposition as an All-Spatial Concept toward High-Rate Room Temperature Atomic Layer Etching. *ECS J. Solid State Sci. Technol.* **2015**, *4* (6), N5067−N5076.
(133) Nelson, S. F.; Ellinger, C. R.; Levy, D. H. Improving Yield and Performance in ZnO Thin-Film Transistors Made Using Selective Area Deposition. *ACS Appl. Mater. Interfaces* **2015**, *7* (4), 2754−2759.
(134) Färm, E.; Kemell, M.; Ritala, M.; Leskela, M. Selective-Area Atomic Layer Deposition Using Poly (Methyl Methacrylate) Films as Mask Layers. *J. Phys. Chem. C* **2008**, *112*, 15791−15795.
(135) Sinha, A.; Hess, D. W.; Henderson, C. L. Area-Selective ALD of Titanium Dioxide Using Lithographically Defined Poly(Methyl Methacrylate) Films. *J. Electrochem. Soc.* **2006**, *153* (5), G465.
(136) Bobb-Semple, D.; Nardi, K. L.; Draeger, N.; Hausmann, D. M.; Bent, S. F. Area-Selective Atomic Layer Deposition Assisted by Self-Assembled Monolayers: A Comparison of Cu, Co, W, and Ru. *Chem. Mater.* **2019**, *31* (5), 1635−1645.
(137) Khan, R.; Shong, B.; Ko, B. G.; Lee, J. K.; Lee, H.; Park, J. Y.; Oh, I. K.; Raya, S. S.; Hong, H. M.; Chung, K. B.; Luber, E. J.; Kim, Y. S.; Lee, C. H.; Kim, W. H.; Lee, H. B. R. Area-Selective Atomic Layer Deposition Using Si Precursors as Inhibitors. *Chem. Mater.* **2018**, *30* (21), 7603−7610.
(138) Suh, T.; Yang, Y.; Zhao, P.; Lao, K. U.; Ko, H. Y.; Wong, J.; Distasio, R. A.; Engstrom, J. R. Competitive Adsorption as a Route to

https://dx.doi.org/10.1021/acs.chemmater.0c00722
Chem. Mater. XXXX, XXX, XXX−XXX

Area-Selective Deposition. *ACS Appl. Mater. Interfaces* **2020**, *12* (8), 9989−9999.
(139) Miikkulainen, V.; Väyrynen, K.; Kilpi, V.; Han, Z.; Vehkamäki, M.; Mizohata, K.; Räisänen, J.; Ritala, M. Photo-Assisted ALD: Process Development and Application Perspectives. *ECS Trans.* **2017**, *80* (3), 49−60.
(140) Wojtecki, R.; Mettry, M.; Fine Nathel, N. F.; Friz, A.; De Silva, A.; Arellano, N.; Shobha, H. Fifteen Nanometer Resolved Patterns in Selective Area Atomic Layer Deposition - Defectivity Reduction by Monolayer Design. *ACS Appl. Mater. Interfaces* **2018**, *10*, 38630−38637.
(141) Wojtecki, R. J.; DeSilva, A.; Nathel, N. F. F.; Shobha, H.; Arellano, N.; Friz, A.; Wallraff, G. Reactive Monolayers in Directed Additive Manufacturing - Area Selective Atomic Layer Deposition. *J. Photopolym. Sci. Technol.* **2018**, *31* (3), 431−436.
(142) Kumar, N.; Yanguas-Gil, A.; Daly, S. R.; Girolami, G. S.; Abelson, J. R. Growth Inhibition to Enhanced Conformal Coverage in Thin Film Chemical Vapor Deposition. *J. Am. Chem. Soc.* **2008**, *130* (52), 17660−17661.
(143) Talukdar, T. K.; Girolami, G. S.; Abelson, J. R. Seamless Fill of Deep Trenches by Chemical Vapor Deposition: Use of a Molecular Growth Inhibitor to Eliminate Pinch-Off. *J. Vac. Sci. Technol., A* **2019**, *37* (2), 021509.
(144) Singh, J. A.; Thissen, N. F. W.; Kim, W.; Johnson, H.; Kessels, W. M. M. M.; Bol, A. A.; Bent, S. F.; Mackus, A. J. M. Area-Selective Atomic Layer Deposition of Metal Oxides on Noble Metals through Catalytic Oxygen Activation. *Chem. Mater.* **2018**, *30* (3), 663−670.
(145) Mackus, A. J. M.; Dielissen, S. A. F.; Mulders, J. J. L.; Kessels, W. M. M. Nanopatterning by Direct-Write Atomic Layer Deposition. *Nanoscale* **2012**, *4* (15), 4477.
(146) Chalker, P. R.; Marshall, P. A.; Dawson, K.; Brunell, I. F.; Sutcliffe, C. J.; Potter, R. J. Vacuum Ultraviolet Photochemical Selective Area Atomic Layer Deposition of Al_2O_3 Dielectrics. *AIP Adv.* **2015**, *5* (1), 017115.
(147) Henke, T.; Knaut, M.; Hossbach, C.; Geidel, M.; Rebohle, L.; Albert, M.; Skorupa, W.; Bartha, J. W. Flash-Enhanced Atomic Layer Deposition: Basics, Opportunities, Review, and Principal Studies on the Flash-Enhanced Growth of Thin Films. *ECS J. Solid State Sci. Technol.* **2015**, *4* (7), P277−P287.
(148) Kim, W. H.; Minaye Hashemi, F. S.; Mackus, A. J. M.; Singh, J.; Kim, Y.; Bobb-Semple, D.; Fan, Y.; Kaufman-Osborn, T.; Godet, L.; Bent, S. F. A Process for Topographically Selective Deposition on 3D Nanostructures by Ion Implantation. *ACS Nano* **2016**, *10* (4), 4451−4458.
(149) Bonvalot, M.; Bsiesy, A.; Chaker, A.; Posseme, N.; Vallat, R.; Vallee, C.; Pesce, V.; Gassilloud, R.; Belahcen, S. Topographically Selective Deposition. *Appl. Phys. Lett.* **2019**, *114* (4), 043101.
(150) Hashemi, F. S. M.; Bent, S. F. Sequential Regeneration of Self-Assembled Monolayers for Highly Selective Atomic Layer Deposition. *Adv. Mater. Interfaces* **2016**, *3* (21), 1600464.
(151) Vallat, R.; Gassilloud, R.; Salicio, O.; El Hajjam, K.; Molas, G.; Pelissier, B.; Vallée, C. Area Selective Deposition of TiO_2 by Intercalation of Plasma Etching Cycles in PEALD Process: A Bottom up Approach for the Simplification of 3D Integration Scheme. *J. Vac. Sci. Technol., A* **2019**, *37* (2), 020918.
(152) Vallat, R.; Gassilloud, R.; Eychenne, B.; Vallée, C. Selective Deposition of Ta_2O_5 by Adding Plasma Etching Super-Cycles in Plasma Enhanced Atomic Layer Deposition Steps. *J. Vac. Sci. Technol., A* **2017**, *35* (1), 01B104.
(153) Vos, M. F. J.; Chopra, S. N.; Verheijen, M. A.; Ekerdt, J. G.; Agarwal, S.; Kessels, W. M. M.; Mackus, A. J. M. Area-Selective Deposition of Ruthenium by Combining Atomic Layer Deposition and Selective Etching. *Chem. Mater.* **2019**, *31* (11), 3878−3882.
(154) Reisman, A. Selective Tungsten on Silicon by the Alternating Cyclic, AC, Hydrogen Reduction of WF_6. *J. Electrochem. Soc.* **1990**, *137* (2), 722.
(155) Parsons, G. N. Selective Deposition of Silicon by Plasma-Enhanced Chemical Vapor Deposition Using Pulsed Silane Flow. *Appl. Phys. Lett.* **1991**, *59* (20), 2546−2548.
(156) Frank, M. M.; Chabal, Y. J.; Green, M. L.; Delabie, A.; Brijs, B.; Wilk, G. D.; Ho, M. Y.; Da Rosa, E. B. O. O.; Baumvol, I. J. R. R.; Stedile, F. C. Enhanced Initial Growth of Atomic-Layer-Deposited Metal Oxides on Hydrogen-Terminated Silicon. *Appl. Phys. Lett.* **2003**, *83* (4), 740−742.
(157) Lin, R.-Z.; Cheng, K.-Y.; Pan, F.-M.; Sheu, J.-T. Selective Deposition of Multiple Sensing Materials on Si Nanobelt Devices through Plasma-Enhanced Chemical Vapor Deposition and Device-Localized Joule Heating. *ACS Appl. Mater. Interfaces* **2017**, *9* (46), 39935−39939.
(158) Alaboson, J. M. P. P.; Wang, Q. H.; Emery, J. D.; Lipson, A. L.; Bedzyk, M. J.; Elam, J. W.; Pellin, M. J.; Hersam, M. C. Seeding Atomic Layer Deposition of High-k Dielectrics on Epitaxial Graphene with Organic Self-Assembled Monolayers. *ACS Nano* **2011**, *5* (6), 5223−5232.
(159) Biyikli, N.; Haider, A.; Deminskyi, P.; Yilmaz, M. Self-Aligned Nanoscale Processing Solutions via Selective Atomic Layer Deposition of Oxide, Nitride, and Metallic Films. In *Low-Dimensional Materials and Devices 2017*; Proceedings of SPIE; Kobayashi, N. P., Talin, A. A., Davydov, V. A., Islam, M. S., Eds.; SPIE: 2017; Vol. *10349*, p 20.
(160) Haider, A.; Deminskyi, P.; Khan, T. M.; Eren, H.; Biyikli, N. Area-Selective Atomic Layer Deposition Using Inductively Coupled Plasma Polymerized Fluorocarbon Layer: A Case Study for Metal-Oxides. *J. Phys. Chem. C* **2016**, *120* (46), 26393−26401.
(161) Färm, E.; Kemell, M.; Santala, E.; Ritala, M.; Leskelä, M. Selective-Area Atomic Layer Deposition Using Poly(Vinyl Pyrrolidone) as a Passivation Layer. *J. Electrochem. Soc.* **2010**, *157* (1), K10.
(162) Seo, S.; Yeo, B. C.; Han, S. S.; Yoon, C. M.; Yang, J. Y.; Yoon, J.; Yoo, C.; Kim, H. H.; Lee, Y.; Lee, S. J.; Myoung, J.-M.; Lee, H.-B.-R.; Kim, W.-H.; Oh, I.-K.; Kim, H. H. Reaction Mechanism of Area-Selective Atomic Layer Deposition for Al_2O_3 Nanopatterns. *ACS Appl. Mater. Interfaces* **2017**, *9* (47), 41607−41617.
(163) Biercuk, M. J.; Monsma, D. J.; Marcus, C. M.; Becker, J. S.; Gordon, R. G. Low-Temperature Atomic-Layer-Deposition Lift-off Method for Microelectronic and Nanoelectronic Applications. *Appl. Phys. Lett.* **2003**, *83* (12), 2405−2407.
(164) Sampson, M. D.; Emery, J. D.; Pellin, M. J.; Martinson, A. B. F. Inhibiting Metal Oxide Atomic Layer Deposition: Beyond Zinc Oxide. *ACS Appl. Mater. Interfaces* **2017**, *9* (39), 33429−33436.
(165) Minaye Hashemi, F. S.; Prasittichai, C.; Bent, S. F. Self-Correcting Process for High Quality Patterning by Atomic Layer Deposition. *ACS Nano* **2015**, *9* (9), 8710−8717.
(166) Dong, W.; Zhang, K.; Zhang, Y.; Wei, T.; Sun, Y.; Chen, X.; Dai, N. Application of Three-Dimensionally Area-Selective Atomic Layer Deposition for Selectively Coating the Vertical Surfaces of Standing Nanopillars. *Sci. Rep.* **2015**, *4*, 4458.
(167) George, A.; Knez, M.; Hlawacek, G.; Hagedoorn, D.; Verputten, H. H. J.; Van Gastel, R.; Ten Elshof, J. E. Nanoscale Patterning of Organosilane Molecular Thin Films from the Gas Phase and Its Applications: Fabrication of Multifunctional Surfaces and Large Area Molecular Templates for Site-Selective Material Deposition. *Langmuir* **2012**, *28* (5), 3045−3052.
(168) Ellinger, C. R.; Nelson, S. F. Selective Area Spatial Atomic Layer Deposition of ZnO, Al_2O_3, and Aluminum-Doped ZnO Using Poly(Vinyl Pyrrolidone). *Chem. Mater.* **2014**, *26* (4), 1514−1522.
(169) Hashemi, F. S. M.; Prasittichai, C.; Bent, S. F. A New Resist for Area Selective Atomic and Molecular Layer Deposition on Metal-Dielectric Patterns. *J. Phys. Chem. C* **2014**, *118* (20), 10957−10962.
(170) Avila, J. R.; Demarco, E. J.; Emery, J. D.; Farha, O. K.; Pellin, M. J.; Hupp, J. T.; Martinson, A. B. F. Real-Time Observation of Atomic Layer Deposition Inhibition: Metal Oxide Growth on Self-Assembled Alkanethiols. *ACS Appl. Mater. Interfaces* **2014**, *6* (15), 11891−11898.
(171) Minaye Hashemi, F. S.; Birchansky, B. R.; Bent, S. F. Selective Deposition of Dielectrics: Limits and Advantages of Alkanethiol Blocking Agents on Metal−Dielectric Patterns. *ACS Appl. Mater. Interfaces* **2016**, *8* (48), 33264−33272.
(172) Ras, R. H. A.; Sahramo, E.; Malm, J.; Raula, J.; Karppinen, M. Blocking the Lateral Film Growth at the Nanoscale in Area-Selective

https://dx.doi.org/10.1021/acs.chemmater.0c00722
Chem. Mater. XXXX, XXX, XXX−XXX

Atomic Layer Deposition. *J. Am. Chem. Soc.* **2008**, *130* (34), 11252−11253.
(173) Gallington, L. C.; Kim, I. S.; Liu, W. G.; Yakovenko, A. A.; Platero-Prats, A. E.; Li, Z.; Wang, T. C.; Hupp, J. T.; Farha, O. K.; Truhlar, D. G.; Martinson, A. B. F.; Chapman, K. W. Regioselective Atomic Layer Deposition in Metal-Organic Frameworks Directed by Dispersion Interactions. *J. Am. Chem. Soc.* **2016**, *138* (41), 13513−13516.
(174) Methaapanon, R.; Bent, S. F. Comparative Study of Titanium Dioxide Atomic Layer Deposition on Silicon Dioxide and Hydrogen-Terminated Silicon. *J. Phys. Chem. C* **2010**, *114* (23), 10498−10504.
(175) Ardalan, P.; Musgrave, C. B.; Bent, S. F. Effects of Surface Functionalization on Titanium Dioxide Atomic Layer Deposition on Ge Surfaces. *ECS Transactions* **2009**, *25*, 131−139.
(176) Sinha, A.; Hess, D. W.; Henderson, C. L. Area Selective Atomic Layer Deposition of Titanium Dioxide: Effect of Precursor Chemistry. *J. Vac. Sci. Technol. B Microelectron. Nanom. Struct.* **2006**, *24* (6), 2523.
(177) Sinha, A.; Hess, D. W.; Henderson, C. L. Transport Behavior of Atomic Layer Deposition Precursors through Polymer Masking Layers: Influence on Area Selective Atomic Layer Deposition. *J. Vac. Sci. Technol. B Microelectron. Nanom. Struct.* **2007**, *25* (5), 1721.
(178) Ghosal, S.; Baumann, T. F.; King, J. S.; Kucheyev, S. O.; Wang, Y.; Worsley, M. A.; Biener, J.; Bent, S. F.; Hamza, V. A. Controlling Atomic Layer Deposition of TiO_2 in Aerogels through Surface Functionalization. *Chem. Mater.* **2009**, *21* (9), 1989−1992.
(179) Finnie, K. S.; Triani, G.; Short, K. T.; Mitchell, D. R. G.; Attard, D. J.; Bartlett, J. R.; Barbé, C. J. Influence of Si(100) Surface Pretreatment on the Morphology of TiO_2 Films Grown by Atomic Layer Deposition. *Thin Solid Films* **2003**, *440* (1−2), 109−116.
(180) Atanasov, S. E.; Kalanyan, B.; Parsons, G. N. Inherent Substrate-Dependent Growth Initiation and Selective-Area Atomic Layer Deposition of TiO_2 Using "Water-Free" Metal-Halide/Metal Alkoxide Reactants. *J. Vac. Sci. Technol., A* **2016**, *34* (1), 01A148.
(181) Green, M. L.; Ho, M.-Y. Y.; Busch, B.; Wilk, G. D.; Sorsch, T.; Conard, T.; Brijs, B.; Vandervorst, W.; Räisänen, P. I.; Muller, D.; Bude, M.; Grazul, J. Nucleation and Growth of Atomic Layer Deposited HfO_2 Gate Dielectric Layers on Chemical Oxide (Si−O−H) and Thermal Oxide (SiO_2 or Si−O−N) Underlayers. *J. Appl. Phys.* **2002**, *92* (12), 7168−7174.
(182) Chen, R.; Kim, H.; McIntyre, P. C.; Bent, S. F. Self-Assembled Monolayer Resist for Atomic Layer Deposition of HfO_2 and ZrO_2 High-κ Gate Dielectrics. *Appl. Phys. Lett.* **2004**, *84* (20), 4017−4019.
(183) Chen, R.; Kim, H.; McIntyre, P. C.; Bent, S. F. Investigation of Self-Assembled Monolayer Resists for Hafnium Dioxide Atomic Layer Deposition. *Chem. Mater.* **2005**, *17* (3), 536−544.
(184) Hu, Z.; Turner, C. H. Initial Surface Reactions of TiO_2 Atomic Layer Deposition onto SiO_2 Surfaces: Density Functional Theory Calculations. *J. Phys. Chem. B* **2006**, *110* (16), 8337−8347.
(185) Ritala, M.; Kukli, K.; Rahtu, A.; Raisanen, P. I.; Leskela, M.; Sajavaara, T.; Keinonen, J. Atomic Layer Deposition of Oxide Thin Films with Metal Alkoxides as Oxygen Sources. *Science* **2000**, *288*, 319−321.
(186) Choi, J. Y.; Ahles, C. F.; Cho, Y.; Anurag, A.; Wong, K. T.; Nemani, S. D.; Yieh, E.; Kummel, A. C. Selective Pulsed Chemical Vapor Deposition of Water-Free HfO_x on Si in Preference to SiCOH and Passivated SiO_2. *Appl. Surf. Sci.* **2020**, *512*, 145733.
(187) Lakomaa, E.-L.; Haukka, S.; Suntola, T. Atomic Layer Growth of TiO_2 on Silica. *Appl. Surf. Sci.* **1992**, *60−61*, 742−748.
(188) Haukka, S.; Lakomaa, E. L.; Root, A. An IR and NMR Study of the Chemisorption of Titanium Tetrachloride on Silica. *J. Phys. Chem.* **1993**, *97* (19), 5085−5094.
(189) Lemaire, P. C.; King, M.; Parsons, G. N. Understanding Inherent Substrate Selectivity during Atomic Layer Deposition: Effect of Surface Preparation, Hydroxyl Density, and Metal Oxide Composition on Nucleation Mechanisms during Tungsten ALD. *J. Chem. Phys.* **2017**, *146* (5), 052811.
(190) Sinha, A.; Hess, D. W.; Henderson, C. L. A Top Surface Imaging Method Using Area Selective ALD on Chemically Amplified Polymer Photoresist Films. *Electrochem. Solid-State Lett.* **2006**, *9* (11), G330.
(191) Chen, R.; Kim, H.; McIntyre, P. C.; Porter, D. W.; Bent, S. F. Achieving Area-Selective Atomic Layer Deposition on Patterned Substrates by Selective Surface Modification. *Appl. Phys. Lett.* **2005**, *86* (19), 191910.
(192) Chen, R.; Bent, S. F. Chemistry for Positive Pattern Transfer Using Area-Selective Atomic Layer Deposition. *Adv. Mater.* **2006**, *18* (8), 1086−1090.
(193) Färm, E.; Kemell, M.; Ritala, M.; Leskelä, M. Selective-Area Atomic Layer Deposition Using Poly(Methyl Methacrylate) Films as Mask Layers. *J. Phys. Chem. C* **2008**, *112* (40), 15791−15795.
(194) Lu, P.; Walker, V. A. Making Nanoflowerbeds : Reaction Pathways Involved in the Selective Chemical Bath Deposition of ZnS on Functionalized Alkanethiolate Self-Assembled Monolayers. *ACS Nano* **2009**, *3* (2), 370−378.
(195) Liu, J.; Mao, Y.; Lan, E.; Banatao, D. R.; Forse, G. J.; Lu, J.; Blom, H. O.; Yeates, T. O.; Dunn, B.; Chang, J. P. Generation of Oxide Nanopatterns by Combining Self-Assembly of S-Layer Proteins and Area-Selective Atomic Layer Deposition. *J. Am. Chem. Soc.* **2008**, *130* (50), 16908−16913.
(196) Surwade, S. P.; Zhou, F.; Wei, B.; Sun, W.; Powell, A.; O'Donnell, C.; Yin, P.; Liu, H. Nanoscale Growth and Patterning of Inorganic Oxides Using DNA Nanostructure Templates. *J. Am. Chem. Soc.* **2013**, *135* (18), 6778−6781.
(197) Park, M. H.; Jang, Y. J.; Sung-Suh, H. M.; Sung, M. M. Selective Atomic Layer Deposition of Titanium Oxide on Patterned Self-Assembled Monolayers Formed by Microcontact Printing. *Langmuir* **2004**, *20* (6), 2257−2260.
(198) Seo, E. K.; Lee, J. W.; Sung-Suh, H. M.; Sung, M. M. Atomic Layer Deposition of Titanium Oxide on Self-Assembled-Monolayer-Coated Gold. *Chem. Mater.* **2004**, *16* (10), 1878−1883.
(199) Hua, Y.; King, W. P.; Henderson, C. L. Nanopatterning Materials Using Area Selective Atomic Layer Deposition in Conjunction with Thermochemical Surface Modification via Heated AFM Cantilever Probe Lithography. *Microelectron. Eng.* **2008**, *85* (5−6), 934−936.
(200) Reinke, M.; Kuzminykh, Y.; Hoffmann, P. Selective Growth of Titanium Dioxide by Low-Temperature Chemical Vapor Deposition. *ACS Appl. Mater. Interfaces* **2015**, *7*, 9736−9743.
(201) Lee, J. P.; Sung, M. M. A New Patterning Method Using Photocatalytic Lithography and Selective Atomic Layer Deposition. *J. Am. Chem. Soc.* **2004**, *126* (1), 28−29.
(202) Zhang, Z.; Dwyer, T.; Sirard, S. M.; Ekerdt, J. G. Area-Selective Atomic Layer Deposition of Cobalt Oxide to Generate Patterned Cobalt Films. *J. Vac. Sci. Technol., A* **2019**, *37* (2), 020905.
(203) Cummins, C.; Weingärtner, T.; Morris, M. A. Enabling Large-Area Selective Deposition on Metal-Dielectric Patterns Using Polymer Brush Deactivation. *J. Phys. Chem. C* **2018**, *122* (26), 14698−14705.
(204) Liu, X.; Zhu, Q.; Lang, Y.; Cao, K.; Chu, S.; Shan, B.; Chen, R. Oxide-Nanotrap-Anchored Platinum Nanoparticles with High Activity and Sintering Resistance by Area-Selective Atomic Layer Deposition. *Angew. Chem., Int. Ed.* **2017**, *56* (6), 1648−1652.
(205) Overhage, K.; Tao, Q.; Jursich, G.; Takoudis, C. G. Selective Atomic Layer Deposition (SALD) of Titanium Dioxide on Silicon and Copper Patterned Substrates. *J. Undergrad. Res.* **2017**, *4* (1), 5−8.
(206) Tao, Q.; Overhage, K.; Jursich, G.; Takoudis, C. On the Initial Growth of Atomic Layer Deposited TiO_2 Films on Silicon and Copper Surfaces. *Thin Solid Films* **2012**, *520* (22), 6752−6756.
(207) Tao, Q.; Jursich, G.; Takoudis, C. Selective Atomic Layer Deposition of HfO_2 on Copper Patterned Silicon Substrates. *Appl. Phys. Lett.* **2010**, *96* (19), 192105.
(208) Haider, A.; Yilmaz, M.; Deminskyi, P.; Eren, H.; Biyikli, N. Nanoscale Selective Area Atomic Layer Deposition of TiO_2 Using E-Beam Patterned Polymers. *RSC Adv.* **2016**, *6* (108), 106109−106119.
(209) Cheng, N.; Banis, M. N.; Liu, J.; Riese, A.; Li, X.; Li, R.; Ye, S.; Knights, S.; Sun, X. Extremely Stable Platinum Nanoparticles Encapsulated in a Zirconia Nanocage by Area-Selective Atomic Layer Deposition for the Oxygen Reduction Reaction. *Adv. Mater.* **2015**, *27* (2), 277−281.

https://dx.doi.org/10.1021/acs.chemmater.0c00722
Chem. Mater. XXXX, XXX, XXX−XXX

(210) Yao, Y.; Coyle, J. P.; Barry, S. T.; Zaera, F. Effect of the Nature of the Substrate on the Surface Chemistry of Atomic Layer Deposition Precursors. *J. Chem. Phys.* **2017**, *146* (5), 052806.
(211) Kannan Selvaraj, S.; Parulekar, J.; Takoudis, C. G. Selective Atomic Layer Deposition of Zirconia on Copper Patterned Silicon Substrates Using Ethanol as Oxygen Source as Well as Copper Reductant. *J. Vac. Sci. Technol., A* **2014**, *32* (1), 010601.
(212) Klesko, J. P.; Rahman, R.; Dangerfield, A.; Nanayakkara, C. E.; L'Esperance, T.; Moser, D. F.; Peña, L. F.; Mattson, E. C.; Dezelah, C. L.; Kanjolia, R. K.; Chabal, Y. J. Selective Atomic Layer Deposition Mechanism for Titanium Dioxide Films with $(EtCp)Ti(NMe_2)_3$: Ozone versus Water. *Chem. Mater.* **2018**, *30* (3), 970.
(213) Hu, Q.; Wang, S.; Gao, Z.; Li, Y.; Zhang, Q.; Xiang, Q.; Qin, Y. The Precise Decoration of Pt Nanoparticles with Fe Oxide by Atomic Layer Deposition for the Selective Hydrogenation of Cinnamaldehyde. *Appl. Catal., B* **2017**, *218*, 591−599.
(214) Choi, J. Y.; Ahles, C. F.; Wong, K. T.; Nemani, S.; Yieh, E.; Kummel, A. C. Highly Selective Atomic Layer Deposition of $MoSiO_x$ Using Inherently Substrate-Dependent Processes. *Appl. Surf. Sci.* **2020**, *512*, 144307.
(215) Yokoyama, S.; Ikeda, N.; Kajikawa, K.; Nakashima, Y. Atomic-Layer Selective Deposition of Silicon Nitride on Hydrogen-Terminated Si Surfaces. *Appl. Surf. Sci.* **1998**, *130*−*132*, 352−356.
(216) Shin, H. K.; Chi, K. M.; Hampden-Smith, M. J.; Kodas, T. T.; Farr, J. D.; Paffett, M. Hot-Wall Chemical Vapor Deposition of Copper from Copper(1) Compounds. 2. Selective, Low-Temperature Deposition of Copper from Copper(1) β-Diketonate Compounds, (β-Diketonate)CuL„ via Thermally Induced Disproportionation Reactions. *Chem. Mater.* **1992**, *4*, 788−795.
(217) Mårtensson, P.; Carlsson, J.-O. Atomic Layer Epitaxy of Copper. *J. Electrochem. Soc.* **1998**, *145* (8), 2926.
(218) Qi, J.; Zimmerman, D. T.; Weisel, G. J.; Willis, B. G. Nucleation and Growth of Copper Selective-Area Atomic Layer Deposition on Palladium Nanostructures. *J. Chem. Phys.* **2017**, *147* (15), 154702.
(219) Lu, J.; Low, K.-B.; Lei, Y.; Libera, J. A.; Nicholls, A.; Stair, P. C.; Elam, J. W. Toward Atomically-Precise Synthesis of Supported Bimetallic Nanoparticles Using Atomic Layer Deposition. *Nat. Commun.* **2014**, *5*, 1−9.
(220) Lin, W.; Warren, T. H.; Nuzzo, R. G.; Girolami, G. S. Surface-Selective Deposition of Palladium and Silver Films from Metal-Organic Precursors: A Novel Metal-Organic Chemical Vapor Deposition Redox Transmetalation Process. *J. Am. Chem. Soc.* **1993**, *115* (24), 11644−11645.
(221) Lin, W.; Wiegand, B. C.; Nuzzo, R. G.; Girolami, G. S. Mechanistic Studies of Palladium Thin Film Growth from Palladium(II) β-Diketonates. 1. Spectroscopic Studies of the Reactions of Bis(Hexafluoroacetylacetonato)Palladium(II) on Copper Surfaces. *J. Am. Chem. Soc.* **1996**, *118* (25), 5977−5987.
(222) Higashi, G. S.; Raghavachari, K.; Steigerwald, M. L. Mechanism of Surface Selectivity in Aluminum Chemical Vapor Deposition. *J. Vac. Sci. Technol., B: Microelectron. Process. Phenom.* **1990**, *8* (1), 103.
(223) Elko-Hansen, T. D. M.; Ekerdt, J. G. Selective Atomic Layer Deposition of Cobalt for Back End of Line. *ECS Trans.* **2017**, *80* (3), 29−37.
(224) Färm, E.; Kemell, M.; Ritala, M.; Leskelä, M. Selective-Area Atomic Layer Deposition with Microcontact Printed Self-Assembled Octadecyltrichlorosilane Monolayers as Mask Layers. *Thin Solid Films* **2008**, *517* (2), 972−975.
(225) Färm, E.; Kemell, M.; Ritala, M.; Leskelä, M. Self-Assembled Octadecyltrimethoxysilane Monolayers Enabling Selective-Area Atomic Layer Deposition of Iridium. *Chem. Vap. Deposition* **2006**, *12* (7), 415−417.
(226) Aaltonen, T.; Rahtu, A.; Ritala, M.; Leskelä, M. Reaction Mechanism Studies on Atomic Layer Deposition of Ruthenium and Platinum. *Electrochem. Solid-State Lett.* **2003**, *6* (9), C130.
(227) Christensen, S. T.; Elam, J. W. Atomic Layer Deposition of Ir−Pt Alloy Films. *Chem. Mater.* **2010**, *22* (8), 2517−2525.
(228) Park, K. J.; Terry, D. B.; Stewart, S. M.; Parsons, G. N. In Situ Auger Electron Spectroscopy Study of Atomic Layer Deposition: Growth Initiation and Interface Formation Reactions during Ruthenium ALD on Si−H, SiO_2, and HfO_2 Surfaces. *Langmuir* **2007**, *23* (11), 6106−6112.
(229) Yim, S.-S.; Lee, D.-J.; Kim, K.-S.; Yoon, T.-S.; Kim, K.-B.; Kim, S.-H. Nucleation Kinetics of Ru on Silicon Oxide and Silicon Nitride Surfaces Deposited by Atomic Layer Deposition. *J. Appl. Phys.* **2008**, *103* (11), 113509.
(230) Park, K. J.; Doub, J. M.; Gougousi, T.; Parsons, G. N. Microcontact Patterning of Ruthenium Gate Electrodes by Selective Area Atomic Layer Deposition. *Appl. Phys. Lett.* **2005**, *86* (5), 051903.
(231) Luo, B.; Wang, Q.; White, J. M. UHV Surface Chemistry of Bis(Ethylcyclopentadienyl)Ruthenium, $(C_2H_5C_5H_4)_2Ru$ on an Oxide Substrate. *Chem. Vap. Deposition* **2004**, *10* (6), 311−317.
(232) Waldfried, C.; Welipitiya, D.; Hutchings, C. W.; de Silva, V. H. S.; Gallup, G. A.; Dowben, P. A.; Pai, W. W.; Zhang, J.; Wendelken, J. F.; Boag, N. M. Preferential Bonding Orientations of Ferrocene on Surfaces. *J. Phys. Chem. B* **1997**, *101* (47), 9782−9789.
(233) Junige, M.; Löffler, M.; Geidel, M.; Albert, M.; Bartha, J. W.; Zschech, E.; Rellinghaus, B.; van Dorp, W. F. Area-Selective Atomic Layer Deposition of Ru on Electron-Beam-Written Pt(C) Patterns versus SiO_2 Substratum. *Nanotechnology* **2017**, *28* (39), 395301.
(234) Mackus, A. J. M.; Mulders, J. J. L.; Van De Sanden, M. C. M.; Kessels, W. M. M. Local Deposition of High-Purity Pt Nanostructures by Combining Electron Beam Induced Deposition and Atomic Layer Deposition. *J. Appl. Phys.* **2010**, *107* (11), 116102.
(235) Mackus, A. J. M.; Thissen, N. F. W.; Mulders, J. J. L.; Trompenaars, P. H. F.; Verheijen, M. A.; Bol, A. A.; Kessels, W. M. M. Direct-Write Atomic Layer Deposition of High-Quality Pt Nanostructures: Selective Growth Conditions and Seed Layer Requirements. *J. Phys. Chem. C* **2013**, *117* (20), 10788−10798.
(236) Mackus, A. J. M.; Verheijen, M. A.; Leick, N.; Bol, A. A.; Kessels, W. M. M. Influence of Oxygen Exposure on the Nucleation of Platinum Atomic Layer Deposition: Consequences for Film Growth, Nanopatterning, and Nanoparticle Synthesis. *Chem. Mater.* **2013**, *25* (9), 1905−1911.
(237) Egorov, V. K.; Lebedinskii, Y. Y.; Soloviev, A. A.; Chouprik, A. A.; Azarov, A. Y.; Markeev, A. M. Initial and Steady-State Ru Growth by Atomic Layer Deposition Studied by in Situ Angle Resolved X-Ray Photoelectron Spectroscopy. *Appl. Surf. Sci.* **2017**, *419*, 107−113.
(238) Kukli, K.; Kemell, M.; Puukilainen, E.; Aarik, J.; Aidla, A.; Sajavaara, T.; Laitinen, M.; Tallarida, M.; Sundqvist, J.; Ritala, M.; Leskelä, M. Atomic Layer Deposition of Ruthenium Films from (Ethylcyclopentadienyl)(Pyrrolyl)Ruthenium and Oxygen. *J. Electrochem. Soc.* **2011**, *158* (3), D158.
(239) Mullings, M. N.; Lee, H.-B.-R.; Marchack, N.; Jiang, X.; Chen, Z.; Gorlin, Y.; Lin, K.-P.; Bent, S. F. Area Selective Atomic Layer Deposition by Microcontact Printing with a Water-Soluble Polymer. *J. Electrochem. Soc.* **2010**, *157* (12), D600.
(240) Zyulkov, I.; Krishtab, M.; De Gendt, S.; Armini, S. Selective Ru ALD as a Catalyst for Sub-Seven-Nanometer Bottom-Up Metal Interconnects. *ACS Appl. Mater. Interfaces* **2017**, *9* (36), 31031−31041.
(241) Xie, R.; Park, C.; Conti, R.; Robison, R.; Zhou, H.; Saraf, I.; Carr, A.; Fan, S. S. C.; Ryan, K.; Belyansky, M.; Pancharatnam, S.; Young, A.; Wang, J.; Greene, A.; Cheng, K.; Li, J.; Conte, R.; Tang, H.; Choi, K.; Amanapu, H.; Peethala, B.; Muthinti, R.; Raymond, M.; Prindle, C.; Liang, Y.; Tsai, S.; Kamineni, V.; Labonte, A.; Cave, N.; Gupta, D.; Basker, V.; Loubet, N.; Guo, D.; Haran, B.; Knorr, A.; Bu, H. Self-Aligned Gate Contact (SAGC) for CMOS Technology Scaling beyond 7nm. *2019 Symp. VLSI Technol. Dig. Technol. Pap.* **2019**, *T148* (T13−3), T148.
(242) King, M. J.; Theofanis, P. L.; Lemaire, P. C.; Santiso, E. E.; Parsons, G. N. Ab Initio Analysis of Nucleation Reactions during Tungsten Atomic Layer Deposition on Si(100) and W(110) Substrates. *J. Vac. Sci. Technol., A* **2018**, *36* (6), 061507.
(243) Kalanyan, B.; Lemaire, P. C.; Atanasov, S. E.; Ritz, M. J.; Parsons, G. N. Using Hydrogen to Expand the Inherent Substrate Selectivity Window during Tungsten Atomic Layer Deposition. *Chem. Mater.* **2016**, *28* (1), 117−126.

https://dx.doi.org/10.1021/acs.chemmater.0c00722
Chem. Mater. XXXX, XXX, XXX−XXX

(244) Lee, H.-B.-R.; Kim, W.-H.; Lee, J. W.; Kim, J.-M.; Heo, K.; Hwang, I. C.; Park, Y.; Hong, S.; Kim, H. High Quality Area-Selective Atomic Layer Deposition Co Using Ammonia Gas as a Reactant. *J. Electrochem. Soc.* **2010**, *157* (1), D10.
(245) Lee, H.-B.-R.; Kim, H. Area Selective Atomic Layer Deposition of Cobalt Thin Films. *ECS Transactions* **2008**, *16*, 219−225.
(246) Kerrigan, M. M.; Klesko, J. P.; Rupich, S. M.; Dezelah, C. L.; Kanjolia, R. K.; Chabal, Y. J.; Winter, C. H. Substrate Selectivity in the Low Temperature Atomic Layer Deposition of Cobalt Metal Films from Bis(1,4-Di- Tert -Butyl-1,3-Diazadienyl)Cobalt and Formic Acid. *J. Chem. Phys.* **2017**, *146* (5), 052813.
(247) Wolf, S.; Breeden, M.; Ueda, S.; Kummel, A. Hyper-Selective Co Metal ALD on Metals vs. SiO_2 without Passivation. *2019 Int. Symp. VLSI Technol. Syst. Appl. VLSI-TSA 2019* **2019**, 31−32.
(248) Kerrigan, M. M.; Klesko, J. P.; Winter, C. H. Low Temperature, Selective Atomic Layer Deposition of Cobalt Metal Films Using Bis(1,4-Di- Tert -Butyl-1,3-Diazadienyl)Cobalt and Alkylamine Precursors. *Chem. Mater.* **2017**, *29* (17), 7458−7466.
(249) Jeon, N. L.; Nuzzo, R. G.; Xia, Y.; Mrksich, M.; Whitesides, G. M. Patterned Self-Assembled Monolayers Formed by Microcontact Printing Direct Selective Metalization by Chemical Vapor Deposition on Planar and Nonplanar Substrates. *Langmuir* **1995**, *11* (8), 3024−3026.
(250) Lee, B. H.; Hwang, J. K.; Nam, J. W.; Lee, S. U.; Kim, J. T.; Koo, S. M.; Baunemann, A.; Fischer, R. A.; Sung, M. M. Low-Temperature Atomic Layer Deposition of Copper Metal Thin Films: Self-Limiting Surface Reaction of Copper Dimethylamino-2-Propoxide with Diethylzinc. *Angew. Chem., Int. Ed.* **2009**, *48* (25), 4536−4539.
(251) Färm, E.; Vehkamäki, M.; Ritala, M.; Leskelä, M. Passivation of Copper Surfaces for Selective-Area ALD Using a Thiol Self-Assembled Monolayer. *Semicond. Sci. Technol.* **2012**, *27* (7), 074004.
(252) Kim, W.-H.; Lee, H.-B.-R.; Heo, K.; Lee, Y. K.; Chung, T.-M.; Kim, C. G.; Hong, S.; Heo, J.; Kim, H. Atomic Layer Deposition of Ni Thin Films and Application to Area-Selective Deposition. *J. Electrochem. Soc.* **2011**, *158* (1), D1.
(253) Park, K. J.; Parsons, G. N. Selective Area Atomic Layer Deposition of Rhodium and Effective Work Function Characterization in Capacitor Structures. *Appl. Phys. Lett.* **2006**, *89* (4), 043111.
(254) Funakubo, H.; Shiraishi, T.; Oikawa, T.; Hirano, M.; Chiba, H.; Kawano, K. Effect of Incubation Time on Preparation of Continuous and Flat Ru Films. *J. Vac. Sci. Technol., A* **2015**, *33*, 01A149.
(255) Kastelic, M.; Oh, I.; Takoudis, C. G.; Friedrich, J. A.; Neudeck, G. W. Selective Epitaxial Growth of Silicon in Pancake Reactors. *Chem. Eng. Sci.* **1988**, *43* (8), 2031−2036.
(256) Hartmann, J. M.; Bertin, F.; Rolland, G.; Laugier, F.; Semeria, M. N. Selective Epitaxial Growth of Si and SiGe for Metal Oxide Semiconductor Transistors. *J. Cryst. Growth* **2003**, *259* (4), 419−427.
(257) Gannavaram, S.; Pesovic, N.; Ozturk, M. C. Low Temperature (<800C) Recessed Junction Selective Silicon-Germanium SourceDrain Technology for Sub-70 nm CMOS. In *IEDM Proceedings*; IEEE: 2000; pp 437−440.
(258) Nagahara, M.; Miyoshi, S.; Yaguchi, H.; Onabe, K.; Shiraki, Y.; Ito, R. Selective Growth of Cubic GaN in Small Areas on Patterned GaAs(100) Substrates by Metalorganic Vapor Phase Epitaxy. *Jpn. J. Appl. Phys.* **1994**, *33* (1), 694−697.
(259) Hersee, S. D.; Sun, X.; Wang, X. The Controlled Growth of GaN Nanowires. *Nano Lett.* **2006**, *6* (8), 1808−1811.
(260) Han, W.; Fan, S.; Li, Q.; Hu, Y. Synthesis of Gallium Nitride Nanorods Through a Carbon Nanotube-Confined Reaction. *Science* **1997**, *277* (5330), 1287−1289.
(261) Kondo, D.; Sato, S.; Yagi, K.; Harada, N.; Sato, M.; Nihei, M.; Yokoyama, N. Low-Temperature Synthesis of Graphene and Fabrication of Top-Gated Field Effect Transistors without Using Transfer Processes. *Appl. Phys. Express* **2010**, *3* (2), 025102.
(262) Parsons, G. N.; Boland, J. J.; Tsang, J. C. Selective Deposition and Bond Strain Relaxation in Silicon PECVD Using Time Modulated Silane Flow. *Jpn. J. Appl. Phys.* **1992**, *31* (6S), 1943−1947.
(263) Heyne, M. H.; de Marneffe, J.-F.; Delabie, A.; Caymax, M.; Neyts, E. C.; Radu, I.; Huyghebaert, C.; De Gendt, S. Two-Dimensional WS_2 Nanoribbon Deposition by Conversion of Pre-Patterned Amorphous Silicon. *Nanotechnology* **2017**, *28* (4), 04LT01.
(264) Han, G. H.; Kybert, N. J.; Naylor, C. H.; Lee, B. S.; Ping, J.; Park, J. H.; Kang, J.; Lee, S. Y.; Lee, Y. H.; Agarwal, R.; Johnson, A. T. C. Seeded Growth of Highly Crystalline Molybdenum Disulphide Monolayers at Controlled Locations. *Nat. Commun.* **2015**, *6*, 1−6.
(265) Sun, D.; Nguyen, A. E.; Barroso, D.; Zhang, X.; Preciado, E.; Bobek, S.; Klee, V.; Mann, J.; Bartels, L. Chemical Vapor Deposition Growth of a Periodic Array of Single-Layer MoS_2 Islands via Lithographic Patterning of an SiO_2/Si Substrate. *2D Mater.* **2015**, *2* (4), 045014.
(266) Chen, X.; Park, Y. J.; Das, T.; Jang, H.; Lee, J. B.; Ahn, J. H. Lithography-Free Plasma-Induced Patterned Growth of MoS_2 and Its Heterojunction with Graphene. *Nanoscale* **2016**, *8* (33), 15181−15188.
(267) Bartolucci, S. F.; Kaplan, D.; Maurer, J. A. Ion Beam-Induced Hydroxylation Controls Molybdenum Disulfide Growth. *2D Mater.* **2017**, *4* (2), 021017.
(268) Ryu, B.; Li, D.; Park, C.; Rokni, H.; Lu, W.; Liang, X. Rubbing-Induced Site-Selective Growth of MoS_2 Device Patterns. *ACS Appl. Mater. Interfaces* **2018**, *10* (50), 43774−43784.
(269) Gong, X.; Zhao, X.; Pam, M. E.; Yao, H.; Li, Z.; Geng, D.; Pennycook, S. J.; Shi, Y.; Yang, H. Y. Location-Selective Growth of Two-Dimensional Metallic/Semiconducting Transition Metal Dichalcogenide Heterostructures. *Nanoscale* **2019**, *11* (10), 4183−4189.
(270) Choi, B. J.; Choi, S.; Shin, Y. C.; Kim, K. M.; Hwang, C. S.; Kim, Y. J.; Son, Y. J.; Hong, S. K. Combined Atomic Layer and Chemical Vapor Deposition, and Selective Growth of $Ge_2Sb_2Te_5$ Films on TiN/W Contact Plug. *Chem. Mater.* **2007**, *19* (18), 4387−4389.
(271) Benjamin, S. L.; de Groot, C. H.; Hector, a. L.; Huang, R.; Koukharenko, E.; Levason, W.; Reid, G. Chemical Vapour Deposition of Antimony Chalcogenides with Positional and Orientational Control: Precursor Design and Substrate Selectivity. *J. Mater. Chem. C* **2015**, *3* (2), 423−430.
(272) Chen, H. Y.; Lai, J. H.; Jiang, X.; Lahann, J. Substrate-Selective Chemical Vapor Deposition of Reactive Polymer Coatings. *Adv. Mater.* **2008**, *20* (18), 3474−3480.
(273) Bally-Le Gall, F.; Friedmann, C.; Heinke, L.; Arslan, H.; Azucena, C.; Welle, A.; Ross, A. M.; Wöll, C.; Lahann, J. Free-Standing Nanomembranes Based on Selective CVD Deposition of Functional Poly-p-Xylylenes. *ACS Nano* **2015**, *9* (2), 1400−1407.
(274) Vaeth, K. M.; Jackman, R. J.; Black, A. J.; Whitesides, G. M.; Jensen, K. F. Use of Microcontact Printing for Generating Selectively Grown Films of Poly(p-Phenylene Vinylene) and Parylenes Prepared by Chemical Vapor Deposition. *Langmuir* **2000**, *16* (22), 8495−8500.
(275) Vaeth, K. M.; Jensen, K. F. Transition Metals for Selective Chemical Vapor Deposition of Parylene-Based Polymers. *Chem. Mater.* **2000**, *12* (5), 1305−1313.
(276) Huang, Z.; Wang, P.-C.; Macdiarmid, A. G.; Xia, Y.; Whitesides, G. Selective Deposition of Conducting Polymers on Hydroxyl-Terminated Surfaces with Printed Monolayers of Alkylsiloxanes as Templates. *Langmuir* **1997**, *13* (24), 6480−6484.
(277) Hermes, S.; Zacher, D.; Baunemann, A.; Wöll, C.; Fischer, R. A. Selective Growth and MOCVD Loading of Small Single Crystals of MOF-5 at Alumina and Silica Surfaces Modified with Organic Self-Assembled Monolayers. *Chem. Mater.* **2007**, *19* (9), 2168−2173.
(278) Zhuang, J.-L.; Kind, M.; Grytz, C. M.; Farr, F.; Diefenbach, M.; Tussupbayev, S.; Holthausen, M. C.; Terfort, A. Insight into the Oriented Growth of Surface-Attached Metal−Organic Frameworks: Surface Functionality, Deposition Temperature, and First Layer Order. *J. Am. Chem. Soc.* **2015**, *137* (25), 8237−8243.
(279) Peters, A. W.; Li, Z.; Farha, O. K.; Hupp, J. T. Atomically Precise Growth of Catalytically Active Cobalt Sulfide on Flat Surfaces and within a Metal-Organic Framework via Atomic Layer Deposition. *ACS Nano* **2015**, *9* (8), 8484−8490.
(280) Hermes, S.; Schröder, F.; Chelmowski, R.; Wöll, C.; Fischer, R. A. Selective Nucleation and Growth of Metal−Organic Open Framework Thin Films on Patterned $COOH/CF_3$-Terminated Self-Assembled Monolayers on Au(111). *J. Am. Chem. Soc.* **2005**, *127* (40), 13744−13745.

(281) Prasittichai, C.; Pickrahn, K. L.; Minaye Hashemi, F. S.; Bergsman, D. S.; Bent, S. F. Improving Area-Selective Molecular Layer Deposition by Selective SAM Removal. *ACS Appl. Mater. Interfaces* **2014**, *6* (20), 17831−17836.
(282) Closser, R. G.; Bergsman, D. S.; Ruelas, L.; Hashemi, F. S. M.; Bent, S. F. Correcting Defects in Area Selective Molecular Layer Deposition. *J. Vac. Sci. Technol., A* **2017**, *35* (3), 031509.
(283) Prasittichai, C.; Zhou, H.; Bent, S. F. Area Selective Molecular Layer Deposition of Polyurea Films. *ACS Appl. Mater. Interfaces* **2013**, *5* (24), 13391−13396.
(284) Bergsman, D.; Zhou, H.; Bent, S. F. Molecular Layer Deposition of Nanoscale Organic Films for Nanoelectronics Applications. *ECS Trans.* **2014**, *64* (9), 87−96.
(285) Jeon, N. L.; Choi, I. S.; Whitesides, G. M.; Kim, N. Y.; Laibinis, P. E.; Harada, Y.; Finnie, K. R.; Girolami, G. S.; Nuzzo, R. G. Patterned Polymer Growth on Silicon Surfaces Using Microcontact Printing and Surface-Initiated Polymerization. *Appl. Phys. Lett.* **1999**, *75* (26), 4201−4203.
(286) Gu, H.; Xu, C.; Weng, L. T.; Xu, B. Solventless Polymerization: Spatial Migration of a Catalyst to Form Polymeric Thin Films in Microchannels. *J. Am. Chem. Soc.* **2003**, *125* (31), 9256−9257.
(287) O'Connell, C. D.; Higgins, M. J.; Nakashima, H.; Moulton, S. E.; Wallace, G. G. Vapor Phase Polymerization of EDOT from Submicrometer Scale Oxidant Patterned by Dip-Pen Nanolithography. *Langmuir* **2012**, *28* (26), 9953−9960.
(288) Brooke, R.; Evans, D.; Dienel, M.; Hojati-Talemi, P.; Murphy, P.; Fabretto, M. Inkjet Printing and Vapor Phase Polymerization: Patterned Conductive PEDOT for Electronic Applications. *J. Mater. Chem. C* **2013**, *1* (20), 3353−3358.
(289) Kwong, P.; Flowers, C. A.; Gupta, M. Directed Deposition of Functional Polymers onto Porous Substrates Using Metal Salt Inhibitors. *Langmuir* **2011**, *27* (17), 10634−10641.
(290) Kwong, P.; Seidel, S.; Gupta, M. Effect of Transition Metal Salts on the Initiated Chemical Vapor Deposition of Polymer Thin Films. *J. Vac. Sci. Technol., A* **2015**, *33* (3), 031504.
(291) Pattison, T. G.; Hess, A. E.; Arellano, N.; Lanzillo, N.; Nguyen, S.; Bui, H.; Rettner, C.; Truong, H.; Friz, A.; Topuria, T.; Fong, A.; Hughes, B.; Tek, A. T.; DeSilva, A.; Miller, R. D.; Qiao, G. G.; Wojtecki, R. J. Surface Initiated Polymer Thin Films for the Area Selective Deposition and Etching of Metal Oxides. *ACS Nano* **2020**, *14* (4), 4276−4288.
(292) Yoo, P. J.; Nam, K. T.; Belcher, A. M.; Hammond, P. T. Solvent-Assisted Patterning of Polyelectrolyte Multilayers and Selective Deposition of Virus Assemblies. *Nano Lett.* **2008**, *8* (4), 1081−1089.
(293) Calais, T.; Playe, B.; Ducéré, J. M.; Veyan, J. F.; Rupich, S.; Hemeryck, A.; Djafari Rouhani, M.; Rossi, C.; Chabal, Y. J.; Estève, A. Role of Alumina Coatings for Selective and Controlled Bonding of DNA on Technologically Relevant Oxide Surfaces. *J. Phys. Chem. C* **2015**, *119* (41), 23527−23543.
(294) Klosterman, L.; Riley, J. K.; Bettinger, C. J. Control of Heterogeneous Nucleation and Growth Kinetics of Dopamine-Melanin by Altering Substrate Chemistry. *Langmuir* **2015**, *31* (11), 3451−3458.
(295) Furukawa, H.; Cordova, K. E.; O'Keeffe, M.; Yaghi, O. M. The Chemistry and Applications of Metal-Organic Frameworks. *Science* **2013**, *341* (6149), 1230444.
(296) Krishtab, M.; Stassen, I.; Stassin, T.; Cruz, A. J.; Okudur, O. O.; Armini, S.; Wilson, C.; De Gendt, S.; Ameloot, R. Vapor-Deposited Zeolitic Imidazolate Frameworks as Gap-Filling Ultra-Low-k Dielectrics. *Nat. Commun.* **2019**, *10* (1), 1−9.
(297) Lemaire, P. C.; Zhao, J.; Williams, P. S.; Walls, H. J.; Shepherd, S. D.; Losego, M. D.; Peterson, G. W.; Parsons, G. N. Copper Benzenetricarboxylate Metal−Organic Framework Nucleation Mechanisms on Metal Oxide Powders and Thin Films Formed by Atomic Layer Deposition. *ACS Appl. Mater. Interfaces* **2016**, *8* (14), 9514−9522.
(298) Zhao, J.; Nunn, W. T.; Lemaire, P. C.; Lin, Y.; Dickey, M. D.; Oldham, C. J.; Walls, H. J.; Peterson, G. W.; Losego, M. D.; Parsons, G. N. Facile Conversion of Hydroxy Double Salts to Metal−Organic Frameworks Using Metal Oxide Particles and Atomic Layer Deposition Thin-Film Templates. *J. Am. Chem. Soc.* **2015**, *137* (43), 13756−13759.
(299) Lausund, K. B.; Nilsen, O. All-Gas-Phase Synthesis of UiO-66 through Modulated Atomic Layer Deposition. *Nat. Commun.* **2016**, *7*, 1−9.
(300) Stassen, I.; Styles, M.; Grenci, G.; Gorp, V. H. V.; Vanderlinden, W.; Feyter, D. S. D.; Falcaro, P.; Vos, D. D.; Vereecken, P.; Ameloot, R. Chemical Vapour Deposition of Zeolitic Imidazolate Framework Thin Films. *Nat. Mater.* **2016**, *15* (3), 304−310.
(301) Stassen, I.; Burtch, N.; Talin, A.; Falcaro, P.; Allendorf, M.; Ameloot, R. An Updated Roadmap for the Integration of Metal-Organic Frameworks with Electronic Devices and Chemical Sensors. *Chem. Soc. Rev.* **2017**, *46* (11), 3185−3241.
(302) Haukka, S. P.; Matero, R. H.; Tois, E.; Niskanen, A.; Huotari, H.; Pore, V. J. Dual Selective Deposition. US Patent Appl. No. 14/687,833; Patent No. US 2015/0299848 A1, 2015.
(303) Gay, G.; Baron, T.; Agraffeil, C.; Salhi, B.; Chevolleau, T.; Cunge, G.; Grampeix, H.; Tortai, J. H.; Martin, F.; Jalaguier, E.; De Salvo, B. CMOS Compatible Strategy Based on Selective Atomic Layer Deposition of a Hard Mask for Transferring Block Copolymer Lithography Patterns. *Nanotechnology* **2010**, *21* (43), 435301.
(304) Hackley, J. C.; Gougousi, T.; Demaree, J. D. Nucleation of HfO_2 Atomic Layer Deposition Films on Chemical Oxide and H-Terminated Si. *J. Appl. Phys.* **2007**, *102* (3), 034101.
(305) Hackley, J. C.; Demaree, J. D.; Gougousi, T. Growth and Interface of HfO_2 Films on H-Terminated Si from a TDMAH and H_2O Atomic Layer Deposition Process. *J. Vac. Sci. Technol., A* **2008**, *26* (5), 1235−1240.
(306) Lu, P.; Campbell, C. T.; Xia, Y. A Sinter-Resistant Catalytic System Fabricated by Maneuvering the Selectivity of SiO_2 Deposition onto the TiO_2 Surface versus the Pt Nanoparticle Surface. *Nano Lett.* **2013**, *13* (10), 4957−4962.
(307) Cummins, C.; Shaw, M. T.; Morris, M. A. Area Selective Polymer Brush Deposition. *Macromol. Rapid Commun.* **2017**, *38* (16), 1700252.
(308) Mameli, A.; Karasulu, B.; Verheijen, M. A.; Mackus, A. J. M.; Kessels, W. M. M.; Roozeboom, F. Area-Selective Atomic Layer Deposition: Role of Surface Chemistry. *ECS Trans.* **2017**, *80* (3), 39−48.
(309) Mameli, A.; Kuang, Y.; Aghaee, M.; Ande, C. K.; Karasulu, B.; Creatore, M.; Mackus, A. J. M.; Kessels, W. M. M.; Roozeboom, F. Area-Selective Atomic Layer Deposition of In_2O_3:H Using a μ-Plasma Printer for Local Area Activation. *Chem. Mater.* **2017**, *29* (3), 921−925.
(310) Avila, J. R.; Emery, J. D.; Pellin, M. J.; Martinson, A. B. F.; Farha, O. K.; Hupp, J. T. Porphyrins as Templates for Site-Selective Atomic Layer Deposition: Vapor Metalation and in Situ Monitoring of Island Growth. *ACS Appl. Mater. Interfaces* **2016**, *8* (31), 19853−19859.
(311) Yang, M.; Aarnink, A. A. I.; Schmitz, J.; Kovalgin, A. Y. Inherently Area-Selective Hot-Wire Assisted Atomic Layer Deposition of Tungsten Films. *Thin Solid Films* **2018**, *649*, 17−23.
(312) Choi, J. Y.; Ahles, C. F.; Hung, R.; Kim, N.; Kummel, A. C. Selective Atomic Layer Deposition of $MoSi_x$ on Si (0 0 1) in Preference to Silicon Nitride and Silicon Oxide. *Appl. Surf. Sci.* **2018**, *462* (May), 1008−1016.
(313) Kwon, J.; Saly, M.; Halls, M. D.; Kanjolia, R. K.; Chabal, Y. J. Substrate Selectivity of (^{t}Bu-Allyl)$Co(CO)_3$ during Thermal Atomic Layer Deposition of Cobalt. *Chem. Mater.* **2012**, *24* (6), 1025−1030.
(314) Minjauw, M. M.; Rijckaert, H.; Van Driessche, I.; Detavernier, C.; Dendooven, J. Nucleation Enhancement and Area-Selective Atomic Layer Deposition of Ruthenium Using RuO_4 and H_2 Gas. *Chem. Mater.* **2019**, *31* (5), 1491−1499.
(315) Xie, J.; Yang, X.; Han, B.; Shao-Horn, Y.; Wang, D. Site-Selective Deposition of Twinned Platinum Nanoparticles on $TiSi_2$ Nanonets by Atomic Layer Deposition and Their Oxygen Reduction Activities. *ACS Nano* **2013**, *7* (7), 6337−6345.
(316) Babar, S.; Davis, L. M.; Zhang, P.; Mohimi, E.; Girolami, G. S.; Abelson, J. R. Chemical Vapor Deposition of Copper: Use of a Molecular Inhibitor to Afford Uniform Nanoislands or Smooth Films. *ECS J. Solid State Sci. Technol.* **2014**, *3* (5), Q79−Q83.

https://dx.doi.org/10.1021/acs.chemmater.0c00722
Chem. Mater. XXXX, XXX, XXX−XXX

(317) Lee, H. B. R.; Bent, S. F. Microstructure-Dependent Nucleation in Atomic Layer Deposition of Pt on TiO_2. *Chem. Mater.* **2012**, *24* (2), 279−286.
(318) Lee, H. B. R.; Mullings, M. N.; Jiang, X.; Clemens, B. M.; Bent, S. F. Nucleation-Controlled Growth of Nanoparticles by Atomic Layer Deposition. *Chem. Mater.* **2012**, *24* (21), 4051−4059.

https://dx.doi.org/10.1021/acs.chemmater.0c00722
Chem. Mater. XXXX, XXX, XXX−XXX